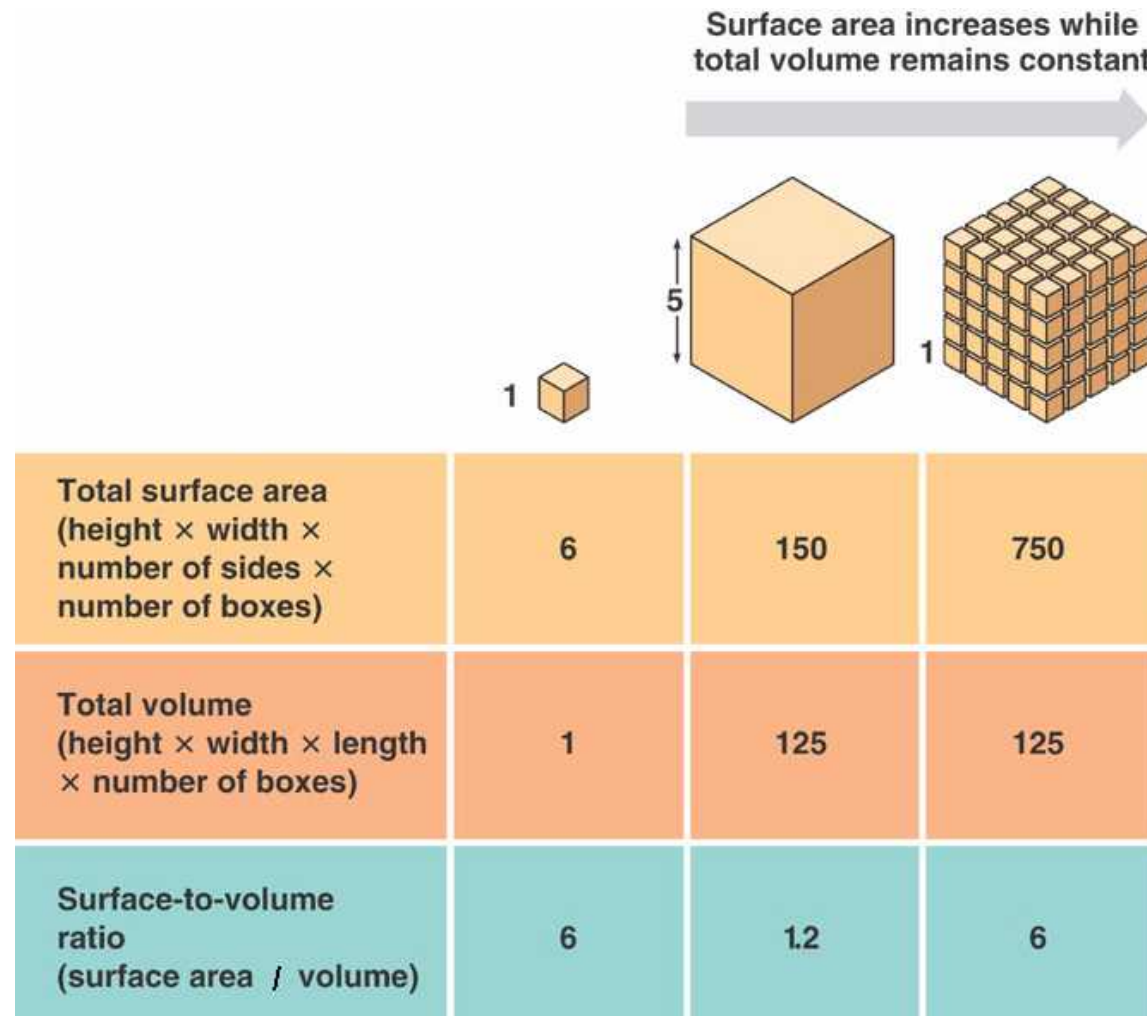


Nanomaterials

- Metals and Alloys
 - Fe, Al, Au
- Semiconductors
 - Band gap, CdS, TiO₂, ZnO
- Ceramic
 - Al₂O₃, Si₃N₄, MgO, , SiO₂, ZrO₂
- Carbon based
 - Diamond, graphite, nanotube, C60, graphene
- Polymers
 - Soft mater, block co-polymer
- Biological
 - Photonic, hydrophobic, adhesive,
- Composites

Surface to Volume Ratio



Surface Energy

One face surface energy: γ

27 cube: $27 \times 6 \gamma$

3 x 9 cube line: 114γ

3 x (3x3) square: 90γ

3 x 3 x 3 cube: 54γ

Surface to Volume Ratio

Au: AAA

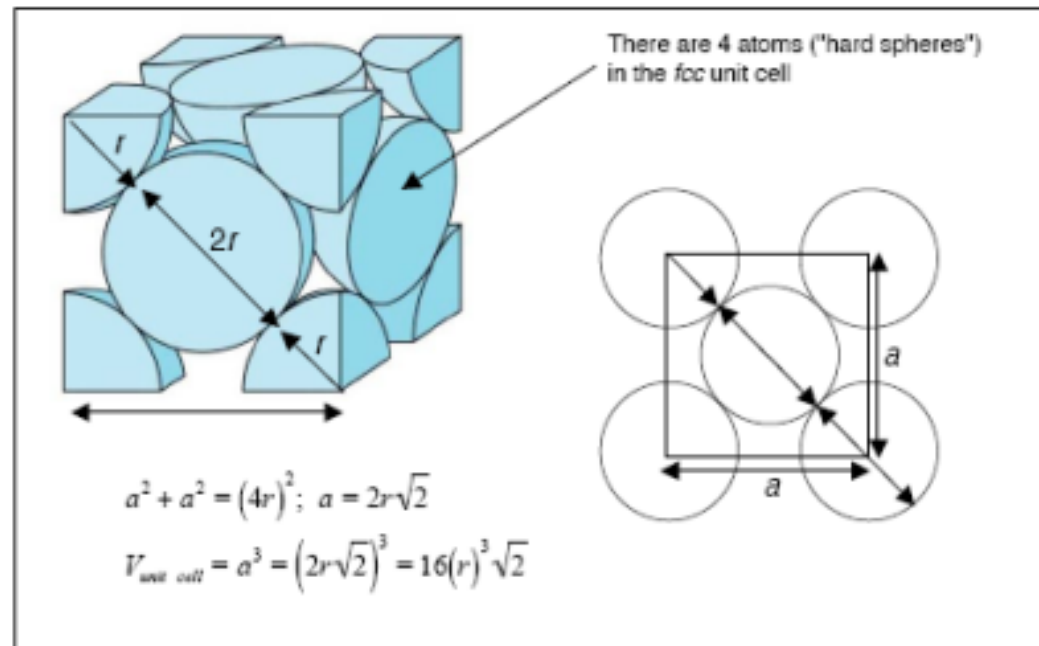
Atomic mass: 196.967

Density 19.31

Radii = 0.144 nm

Number of Au atoms in 1 m	$3.4 \cdot 10^9$
Volume of Au atom	$4.19 \cdot 10^{28}$
Surface area Au atom	$7.22 \cdot 10^{19}$
Surface/volume ratio	$1.72 \cdot 10^{-9}$

fcc



$$V_{\text{unit cell}} = a^3 = (2r\sqrt{2})^3 = 16(0.5\text{nm})^3\sqrt{2} = 2.828 \text{ nm}^3$$

$$\frac{10^{27} \text{ nm}^3}{2.828 \text{ nm}^3} = 3.538 \times 10^{26} \text{ nano-unit cells}$$

$$\frac{S_{\text{plate}}}{S_{\text{unit cell}}} = \frac{4.44 \times 10^8 \text{ m}^2}{6.0 \times 10^7 \text{ m}^2} = 0.74$$

$$\text{Collective Area} = 3.538 \times 10^{26} \text{ nano-unit cells} \left(\frac{4 \text{ spheres}}{\text{unit cell}} \right) \left(\frac{4\pi r^2}{\text{sphere}} \right) = 4.44 \times 10^{27} \text{ nm}^2$$

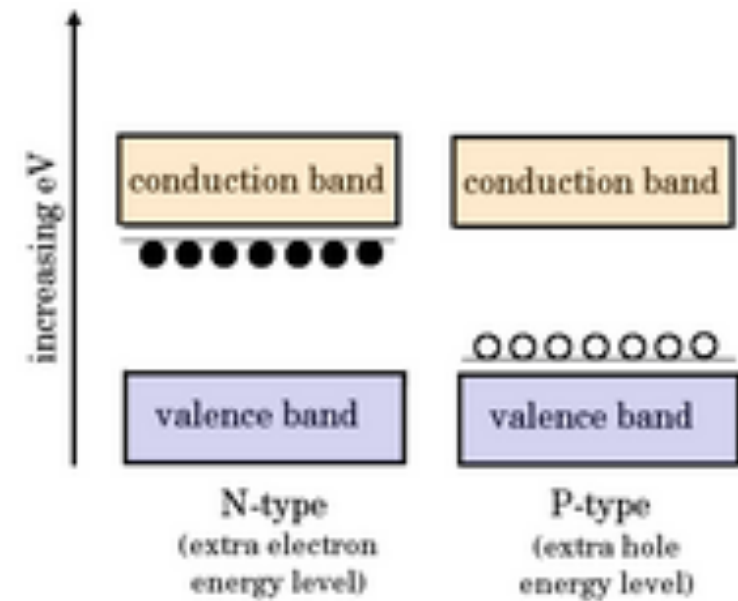
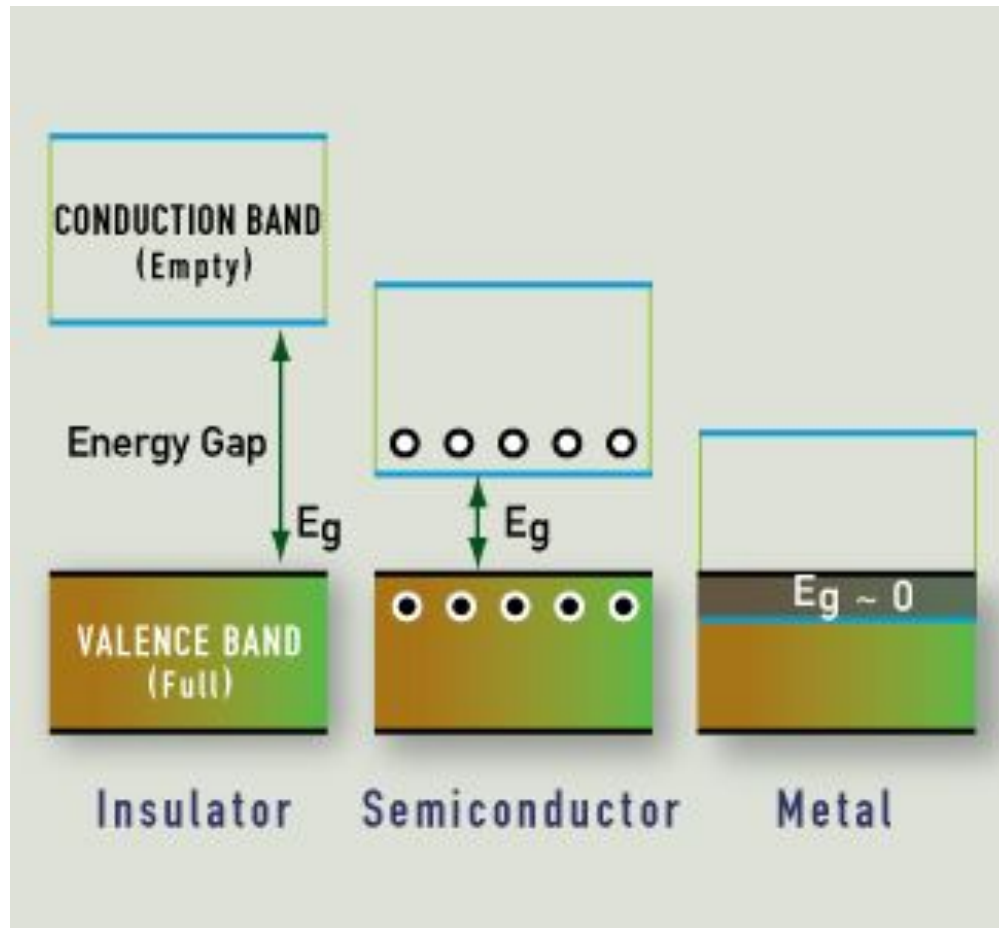
Packing Fraction

$$APF = \frac{N_{\text{atoms}} V_{\text{atom}}}{V_{\text{crystal}}}$$

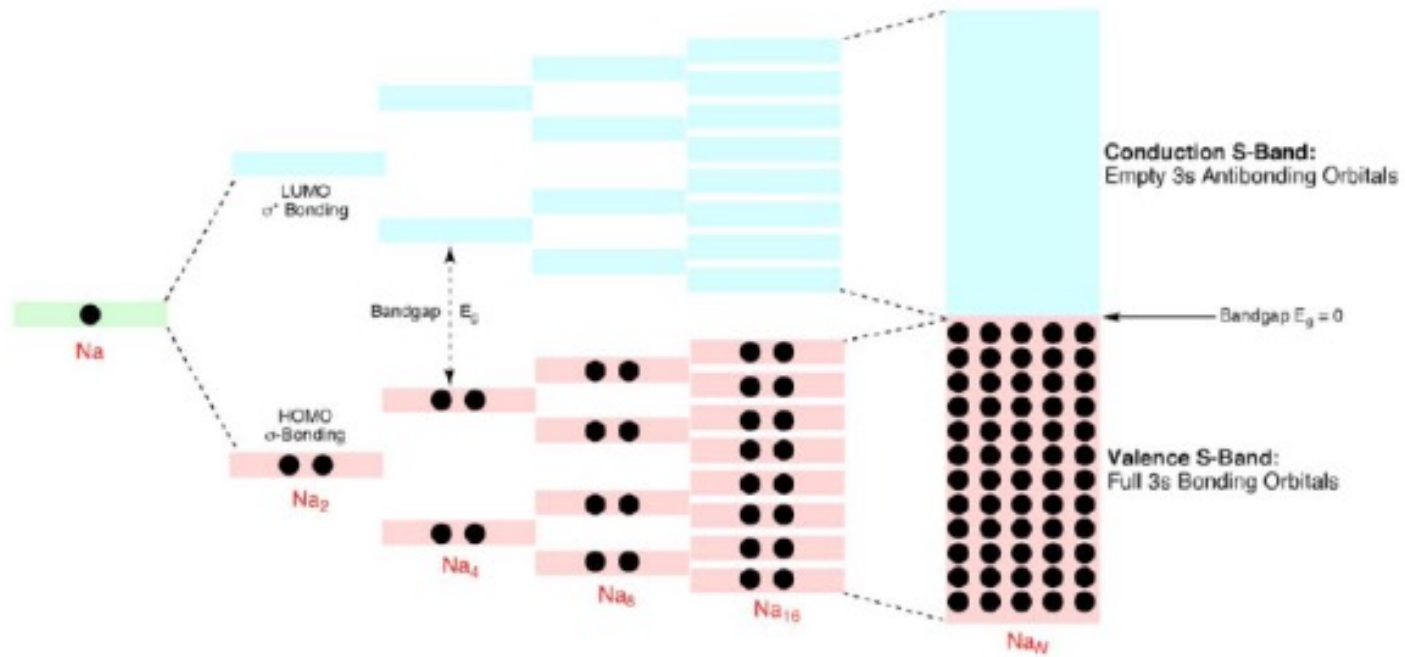
Surfaces

- Collective surface area of nanocube 1 nm
- Porous materials
 - Micropore (<2 nm)
 - Mesopore (2 nm ~ 50 nm)
 - Marcopore (> 50nm)
- Void volume
 - $V_{\text{pore}}/V_{\text{material}}$

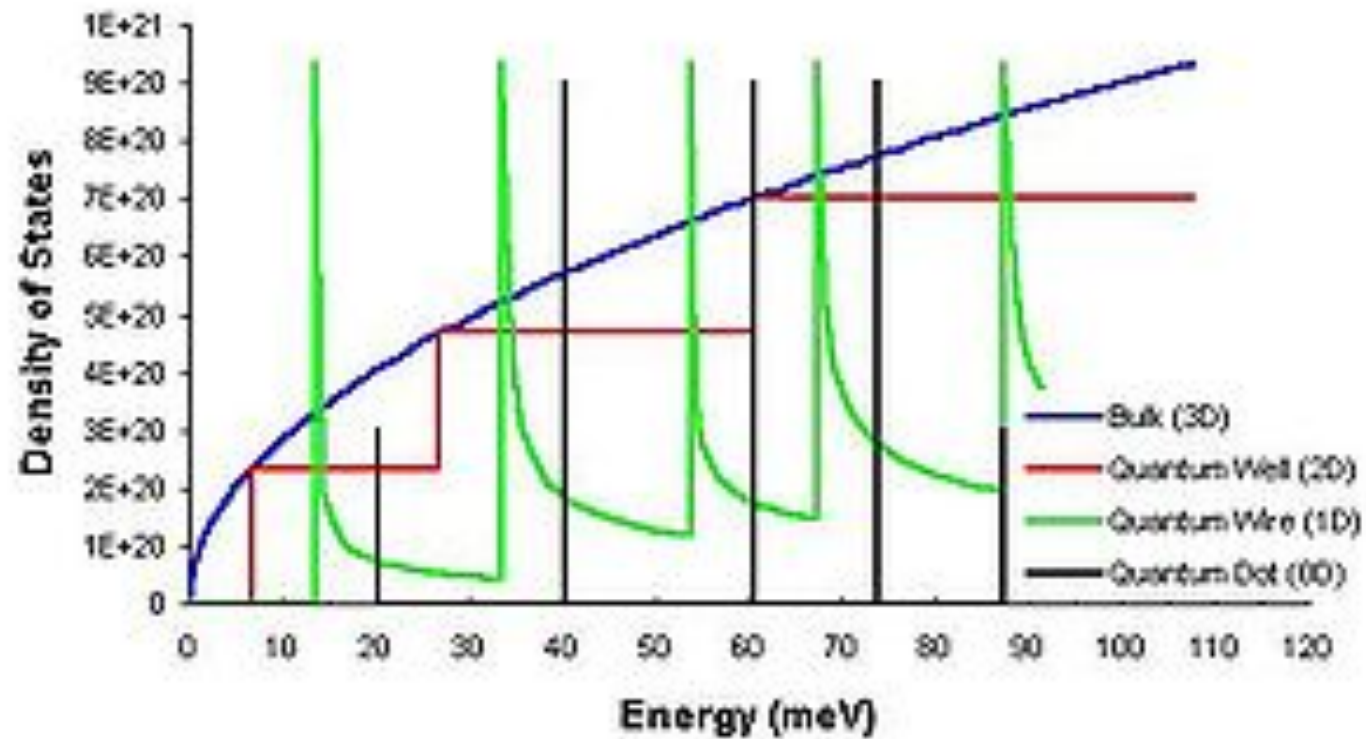
Bandgap



Bandgap



Density of State

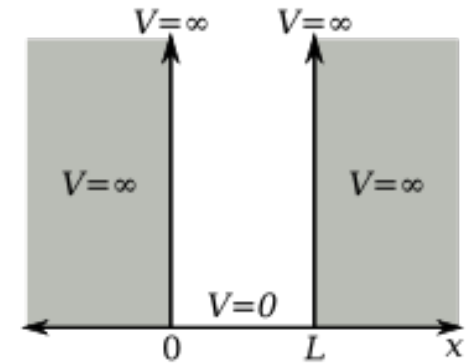


Particle in a Box

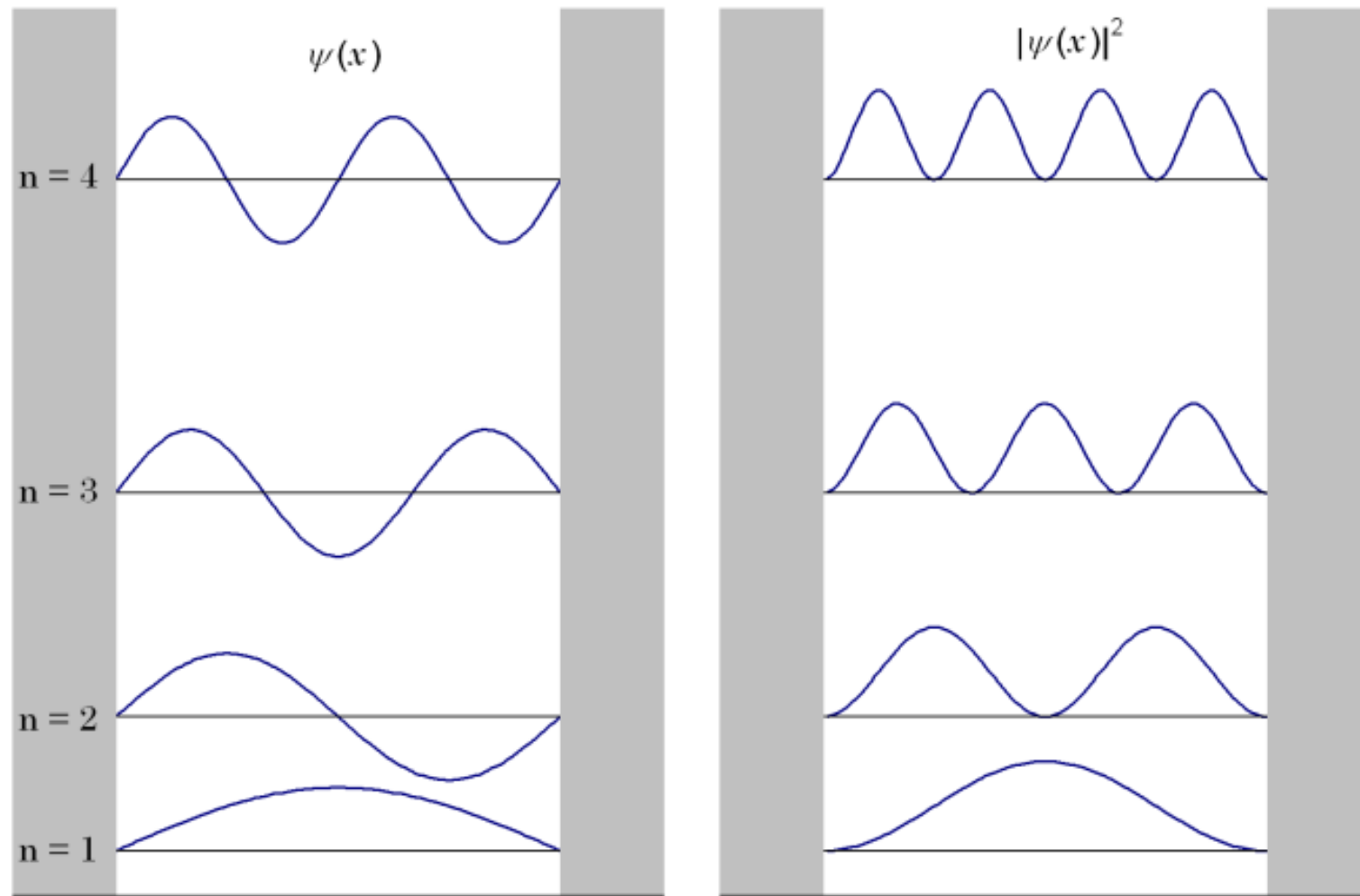
$$-\frac{\hbar^2}{2m} \frac{d^2\psi(x)}{dx^2} + V(x)\psi(x) = E\psi(x) \quad (1)$$

$$\psi_n = \sqrt{\frac{2}{L}} \sin\left(\frac{n\pi x}{L}\right)$$

$$E_n = \frac{\hbar^2 \pi^2}{2mL^2} n^2$$



Particle in a Box



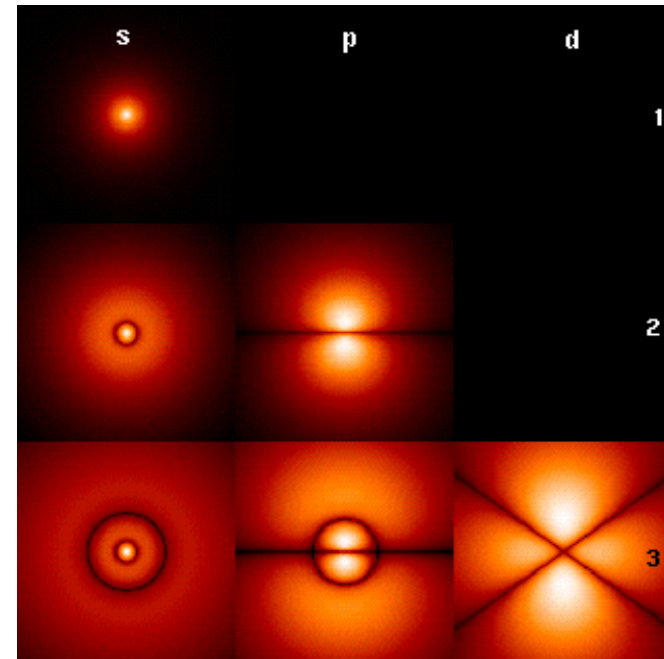
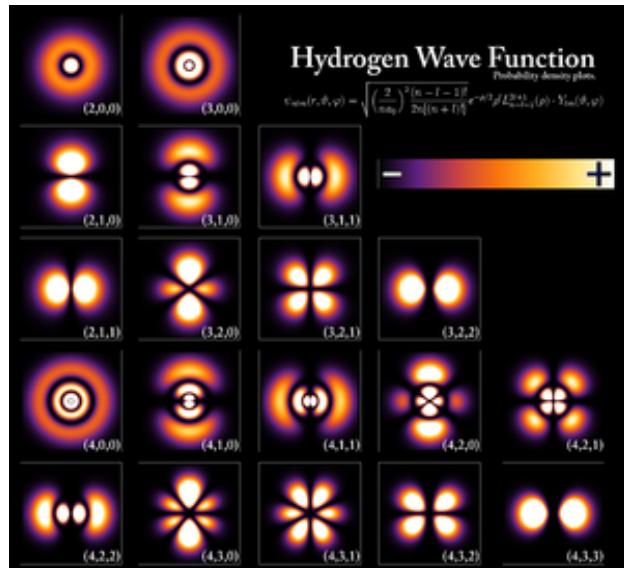
$$\psi_{n_x, n_y} = \sqrt{\frac{4}{L_x L_y}} \sin\left(\frac{n_x \pi x}{L_x}\right) \sin\left(\frac{n_y \pi y}{L_y}\right)$$

$$E_{n_x, n_y} = \frac{\hbar^2 \pi^2}{2m} \left[\left(\frac{n_x}{L_x}\right)^2 + \left(\frac{n_y}{L_y}\right)^2 \right]$$

$$\psi_{n_x, n_y, n_z} = \sqrt{\frac{8}{L_x L_y L_z}} \sin\left(\frac{n_x \pi x}{L_x}\right) \sin\left(\frac{n_y \pi y}{L_y}\right) \sin\left(\frac{n_z \pi z}{L_z}\right) \quad (22)$$

$$E_{n_x, n_y, n_z} = \frac{\hbar^2 \pi^2}{2m} \left[\left(\frac{n_x}{L_x}\right)^2 + \left(\frac{n_y}{L_y}\right)^2 + \left(\frac{n_z}{L_z}\right)^2 \right] \quad (23)$$

Wave Functions



$$i\hbar \frac{\partial}{\partial t} \Psi(\mathbf{r}, t) = \hat{H} \Psi = \left(-\frac{\hbar^2}{2m} \nabla^2 + V(\mathbf{r}) \right) \Psi(\mathbf{r}, t) = -\frac{\hbar^2}{2m} \nabla^2 \Psi(\mathbf{r}, t) + V(\mathbf{r}) \Psi(\mathbf{r}, t)$$

$$V(r) = -\frac{1}{4\pi\epsilon_0} \frac{Ze^2}{r}$$

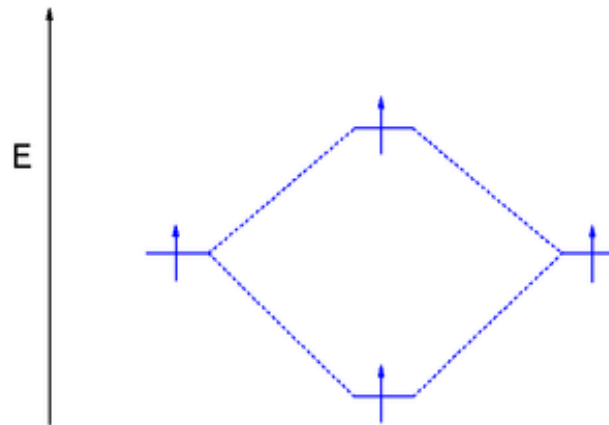
$$\psi_{n\ell m}(r, \vartheta, \varphi) = \sqrt{\left(\frac{2}{na_0}\right)^3 \frac{(n-\ell-1)!}{2n(n+\ell)!}} e^{-\rho/2} \rho^\ell L_{n-\ell-1}^{2\ell+1}(\rho) \cdot Y_\ell^m(\vartheta, \varphi)$$

Linear combination of atomic orbitals molecular orbital method

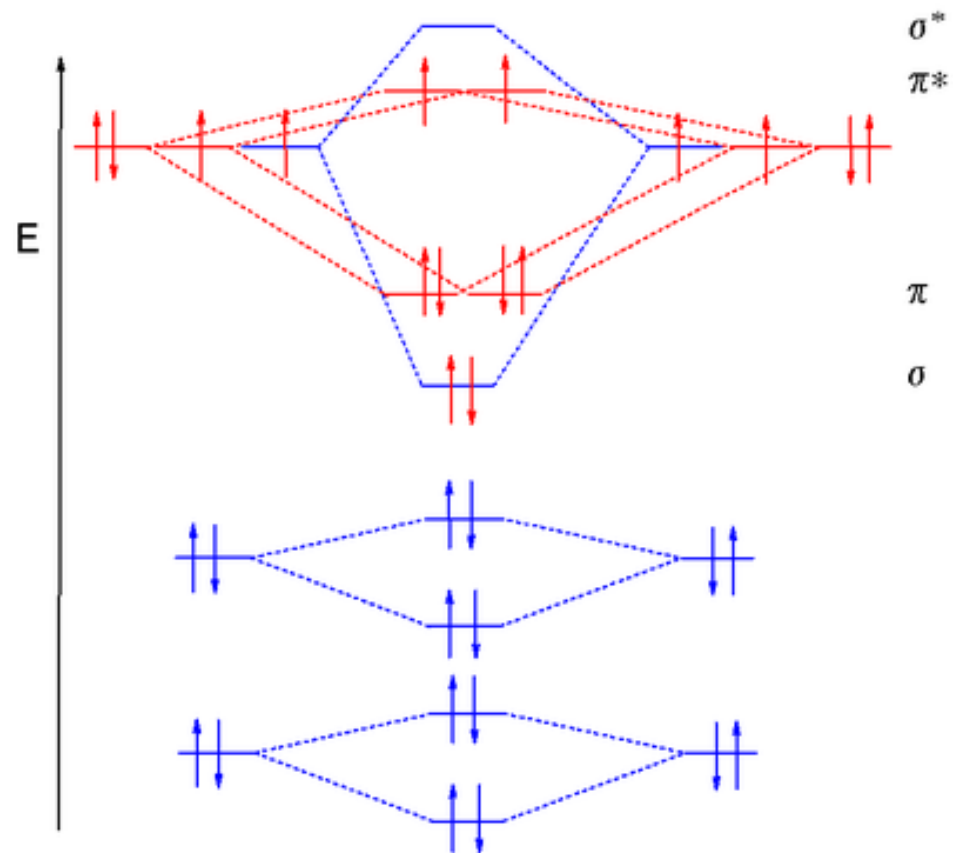
$$\phi_i = c_{1i}\chi_1 + c_{2i}\chi_2 + c_{3i}\chi_3 + \cdots + c_{ni}\chi_n$$

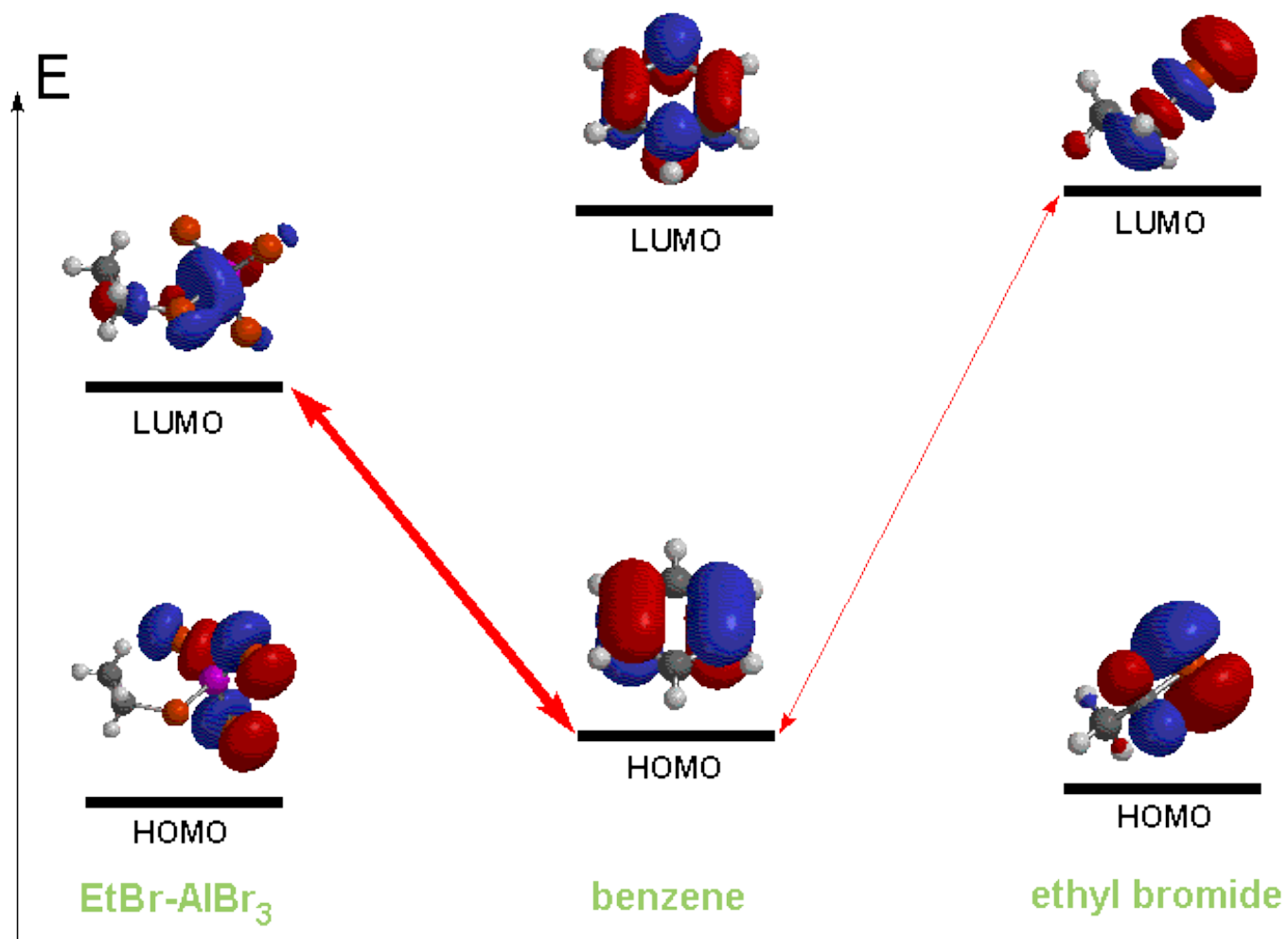
$$\psi_i = \sum_{\mu} c_{\mu i} \phi_{\mu}$$

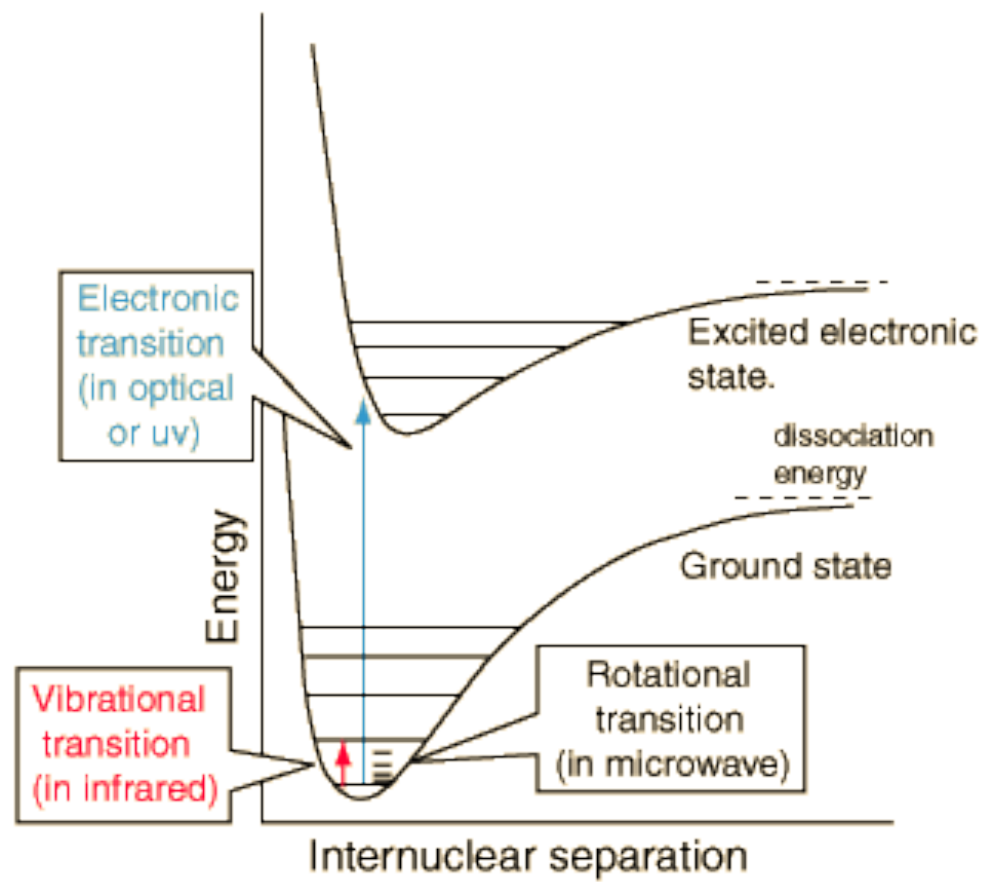
MO \nearrow \nwarrow coefficient of AO_{μ} in MO_i
 \nwarrow AO



Oxygen







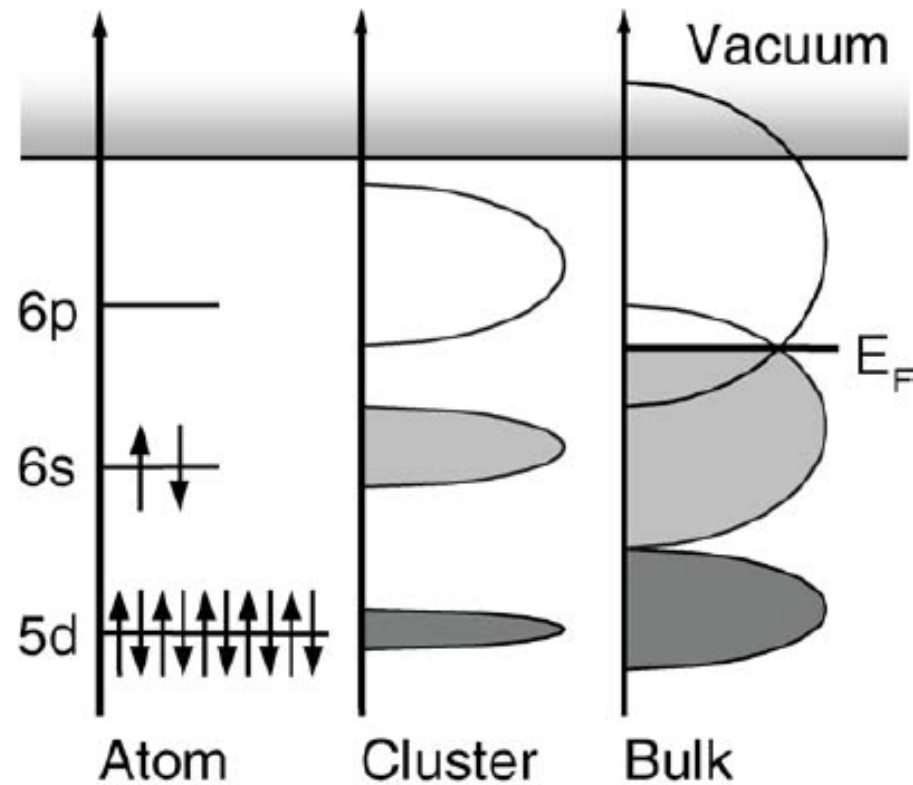


Figure 5 Energy diagram describing a generic Bloch-Wilson MIT in clusters (with specific reference to the energy levels of mercury). For sufficiently large clusters, the *s-p* band gap closes with increasing cluster size (shaded areas represent energy range with occupied electron levels). Overlap leads to a “continuous” DOS at E_F and to an Insulator to Metal transition.

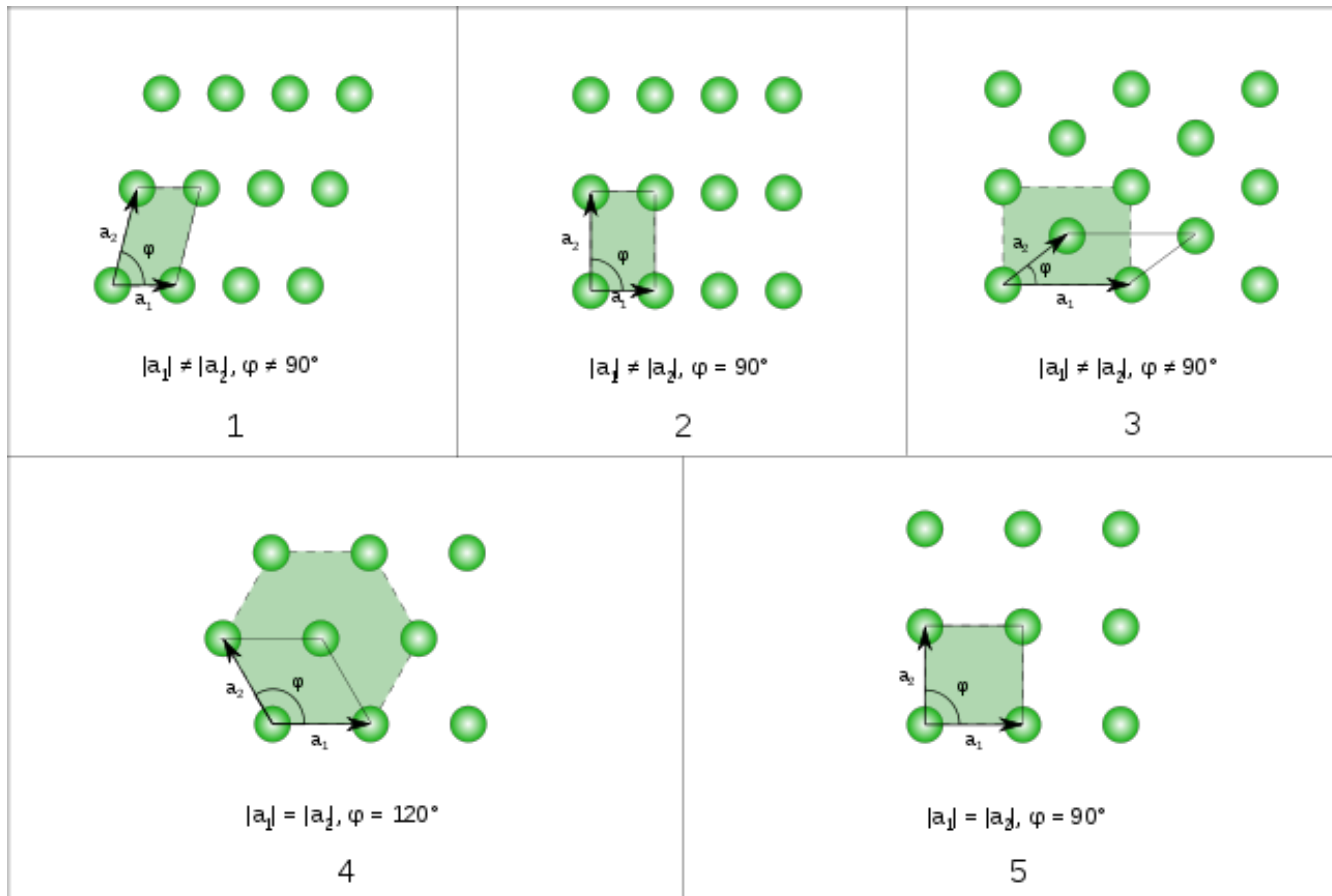
Bloch wave

$$\psi_{n\mathbf{k}}(\mathbf{r}) = e^{i\mathbf{k}\cdot\mathbf{r}} u_{n\mathbf{k}}(\mathbf{r})$$

A **Bloch wave** or **Bloch state**, named after [Felix Bloch](#), is the [wavefunction](#) of a particle (usually, an [electron](#)) placed in a [periodic potential](#).

$$\epsilon_n(\mathbf{k}) = \epsilon_n(\mathbf{k} + \mathbf{K}),$$

The five fundamental two-dimensional Bravais lattices



Unit Cell

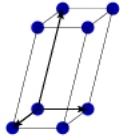
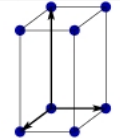
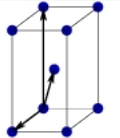
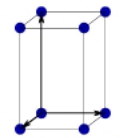
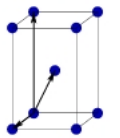
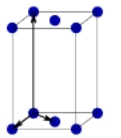
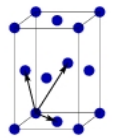
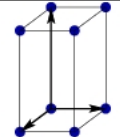
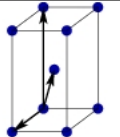
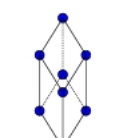
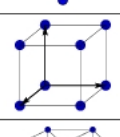
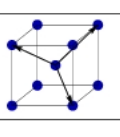
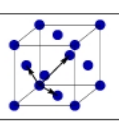
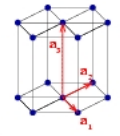
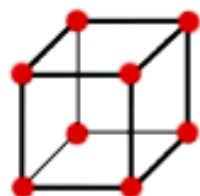
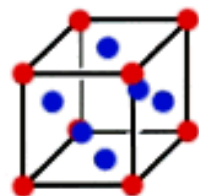
Bravais lattice	Parameters	Simple (P)	Volume centered (I)	Base centered (C)	Face centered (F)
Triclinic	$a_1 \neq a_2 \neq a_3$ $\alpha_{12} \neq \alpha_{23} \neq \alpha_{31}$				
Monoclinic	$a_1 \neq a_2 \neq a_3$ $\alpha_{23} = \alpha_{31} = 90^\circ$ $\alpha_{12} \neq 90^\circ$				
Orthorhombic	$a_1 \neq a_2 \neq a_3$ $\alpha_{12} = \alpha_{23} = \alpha_{31} = 90^\circ$				
Tetragonal	$a_1 = a_2 \neq a_3$ $\alpha_{12} = \alpha_{23} = \alpha_{31} = 90^\circ$				
Trigonal	$a_1 = a_2 = a_3$ $\alpha_{12} = \alpha_{23} = \alpha_{31} < 120^\circ$				
Cubic	$a_1 = a_2 = a_3$ $\alpha_{12} = \alpha_{23} = \alpha_{31} = 90^\circ$				
Hexagonal	$a_1 = a_2 \neq a_3$ $\alpha_{12} = 120^\circ$ $\alpha_{23} = \alpha_{31} = 90^\circ$				

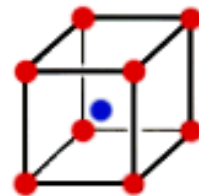
Table 1.1: Bravais lattices in three-dimensions.



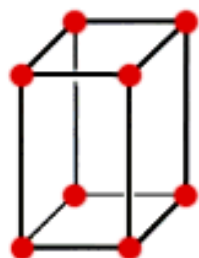
**Simple
cubic**



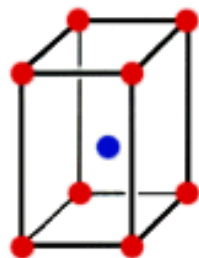
**Face-centered
cubic**



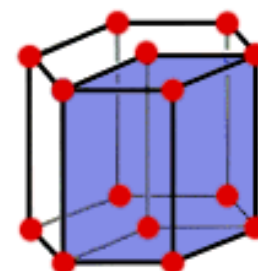
**Body-centered
cubic**



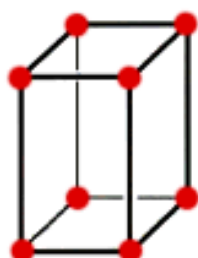
**Simple
tetragonal**



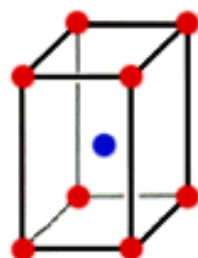
**Body-centered
tetragonal**



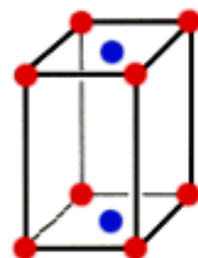
Hexagonal



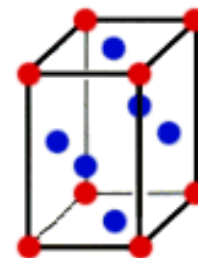
**Simple
orthorhombic**



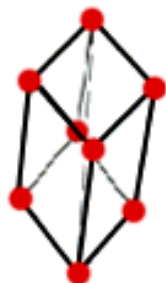
**Body-centered
orthorhombic**



**Base-centered
orthorhombic**



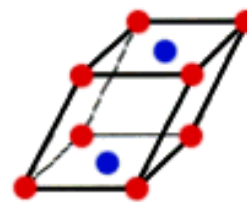
**Face-centered
orthorhombic**



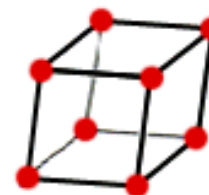
Rhombohedral



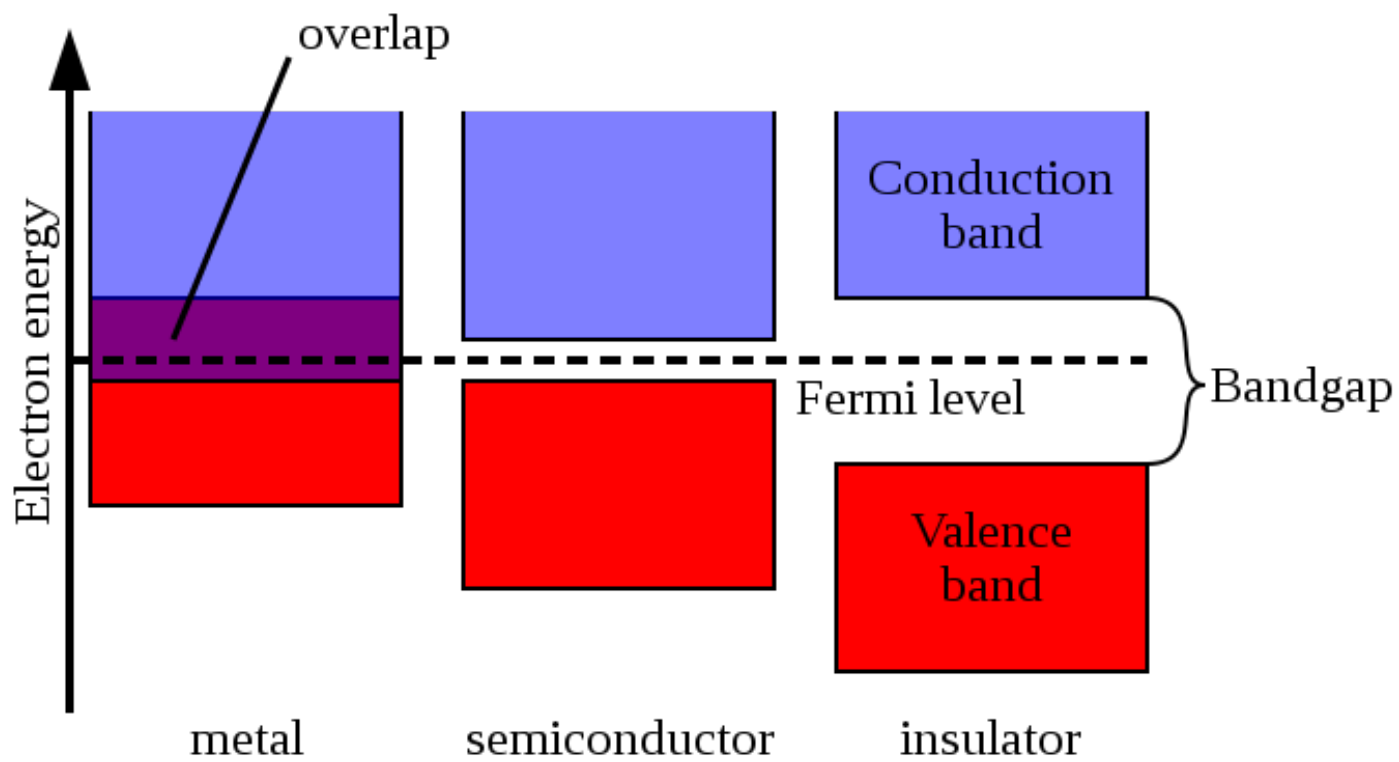
**Simple
Monoclinic**



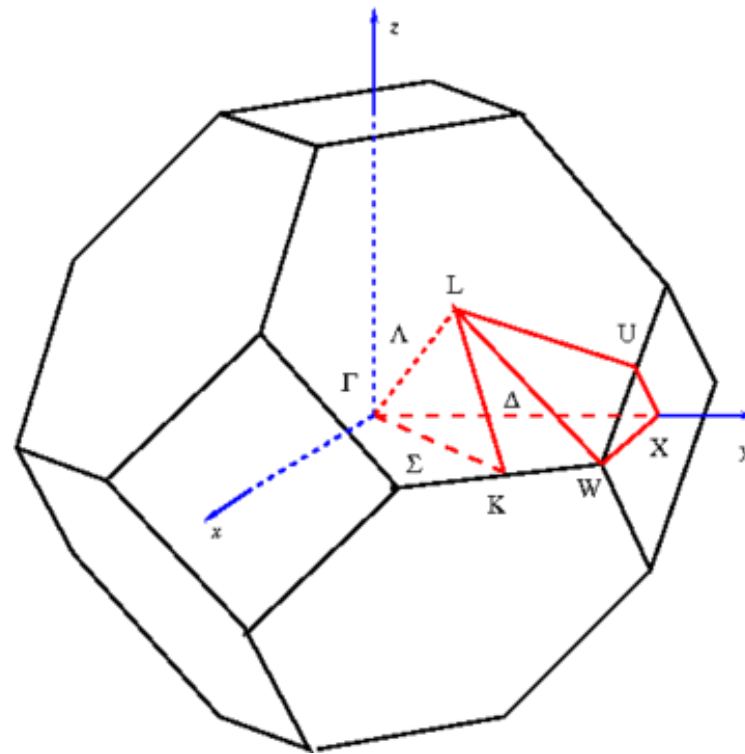
**Base-centered
monoclinic**



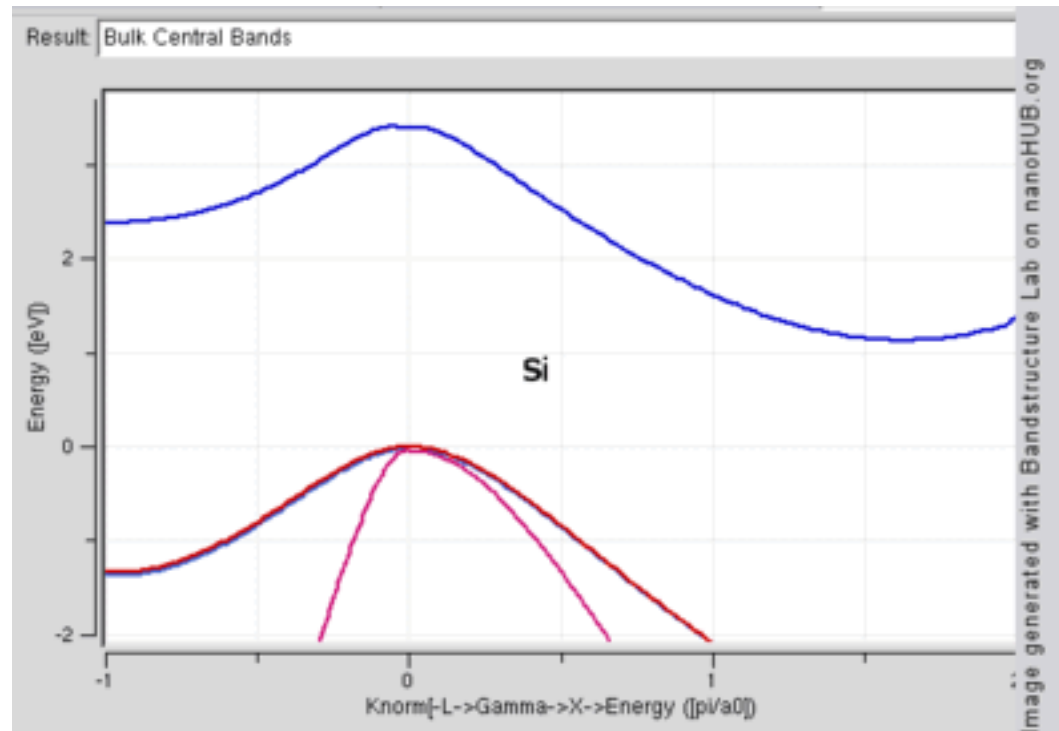
Triclinic



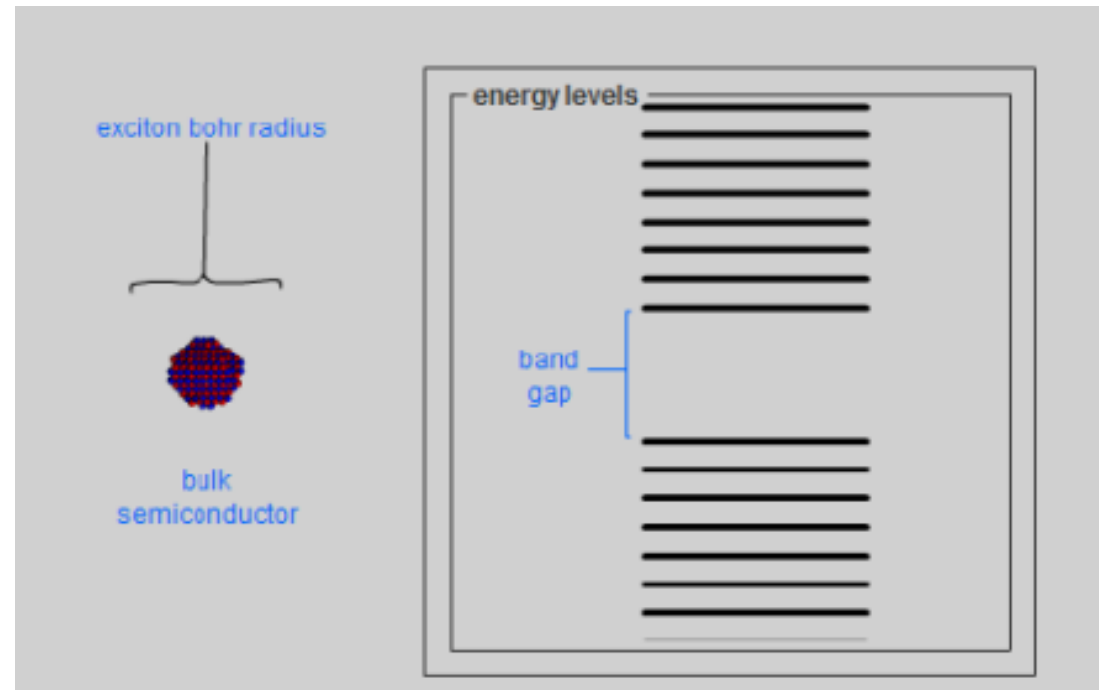
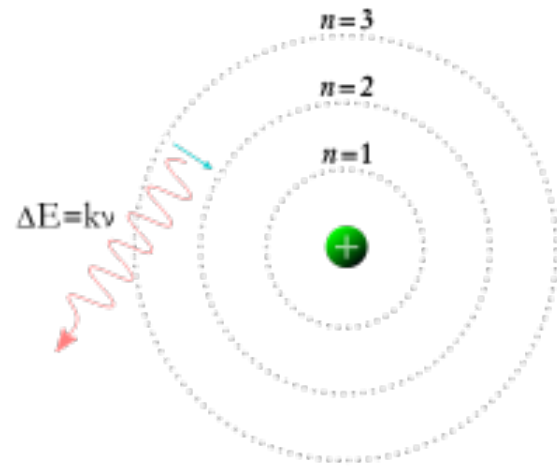
First Brillouin zone of FCC lattice showing symmetry labels



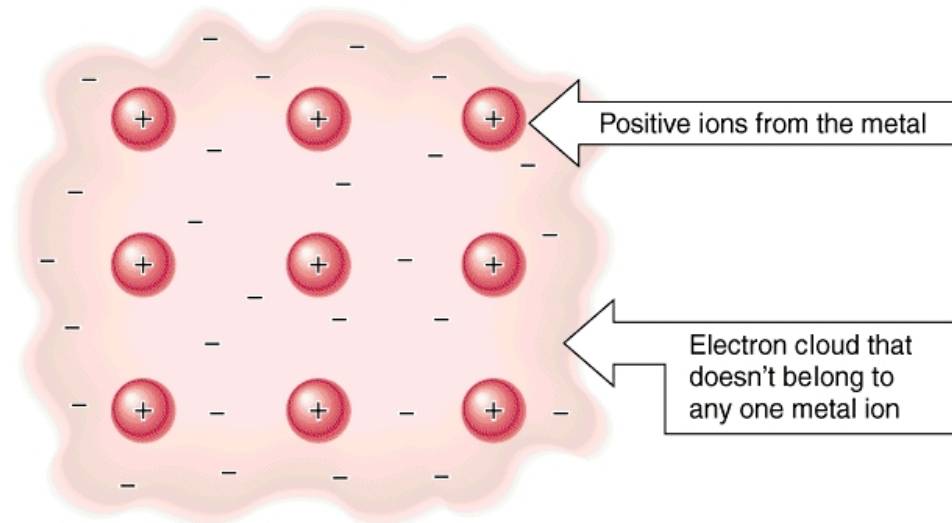
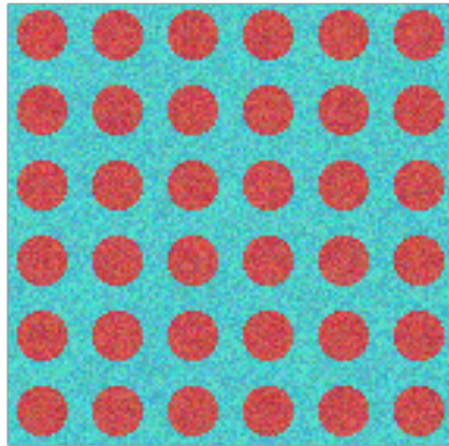
Band Structures



Bohr Exciton Radius



Electron Sea

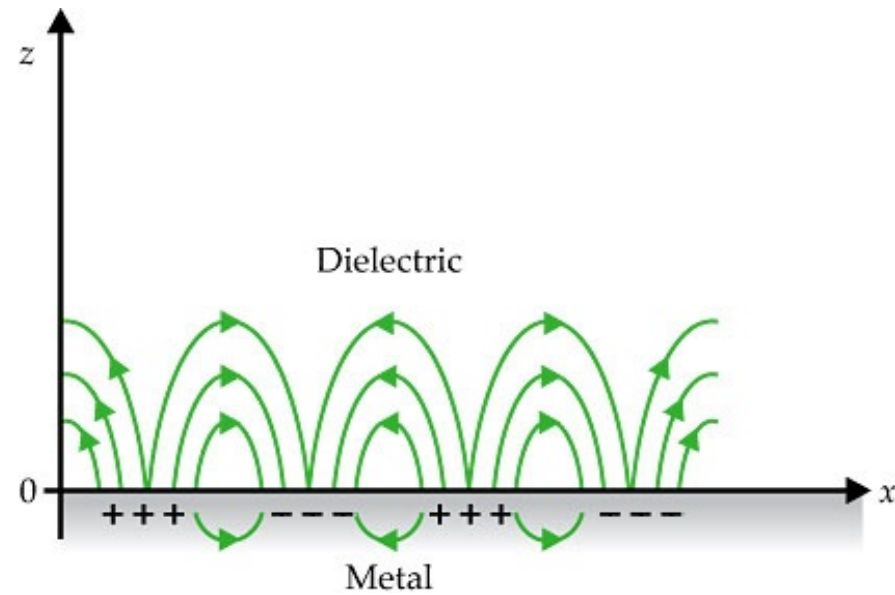


Copyright 1998 by John Wiley and Sons, Inc. All rights reserved.

$$m \frac{d^2 \delta x}{dt^2} = e E_x = -m \omega_p^2 \delta x,$$

$$\omega_p^2 = \frac{n e^2}{\epsilon_0 m},$$

Surface Plasmon



$$\epsilon_m = 1 - \frac{\omega_p^2}{\omega^2}$$

TiO₂

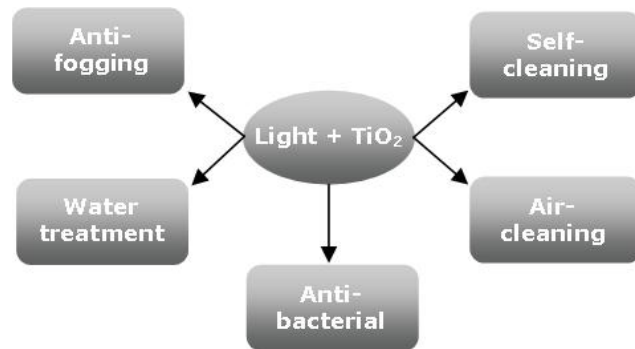
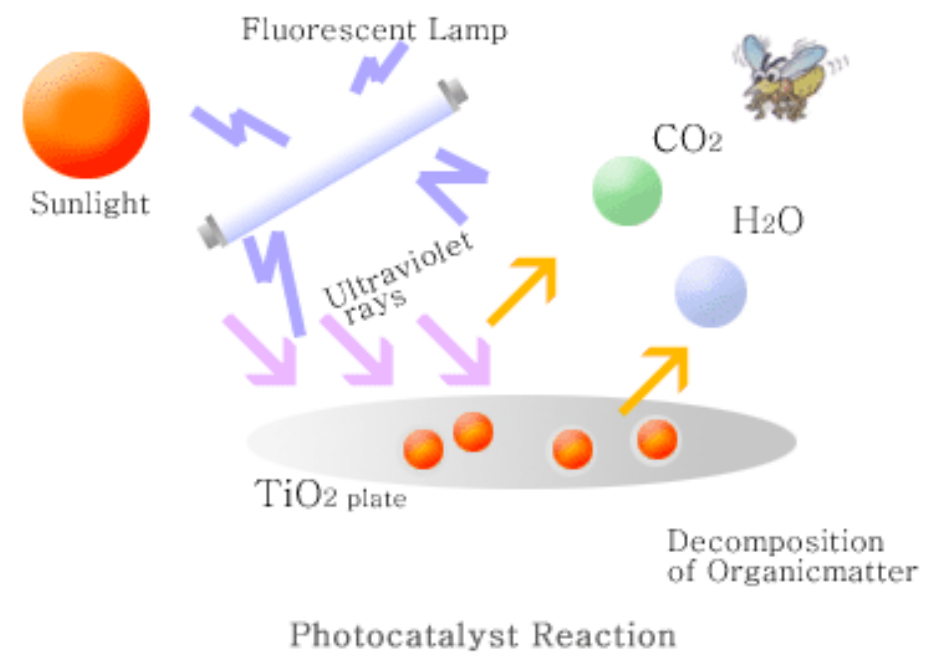
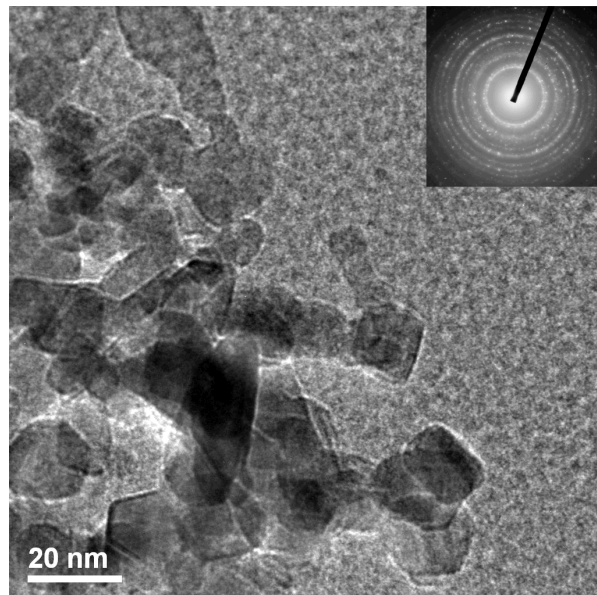
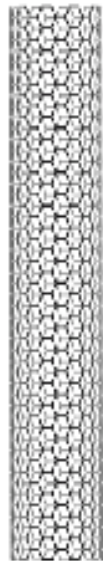


Figure 1. Major areas of activity in titanium dioxide photocatalysis



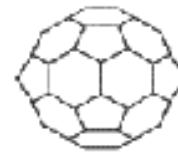
Carbon



SWNT



Poly-C₆₀

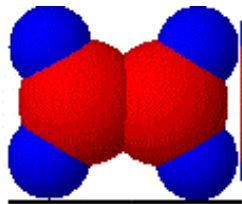


C₆₀

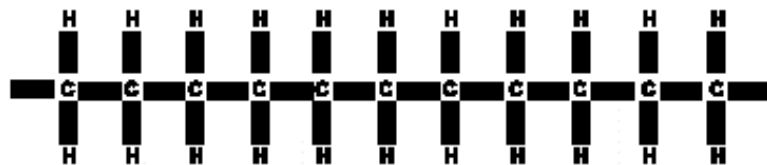
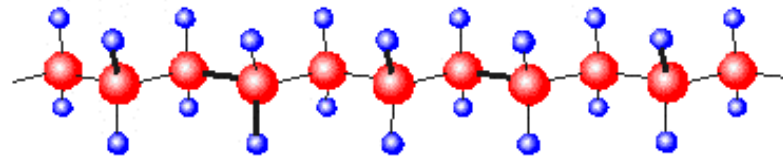
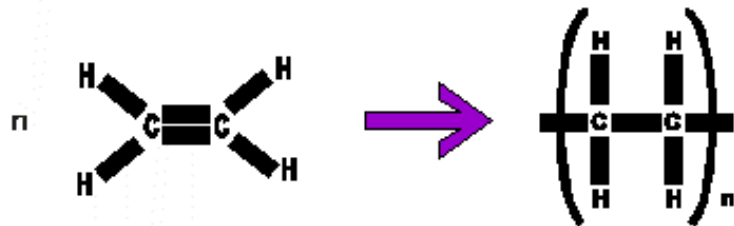
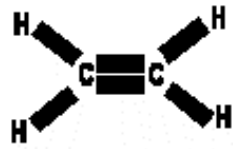


Nanodiamond
~ 2-10 nm

Polymer

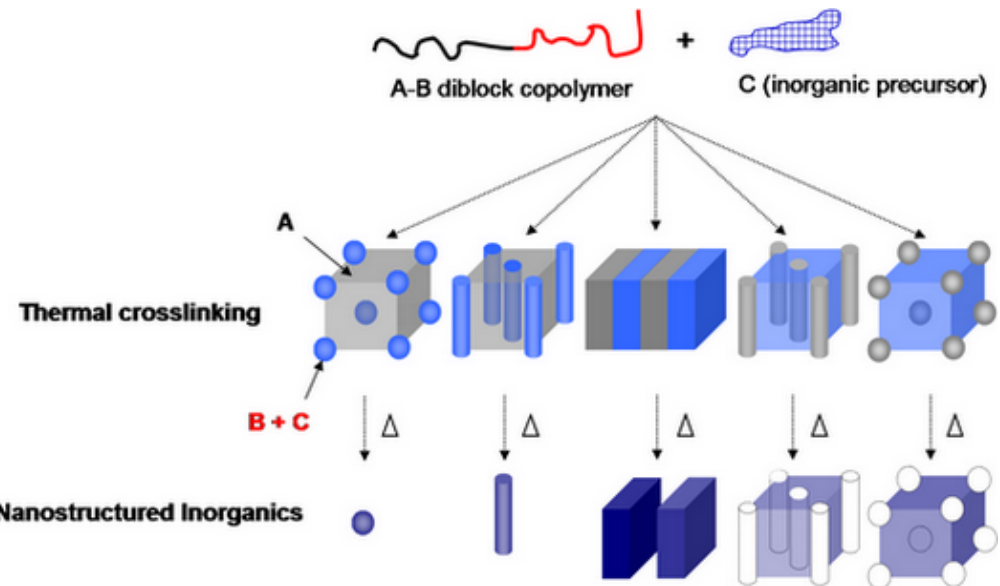


a monomer ethene

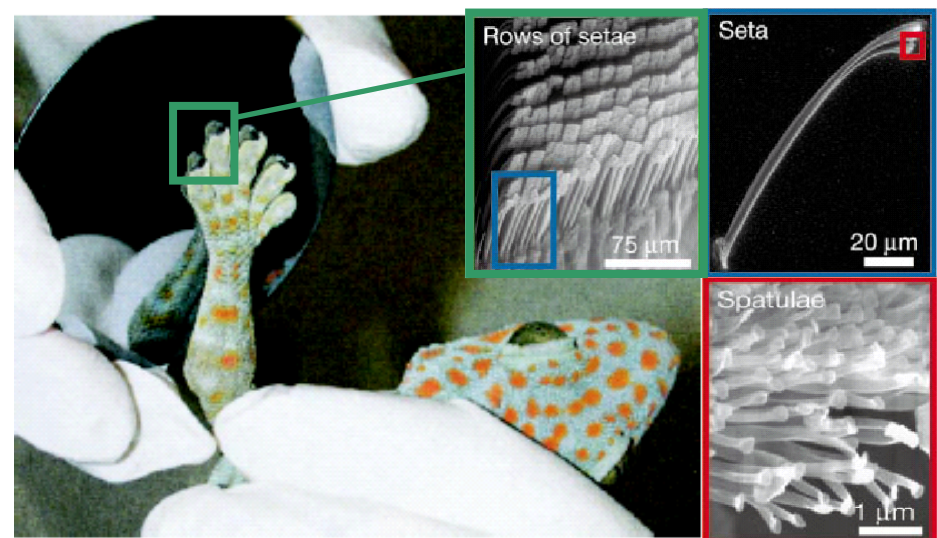
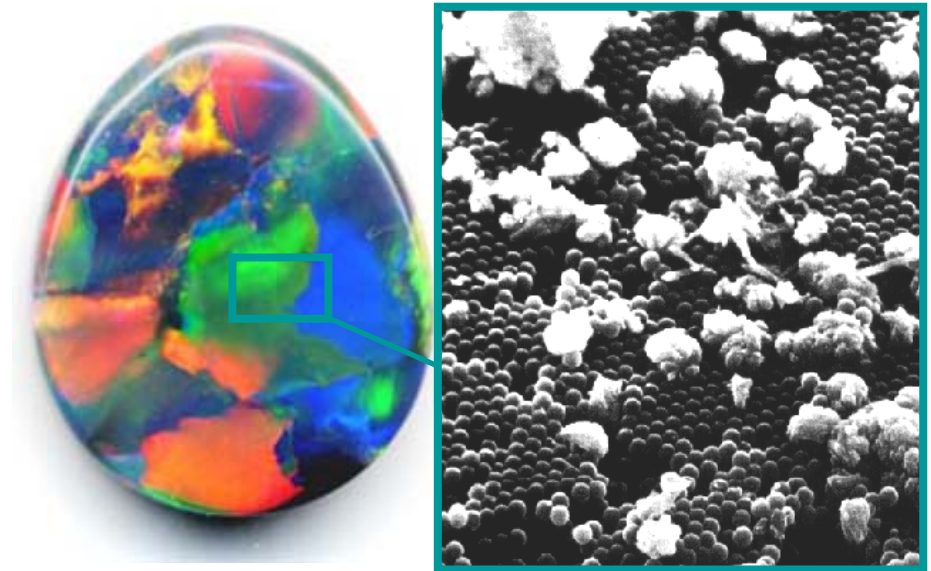
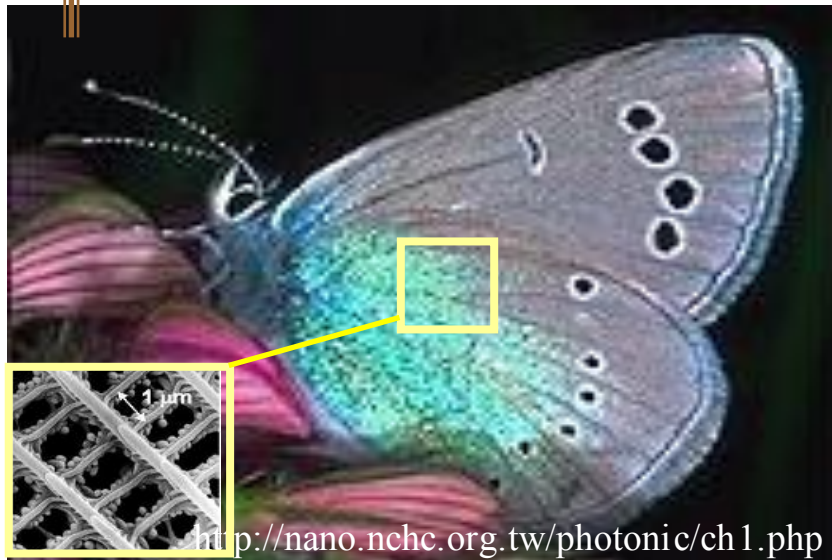


a polymer

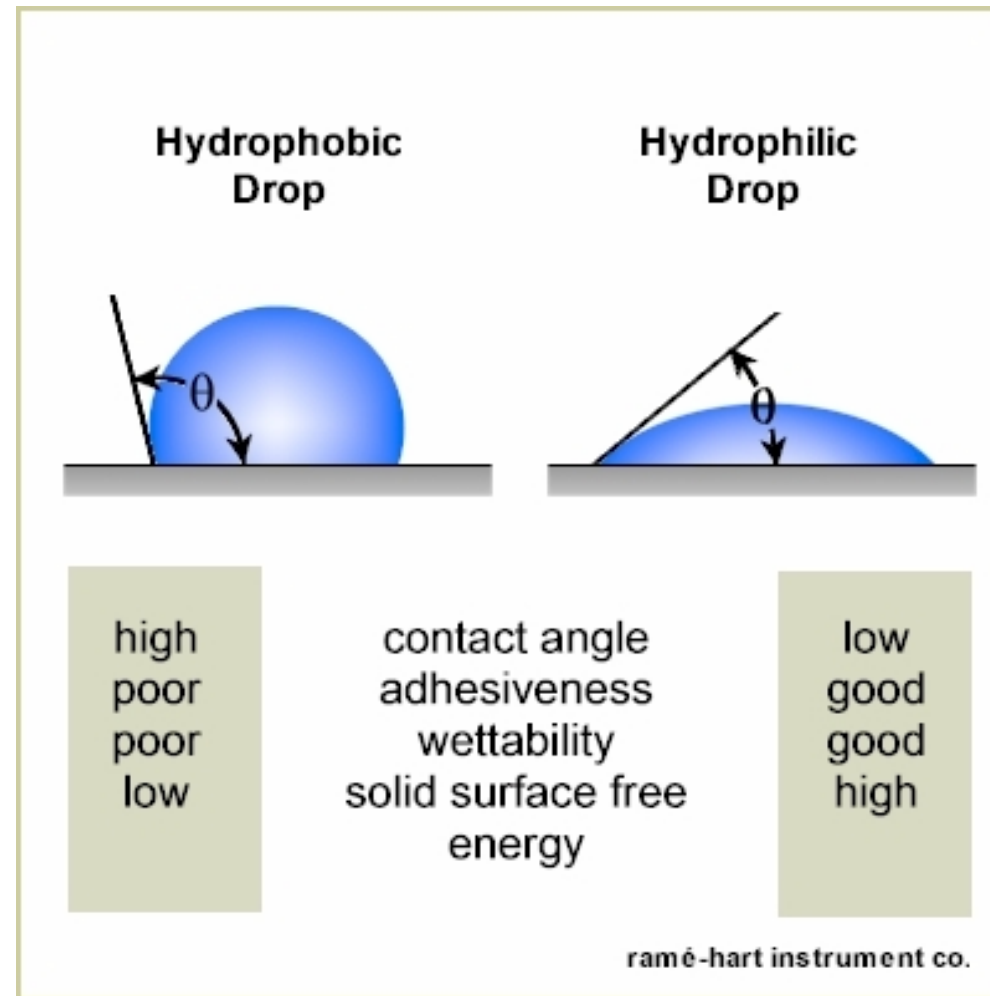
poly(ethene)



Nature Materials

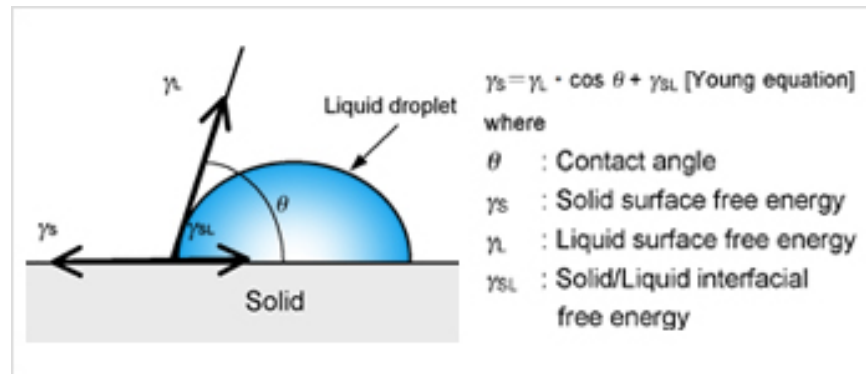


Contact Angle



Young's Equation

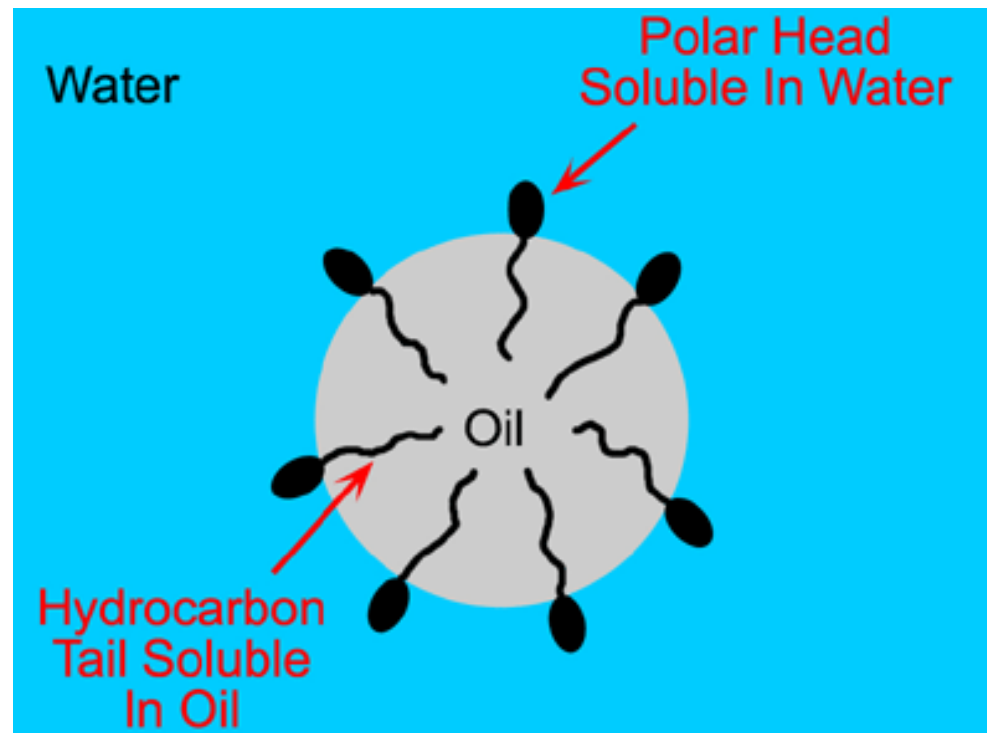
$$\gamma_{SL} + \gamma_{LV} \cos \theta_c = \gamma_{SV}$$



Surface Energy Minimization

- Surfactants
- DLVO
- Polymeric
- Nucleation
- Ostwald Ripening
- Sintering
- Restructure

Surfactant



DLVO Theory

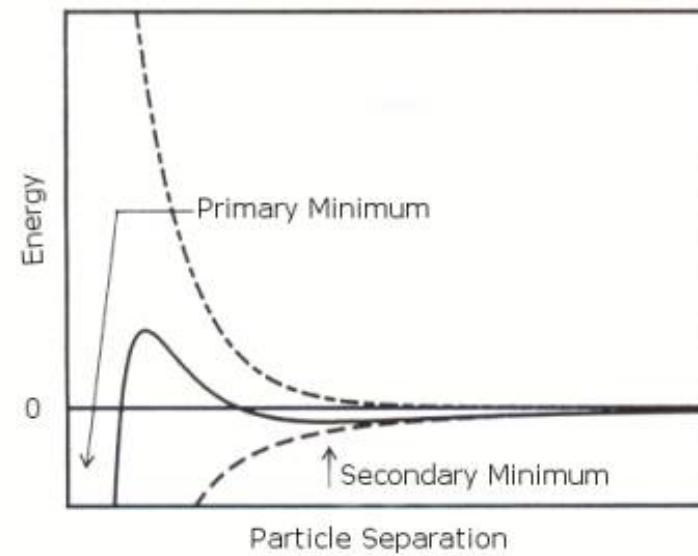
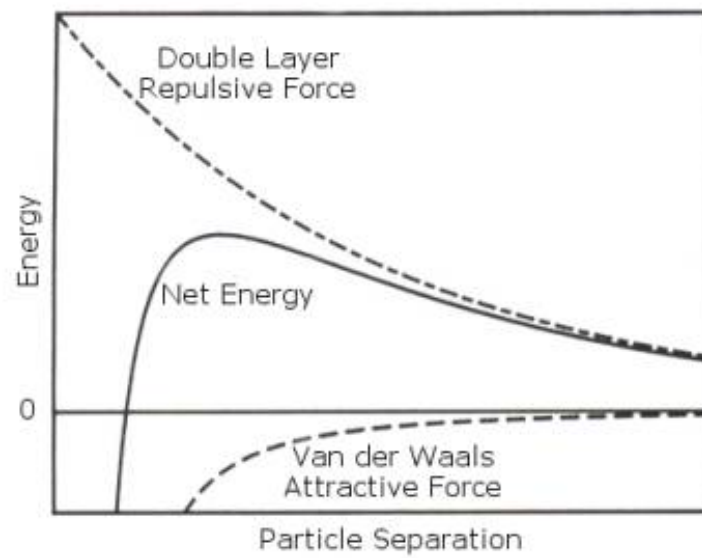
$$V_T = V_A + V_R + V_S$$

$$V_A = -A/(12 \pi D^2)$$

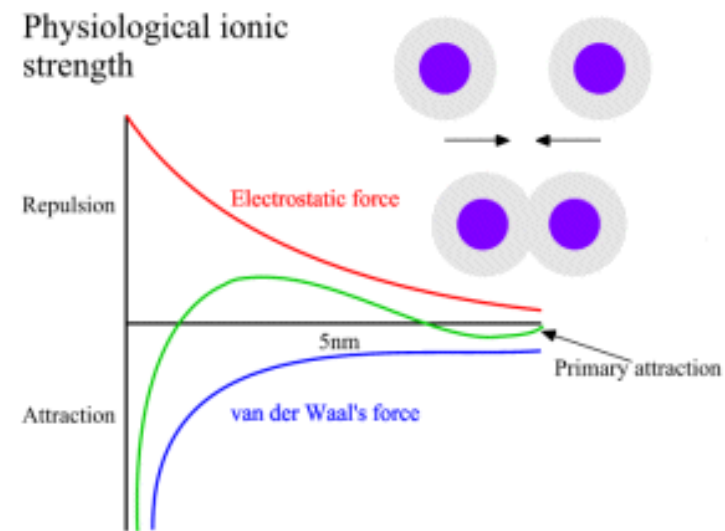
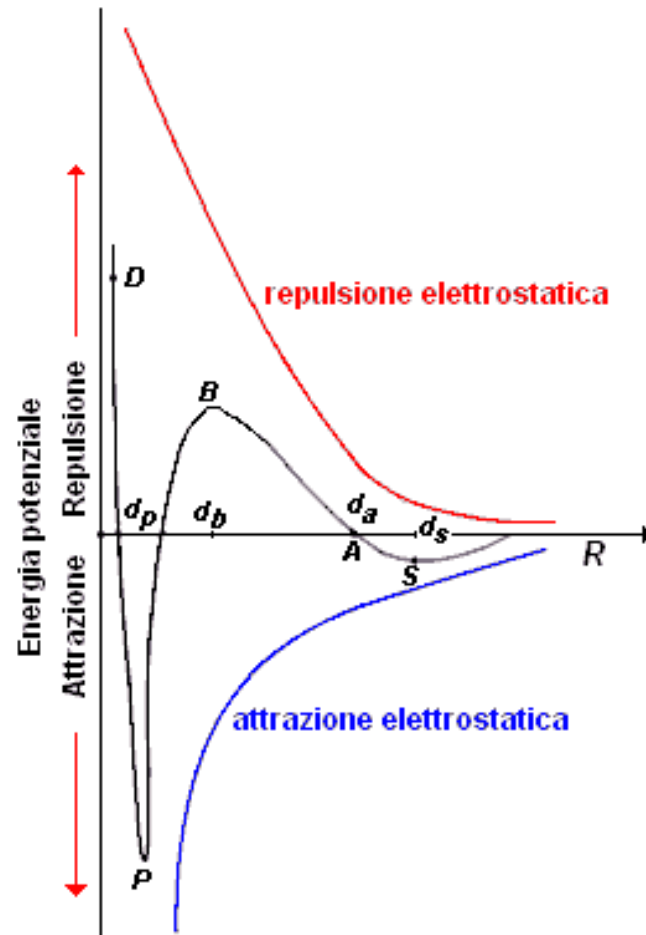
A is the Hamaker constant and D is the particle separation

$$V_R = 2 \pi \varepsilon a \xi^2 \exp(-\kappa D)$$

a is the particle radius, π is the solvent permeability,
 κ is a function of the ionic composition and ξ is the zeta potential



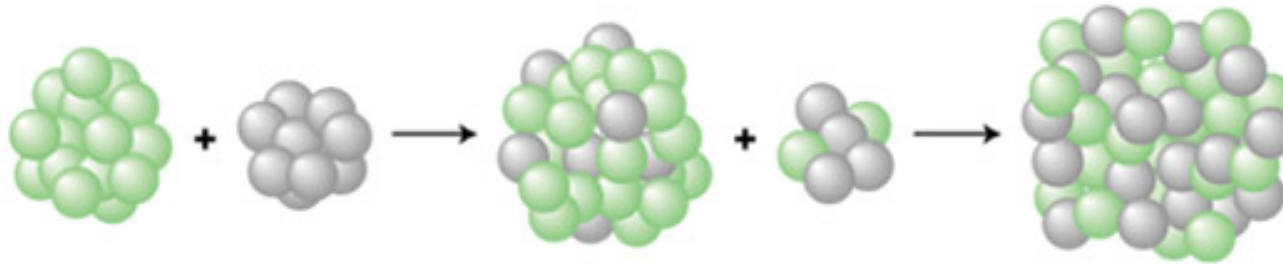
DLVO Theory



a Coalescence



b Ostwald ripening



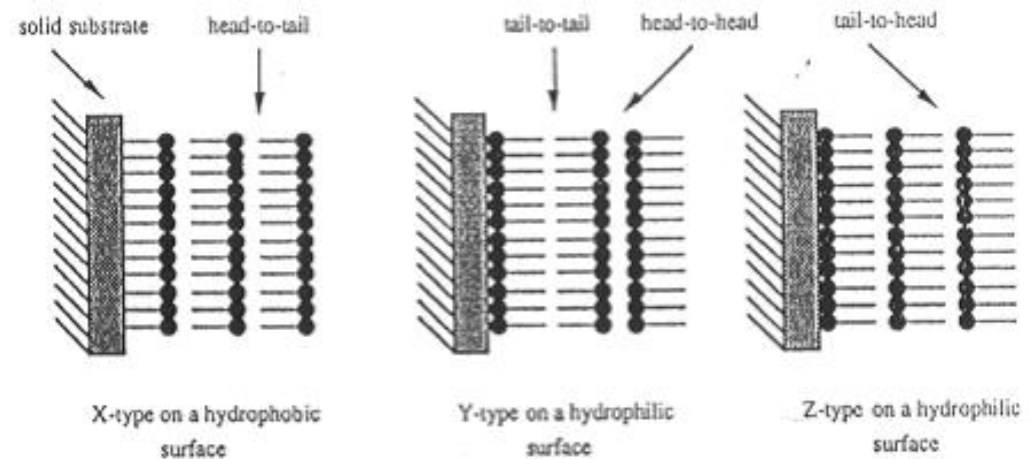
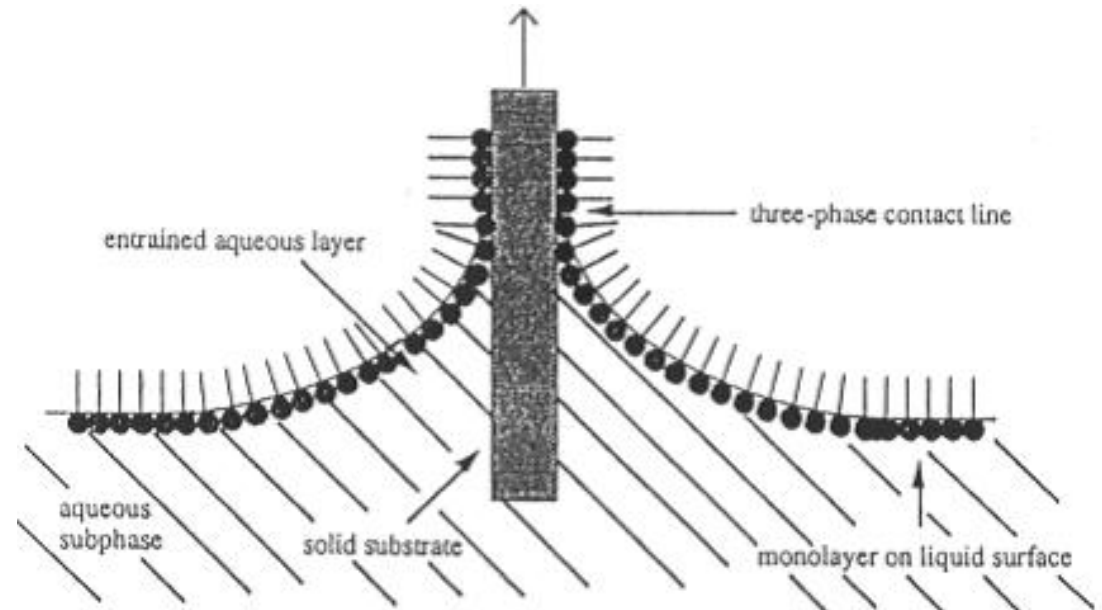
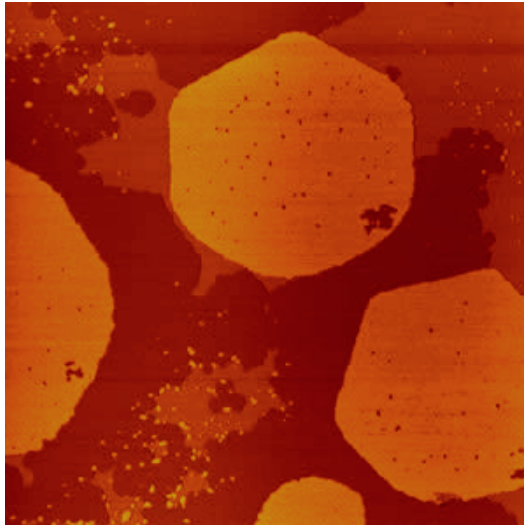
Two main mechanisms are shown here: **a**, coalescence sintering, and **b**, Ostwald ripening sintering. Coalescence sintering occurs when two clusters touch or collide and merge to form one bigger cluster. In contrast, Ostwald ripening sintering occurs by evaporation of atoms from one cluster, which then transfer to another. This is a dynamic process — both clusters exchange atoms, but the rate of loss from the smaller cluster is higher, because of the lower average coordination of atoms at the surface and their relative ease of removal. Thus big clusters get bigger at the expense of smaller clusters, which shrink and eventually disappear. The latter process is the usual form of sintering for metal clusters on a supported surface that are well spaced apart, although coalescence can occur for a high density of clusters. In general, the presence of the surface results in SMORS (surface-mediated Ostwald ripening sintering) in which material is transferred from one cluster to another by diffusion across the surface, and not through the gas phase.

Synthesis of Nanoparticles and Surface Modifications

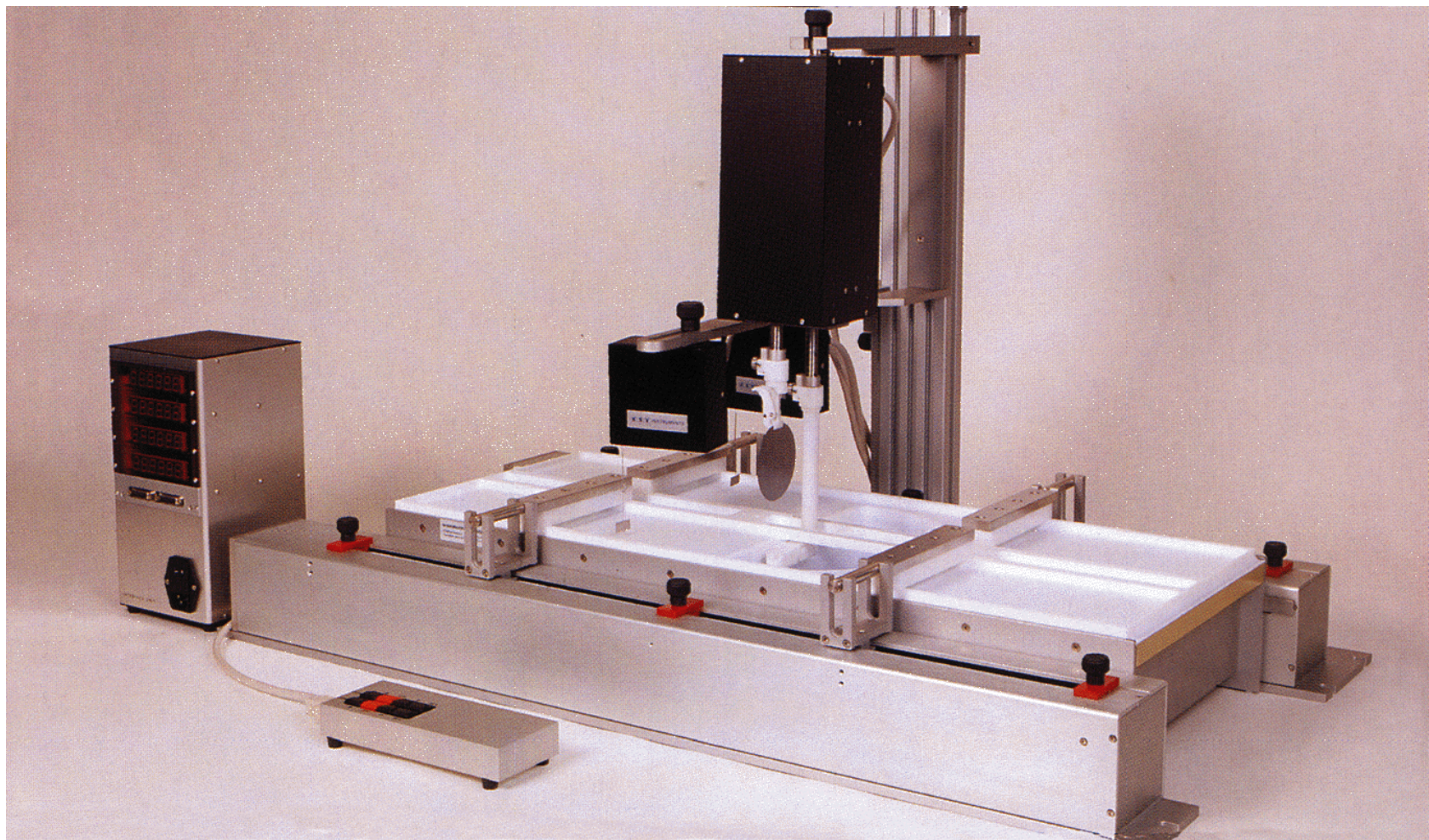
Self-Assembly

- Static assembly
- Dynamic assembly
 - $RT = 8.314 \text{ J/mol} \times 300 = 2.4 \text{ kJ/mol}$
- Driving forces
 - Chemisorption
 - Surface effect
 - Hydrophobic-hydrophilic
 - Intermolecular forces
 - Capillary force

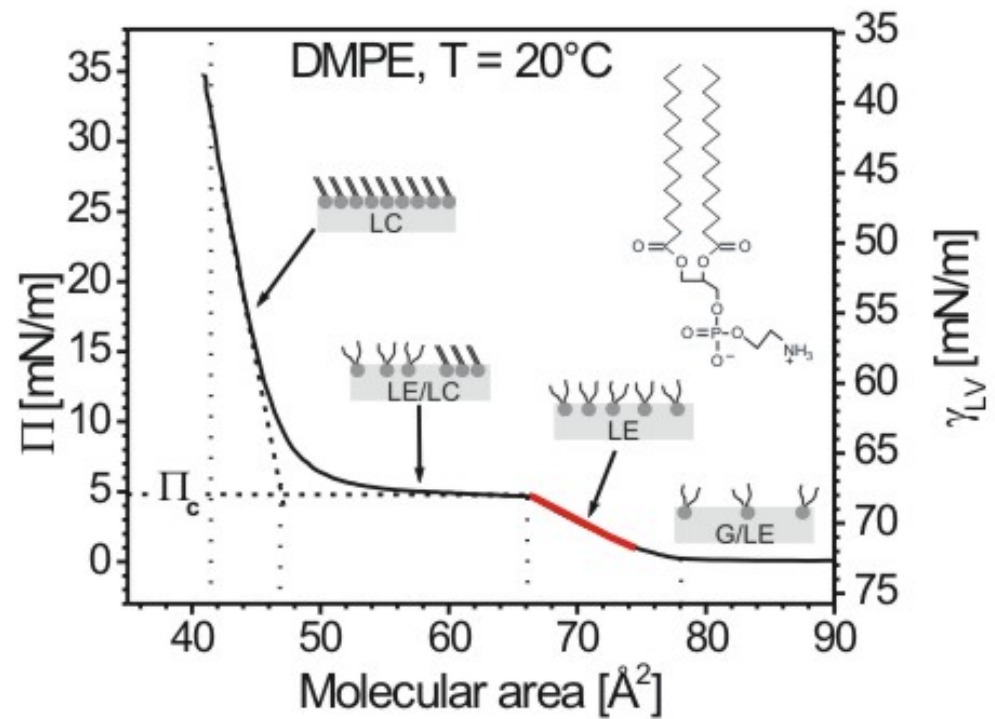
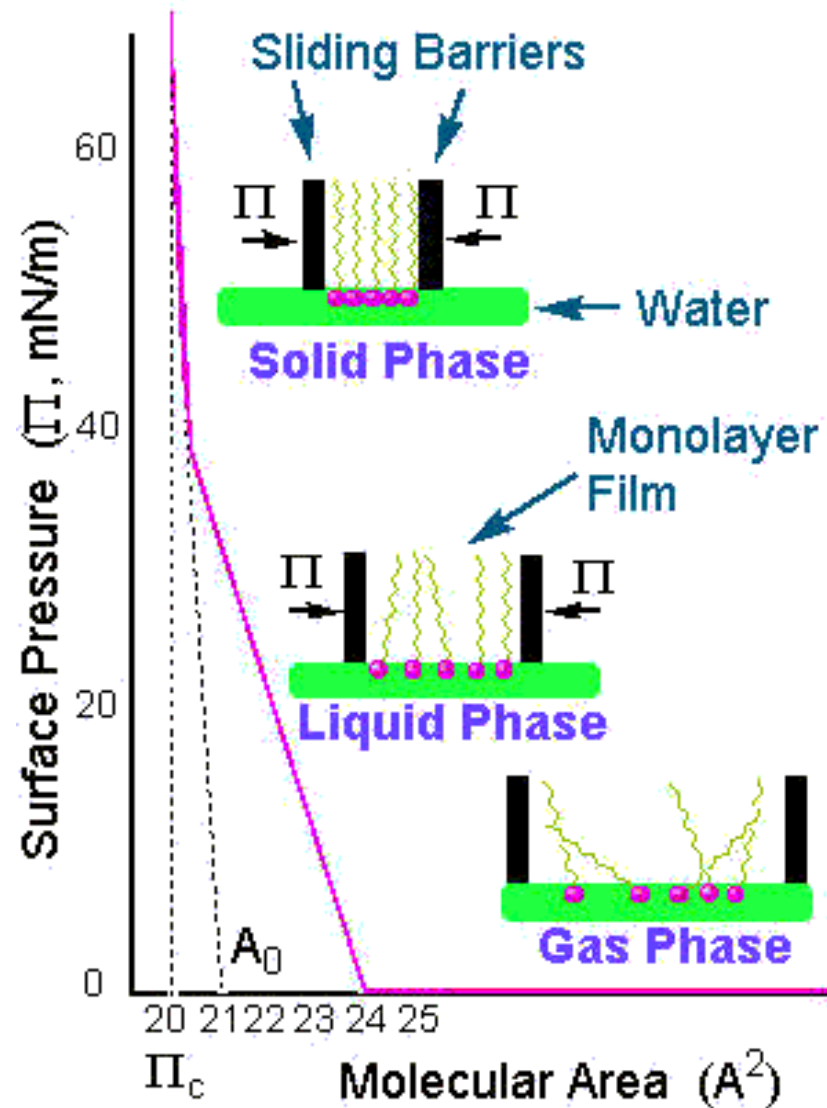
Langmuir-Blodgett Films



Langmuir-Blodgett Films

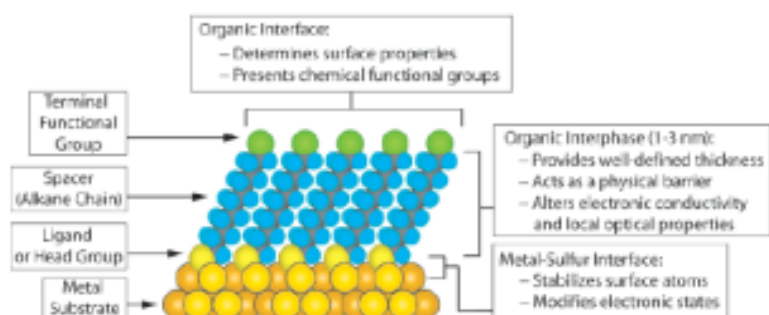


Isotherm



Self-Assemble Monolayer (SAM)

Chem. Rev. 2005, 105, 1103–1169



S-Au 25-30 Kcal/mole
Si-O 190 kcal/mole

Morphology of Substrate				Morphology of Substrate			
Ligand	Substrates	Thin Films or Bulk Material	Nanoparticles or Other Nanostructures	Ligand	Substrates	Thin Films or Bulk Material	Nanoparticles or Other Nanostructures
ROH	Fe ₃ O ₄	36	35	RSSR'	Ag	89	90
	Si-H	37			Au	20	90-92
	Si				CdS		61
RCOO-/RCOOH	α-Al ₂ O ₃	38,39			Pd	30	
	Fe ₃ O ₄		40		Au	93	
	Ni		41,42				
RCOO-OOCR	Ti/TiO ₂	43		RCSSH	Au	94	95
	Si(111):H	44			CdSe		
Ene-diol	Fe ₂ O ₃		45	RS ₂ O ₂ 'Na ⁺	Au	96	98
RNH ₂	FeS ₂	46			Cu	97	
	Mica	47		RSeH	Ag	99	
	Stainless Steel 316L	48			Au	100,101	
	YBa ₂ Cu ₃ O _{7-δ}	49			CdS		60
RC≡N	CdSe		50	RSeSeR'	CdSe		102
	Ag	51			Au	101	
R-N≡N'(BF ₄ ⁻)	Au			R ₃ P	Au		103
	GaAs(100)	52			FeS ₂	46	
	Pd	52			CdS		104
RSH	Si(111):H	52			CdSe		104
	Ag	26	53,54	R ₃ P=O	CdTe		104
	Ag ₉₉ Ni ₁₀	55			Co		105,106
	AgS		56		CdS		104
	Au	26	57		CdSe		104
	AuAg		58	RPO ₂ ²⁻ /RP(O)(OH) ₂	CdTe		104
	AuCu		58		Al	107	
	Au ₉ Pd _{1-x}		58		Al-OH	108	
	CdTe		59		Ca ₁₀ (PO ₄ CO ₃) ₆ (OH) ₂	109	
	CdSe		60		GaAs	110	
	CdS		61,62		GaN	110	
	Cu	26	58		Indium tin oxide	111	
	FePt		63-66		(ITO)		
	GaAs	67			Mica	112	
	Ge	68			TiO ₂	113,114	
	Hg	69-71			ZrO ₂	114,115	
	HgTe		72	RPO ₄ ³⁻	CdSe		116-118
	InP	73	74		CdTe		118,119
	Ir				Al ₂ O ₃	120	
	Ni	75			Nb ₂ O ₅	120	
	PbS		76-78		Ta ₂ O ₅	121	
RSAc	Pd	30	74,79	RN≡C	Pt	123	124
	PdAg		58		Si	37	
	Pt	32	80		Si(111):H	125	
	Ru		81	RHC-CH ₂			
	Stainless Steel 316L	48					
	YBa ₂ Cu ₃ O _{7-δ}	82					
	Zn	83		RC≡CH			
	ZnSe	84					
	ZnS		85				
	Au	86		RSiX ₃ X = H, Cl, OCH ₂ CH ₃	HfO ₂	126	
	Au		87		ITO	127	
					PtO	128	
RSSR'					TiO ₂	113,126,129	
	Au	88			ZrO ₂	126,129	

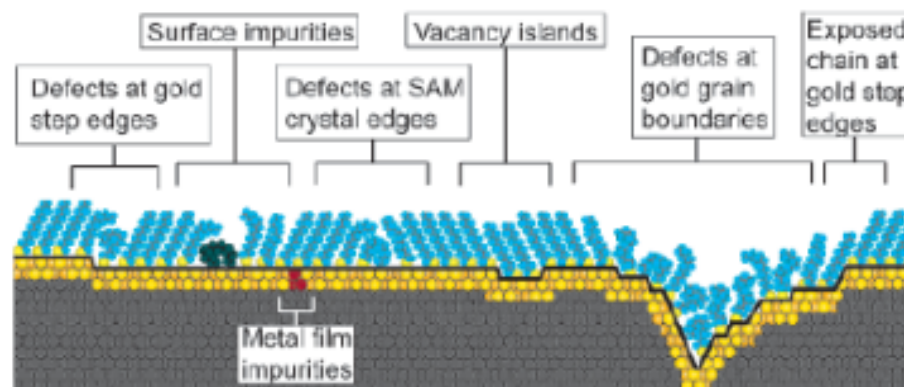
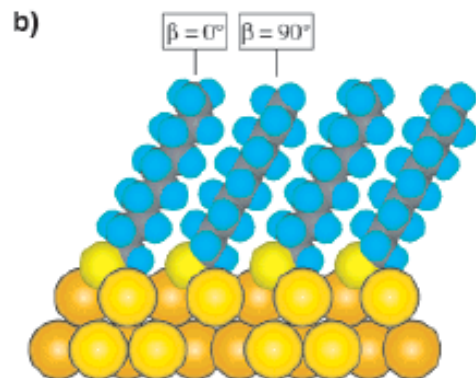
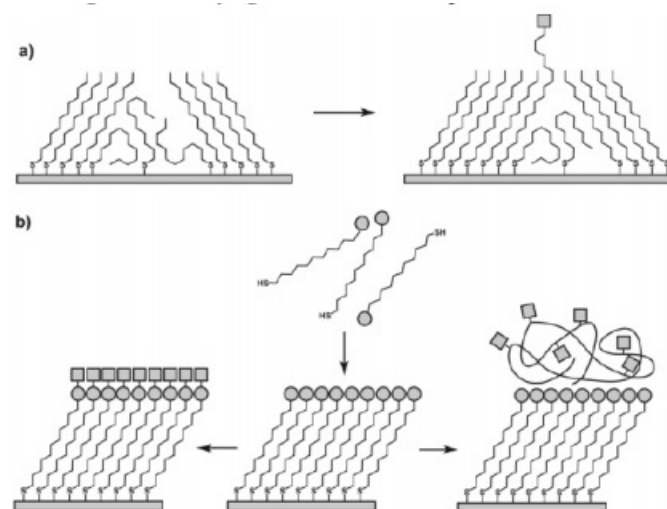
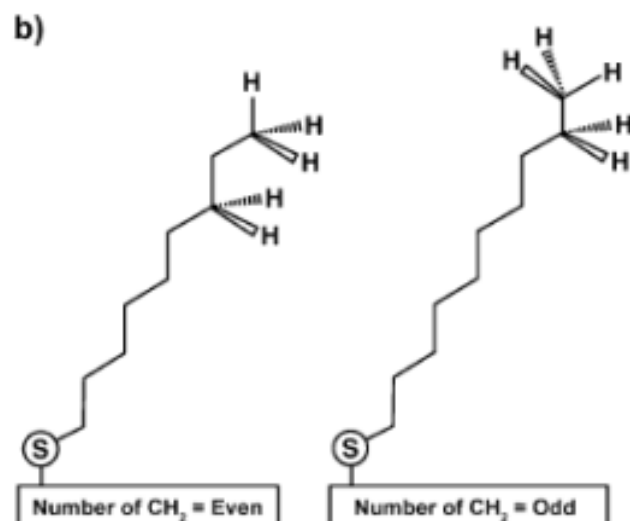


Figure 7. Schematic illustration of some of the intrinsic and extrinsic defects found in SAMs formed on polycrystalline substrates. The dark line at the metal–sulfur interface is a visual guide for the reader and indicates the changing topography of the substrate itself.



^a (a) Insertion of a functional adsorbate at a defect site in a preformed SAM. (b) Transformation of a SAM with exposed functional groups (circles) by either chemical reaction or adsorption of another material.

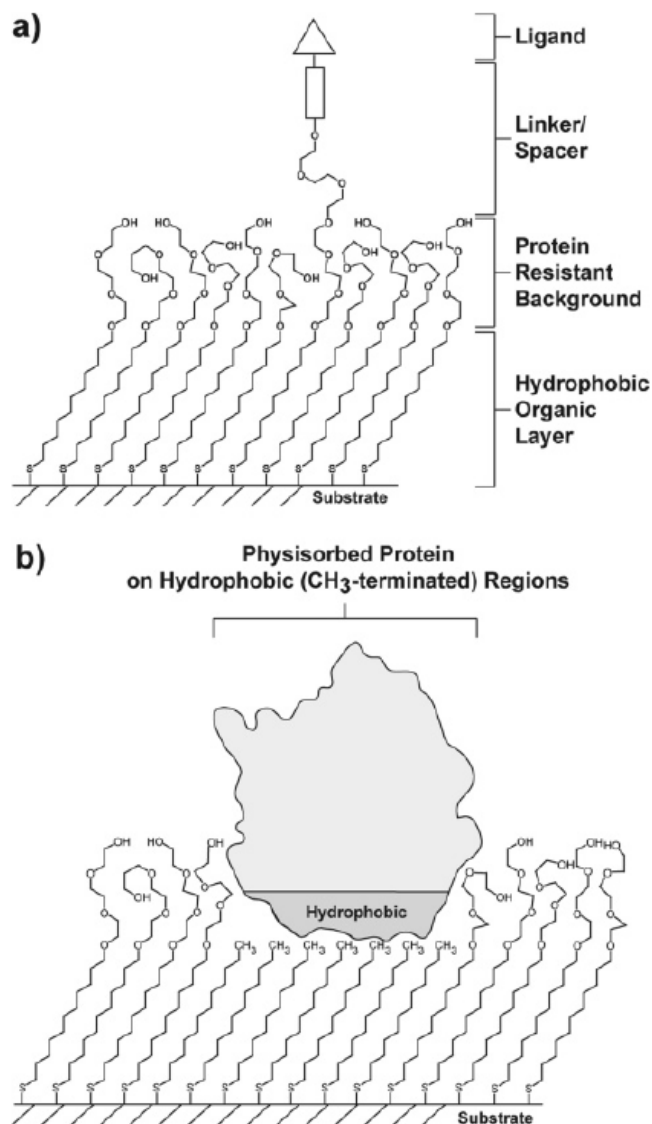


Figure 21. Schematic illustrations of (a) a mixed SAM and (b) a patterned SAM. Both types are used for applications in biology and biochemistry.

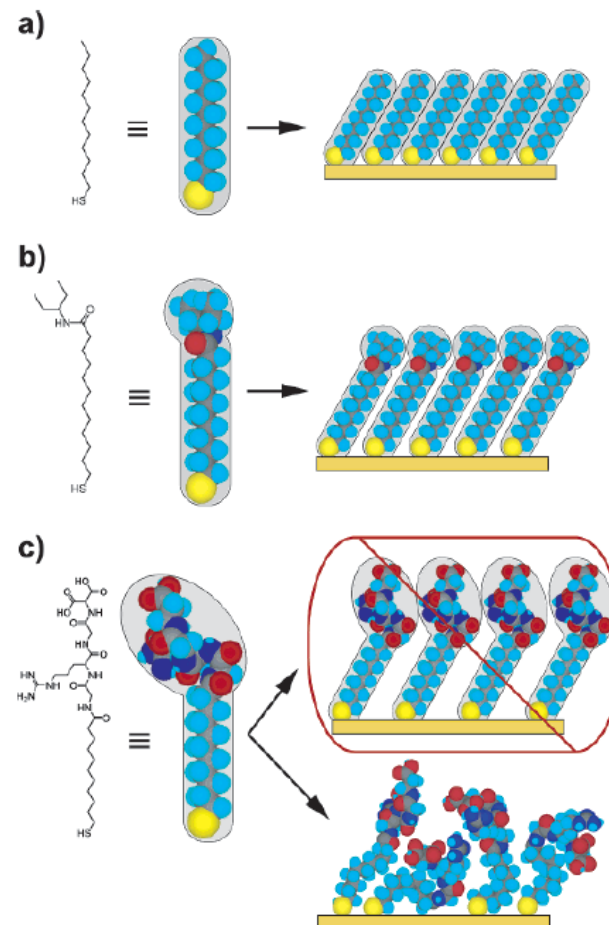


Figure 22. Schematic diagram illustrating the effects that large terminal groups have on the packing density and organization of SAMs. (a) Small terminal groups such as $-\text{CH}_3$, $-\text{CN}$, etc., do not distort the secondary organization of the organic layer and have no effect on the sulfur arrangement. (b) Slightly larger groups (like the branched amide shown here) begin to distort the organization of the organic layer, but the strongly favorable energetics of metal–sulfur binding drive a highly dense arrangement of adsorbates. (c) Large terminal groups (peptides, proteins, antibodies) sterically are unable to adopt a secondary organization similar to that for alkanethiols with small terminal groups. The resulting structures probably are more disordered and less dense than those formed with the types of molecules in a and b.

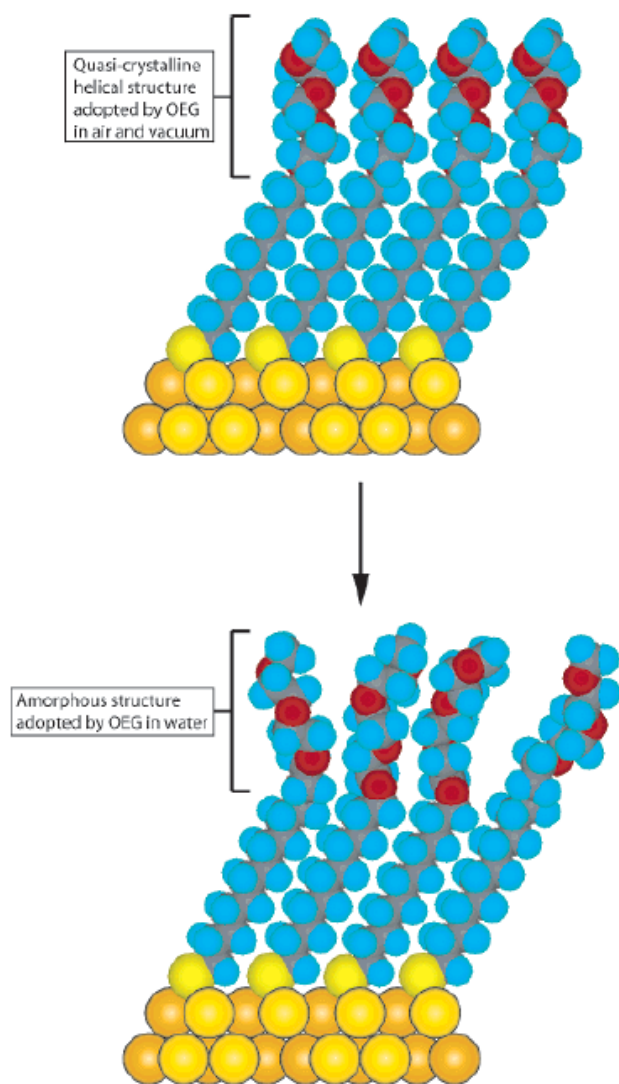
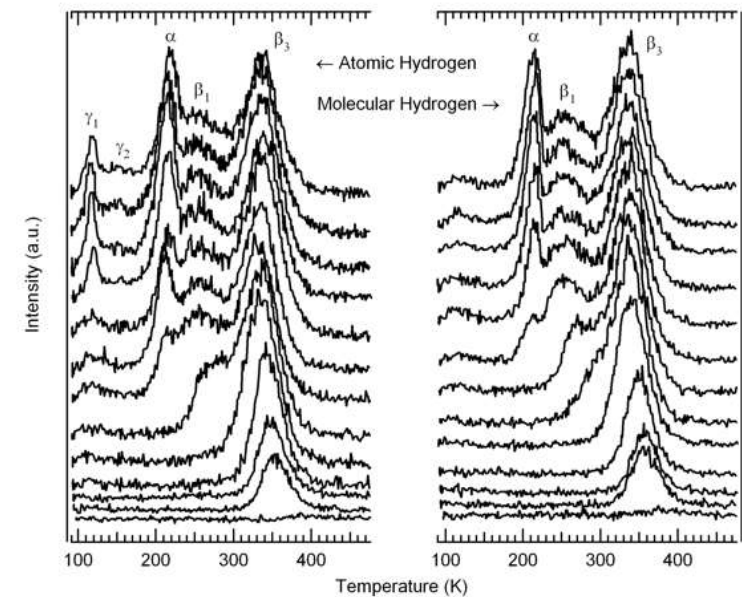
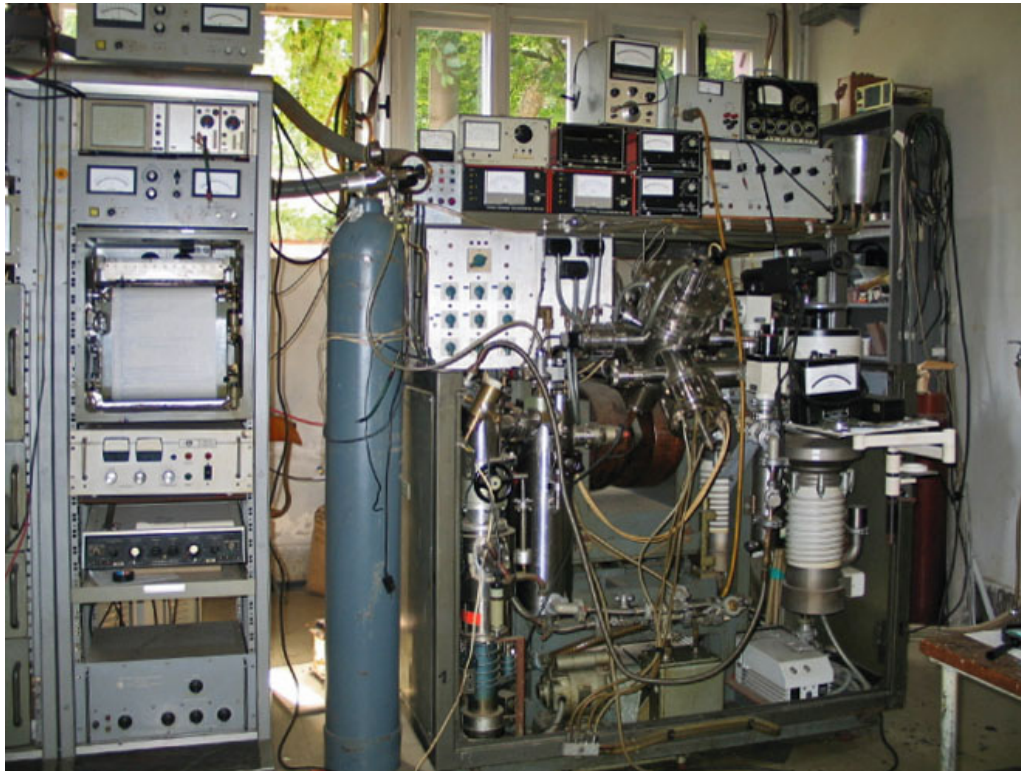


Figure 23. Schematic illustration of the order–disorder transition evidenced by SAMs of alkanethiolates terminated with triethylene glycol. The EG_3 group loses conformational ordering upon solvation in water.

Temperature Programmed Desorption

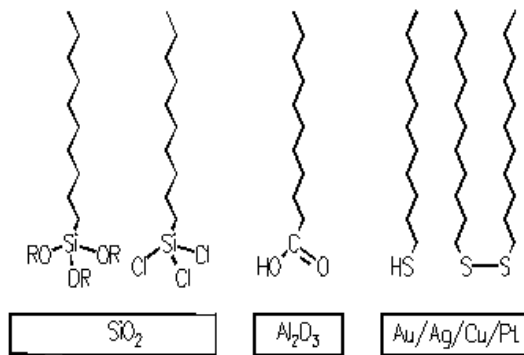


Self-Assembly

- Substrates
- Interstitial adhesion layer
- Noble metal layer
- Organo-sulfur

Organosilanes

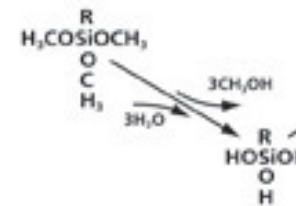
Self-assembled monolayers



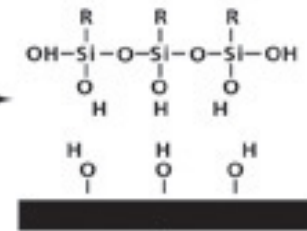
- Surface
- silicon oxide: silanisation
- aluminum oxide: fatty acids
- metals: thiols and sulfides

Immersion of substrate in a solution containing the adequate molecules for 12 - 24 hours yields an ordered monolayer

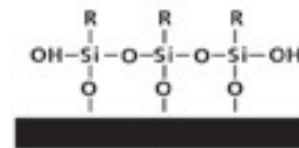
Hydrolysis (1)



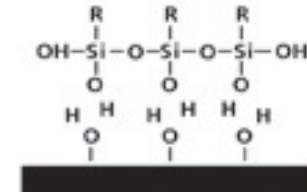
Condensation of Oligomers (2)



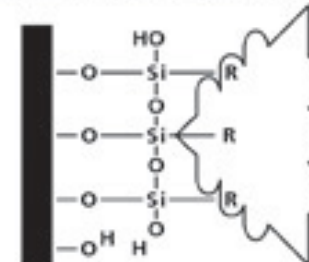
Bond Formation (4)



Hydrogen Bonding (3)

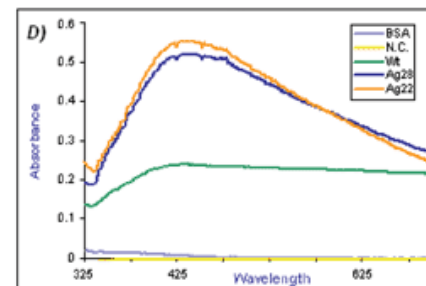
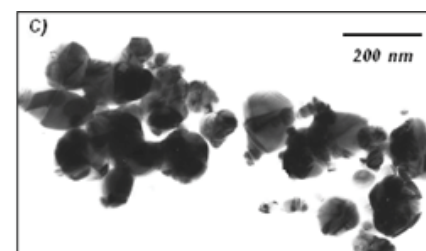
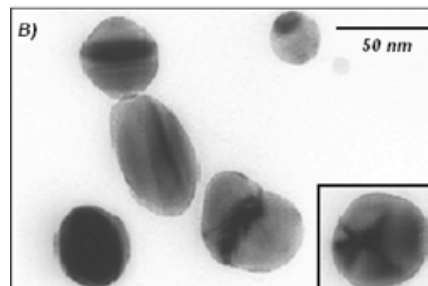
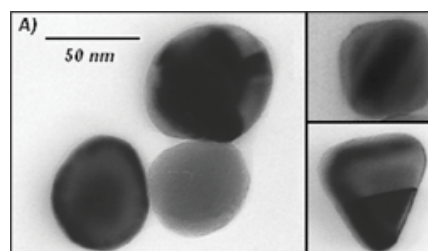
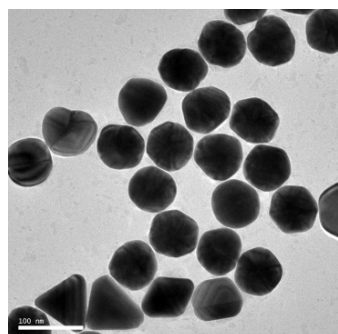
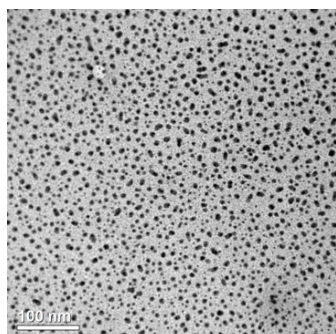
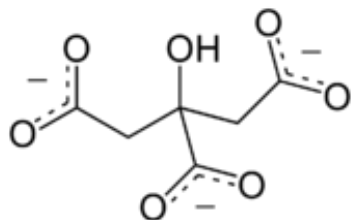


Reaction and bond formation of the R group (5)



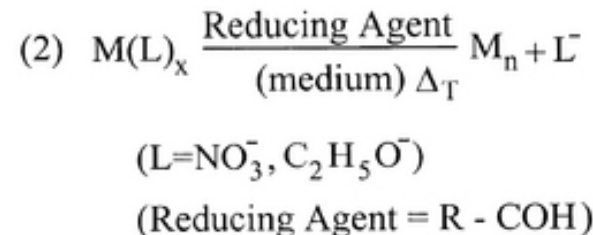
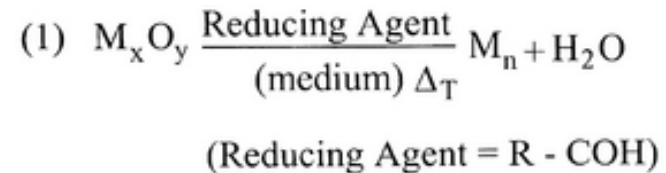
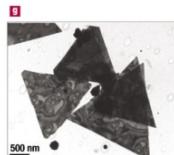
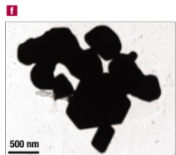
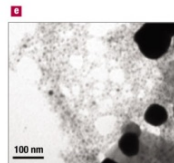
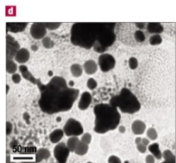
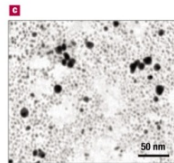
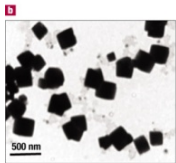
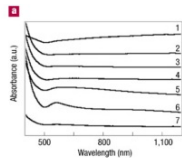
Synthesis of Silver Nanoparticles

1. A solution of AgNO_3 ($1.0 \times 10^{-3} \text{ M}$) in deionized water was heated until it began to boil.
2. Sodium citrate solution was added dropwise to the silver nitrate solution as soon as the boiling commenced. The color of the solution slowly turned into grayish yellow, indicating the reduction of the Ag^+ ions.
3. Heating was continued for an additional 15 min, and then the solution was cooled to room temperature before employing for further experimentation.



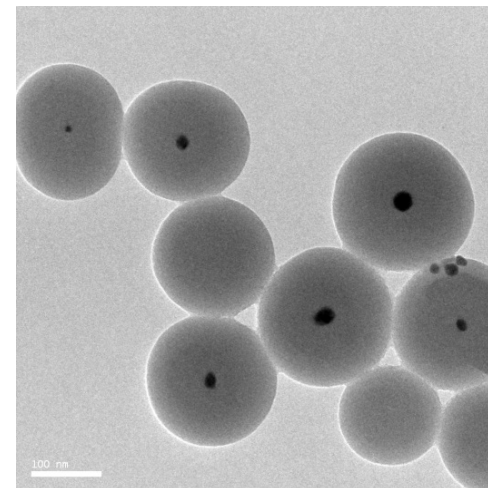
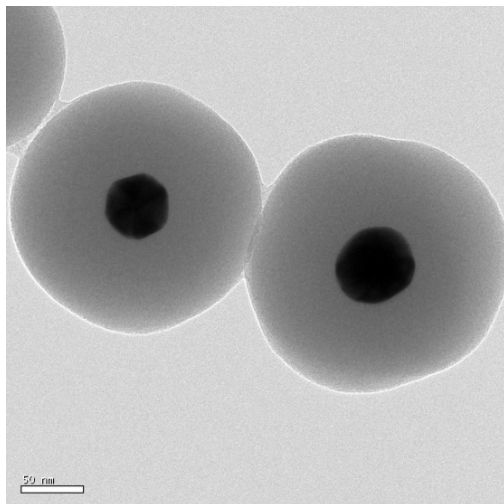
Synthesis of Gold Nanoparticles

1. Add 20 mL of 1.0 mM HAuCl_4 to a 50 mL round bottom flask on a stirring hot plate.
2. Add a magnetic stir bar and bring the solution to a boil.
3. To the boiling solution, add 2 mL of a 1% solution of trisodium citrate dihydrate
4. The gold sol gradually forms as the citrate reduces the gold(III). Stop heating when a deep red color is obtained.

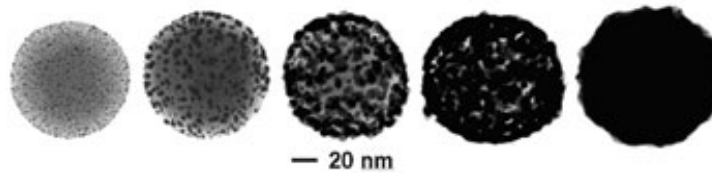
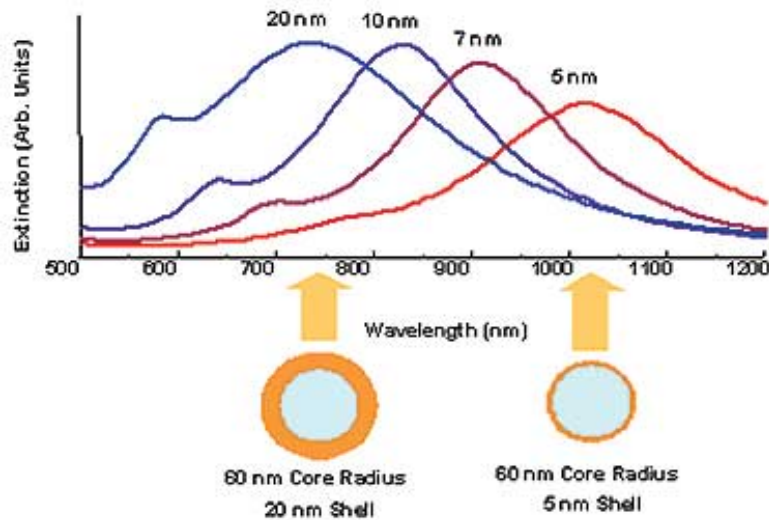


Construction of Core Shell Ag/Au@SiO₂ Nanoparticles

1. Under vigorous stirring, 1 ml of the silver/ gold colloids solution was mixed with 250 mL of isopropanol and 25 mL of deionized water.
2. Immediately after the addition of 4 mL of 30% ammonium hydroxide, different amounts of tetraethoxysilane (TEOS) were added to the reaction mixture.
3. To obtain different silica layer thicknesses, TEOS solutions with a concentration between 50% and 100% was added to the suspension. The reaction was stirred at room temperature for 30 minutes and then was allowed to age without agitation at 4°C overnight.
4. Each suspension of silica-coated silver/gold nanoparticles was washed and centrifuged, followed by re-suspension in water. The thickness of the silica layers was determined from TEM images .



Core-Shell Nanoparticles



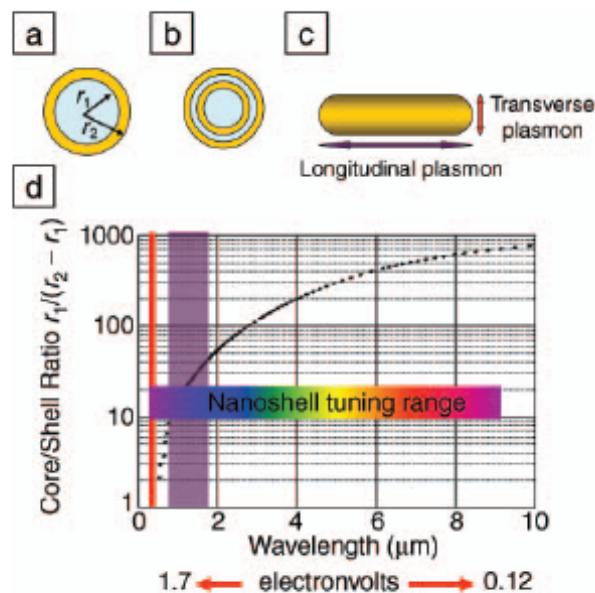


Figure 1. (a) Schematic illustration of a silica-core, gold-shell nanoshell, indicating inner (r_1) and outer (r_2) radii of the shell layers. (b) Depiction of a four-layer, concentric nanoshell. (c) Schematic illustration of a metallic nanorod. (d) Plot of nanoshell resonance as a function of core and shell dimensions, overlaid with reported spectral ranges of nanorod resonances (red, transverse plasmon; purple, longitudinal plasmon), and reported nanoshell and concentric nanoshell combined spectral range of plasmon response.

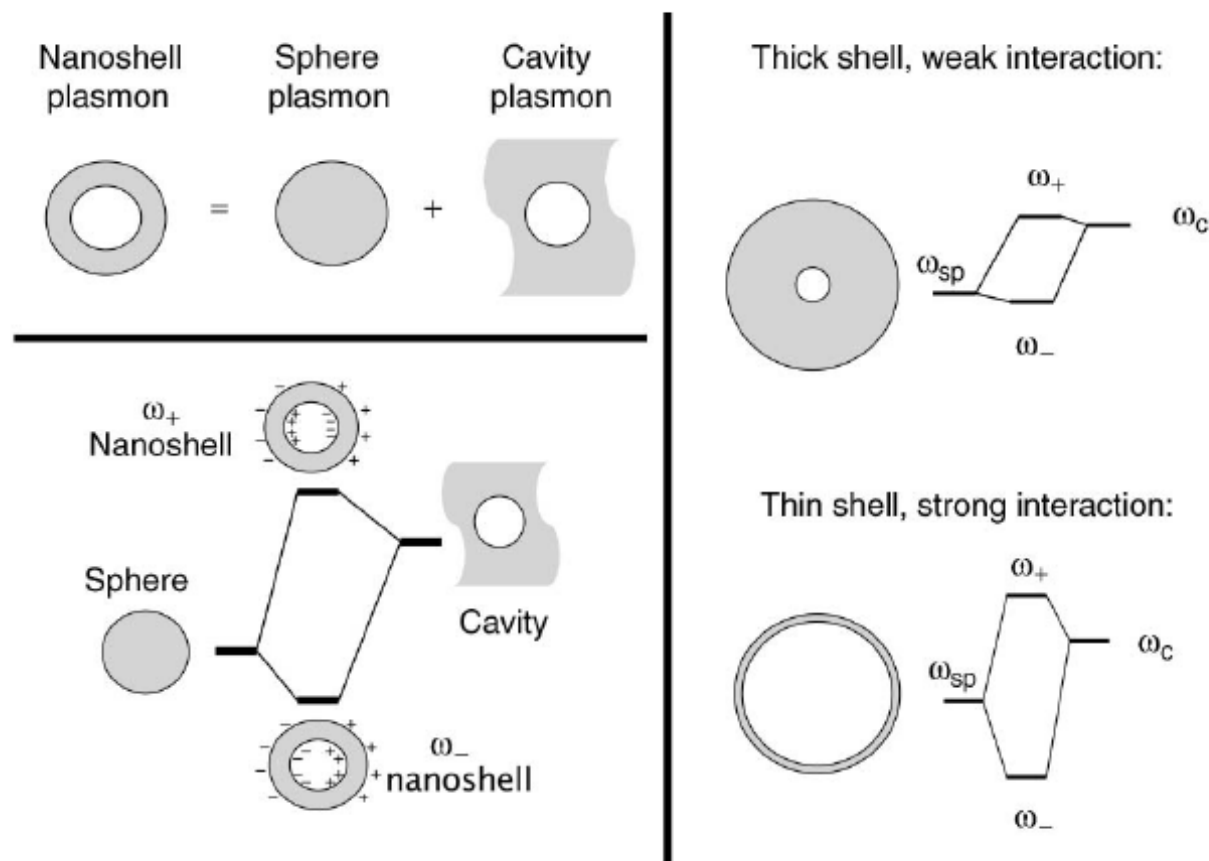


Figure 2. Plasmon hybridization and the sphere-cavity model for nanoshells: the interaction between a sphere (resonance frequency, ω_{sp}) and a cavity plasmon (resonance frequency, ω_c) is tuned by varying the thickness of the shell layer of the nanoparticle. Two hybrid plasmon resonances, the ω_- "bright," or "bonding," plasmon and the ω_+ "dark," or "anti-bonding," plasmon resonances are formed. The lower-energy plasmon couples most strongly to the optical field.

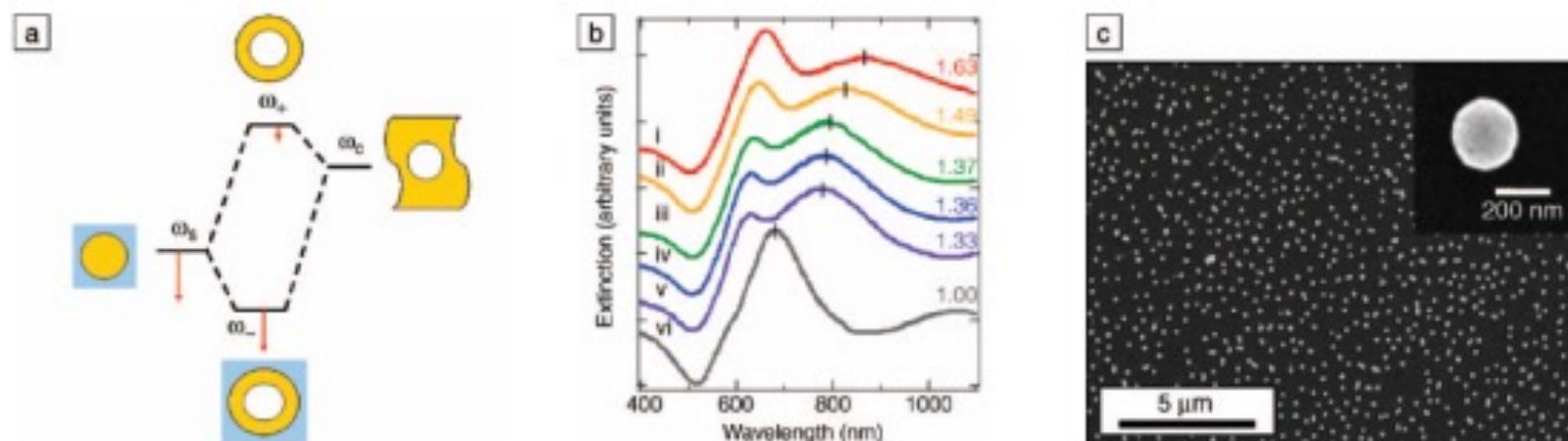


Figure 5. (a) Plasmon hybridization picture applied to surface plasmon resonance sensing with nanoshells: the low-energy "bonding" plasmon, ω_- , is sensitized to changes in its dielectric environment. The blue background schematically denotes the embedding medium for the nanoparticle. (b) Experimental curves showing plasmon resonance shifts for nanoshell-coated films in various media: (i) carbon disulfide, (ii) toluene, (iii) hexane, (iv) ethanol, (v) H_2O , and (vi) air. The index of refraction for each embedding medium is noted on the far right of the spectra. Spectra are offset for clarity. (c) Scanning electron micrograph of nanoshells deposited onto a poly(vinyl pyridine) functionalized glass surface, as used to acquire data in (b). Inset: individual nanoshell.

Preparation of $\text{Fe}_3\text{O}_4@\text{Ag}/\text{Au}$

1. *To the magnetic nanoparticle suspension obtained from commercial company, add 50 ml of a solution of Au (III) salt or Ag (I) salt at concentration of 0.01–1% mmol/L , shaking for 30 minutes, allowing Au (III) or Ag (I) ion to absorb on the surface of magnetic nanoparticle sufficiently,*
 2. *Then adding 15–40 ml of reducing agent, such as hydroxylamine hydrochloride at concentration of 40 mmol/L, reacting for 5–40 minutes.*
 3. *Further adding 1–10 ml of a solution of Au (III) salt or Ag (I) salt at concentration of 0.01–1%, shaking for 10 minutes, coating a reduced layer of gold or silver on the surface of the magnetic nanoparticle, forming super-paramagnetic composite particles having core/shell structure, separating magnetically, washing repeatedly with distilled water.*
- .

Synthesis of Quantum Dots

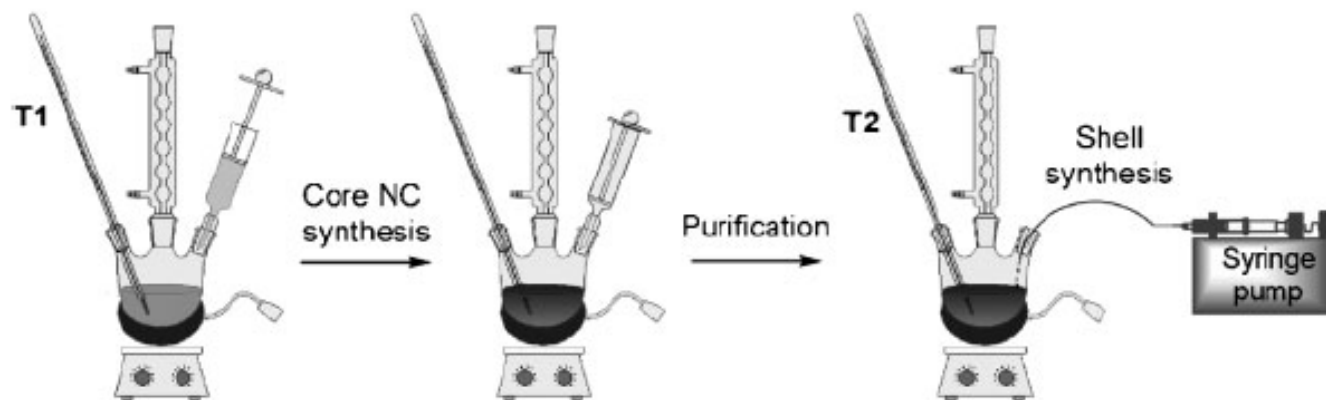
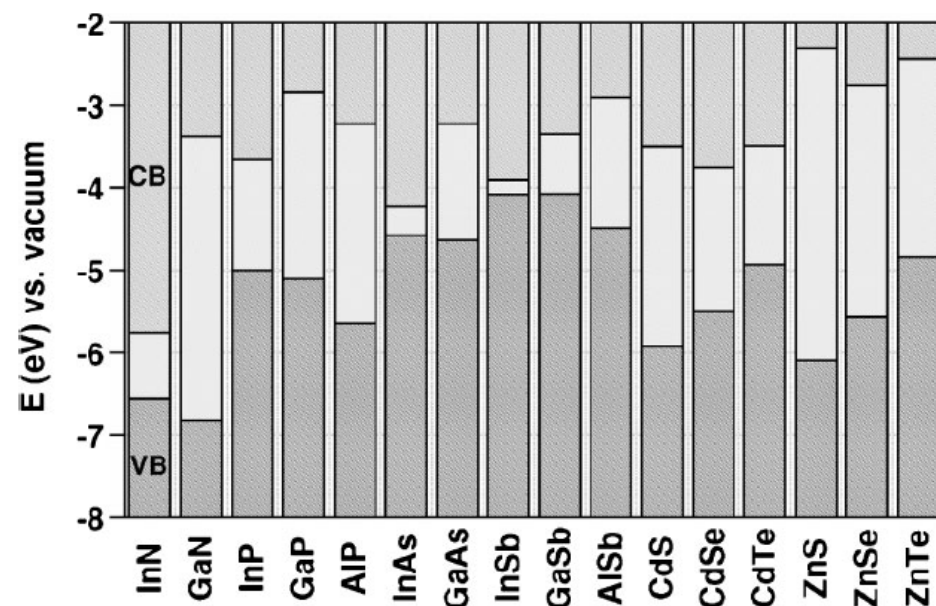


Figure 2. Two-step synthesis of core/shell nanocrystals.



Scheme 1. Electronic energy levels of selected III–V and II–VI semiconductors using the valence-band offsets from Reference [12] (VB: valence band, CB: conduction band).

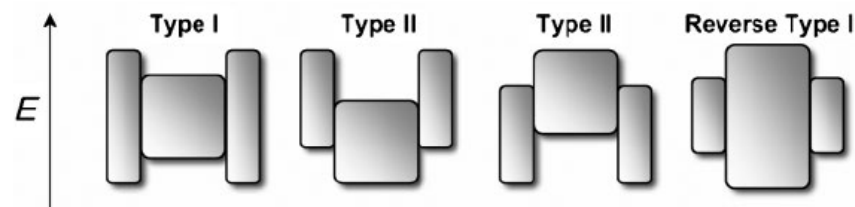
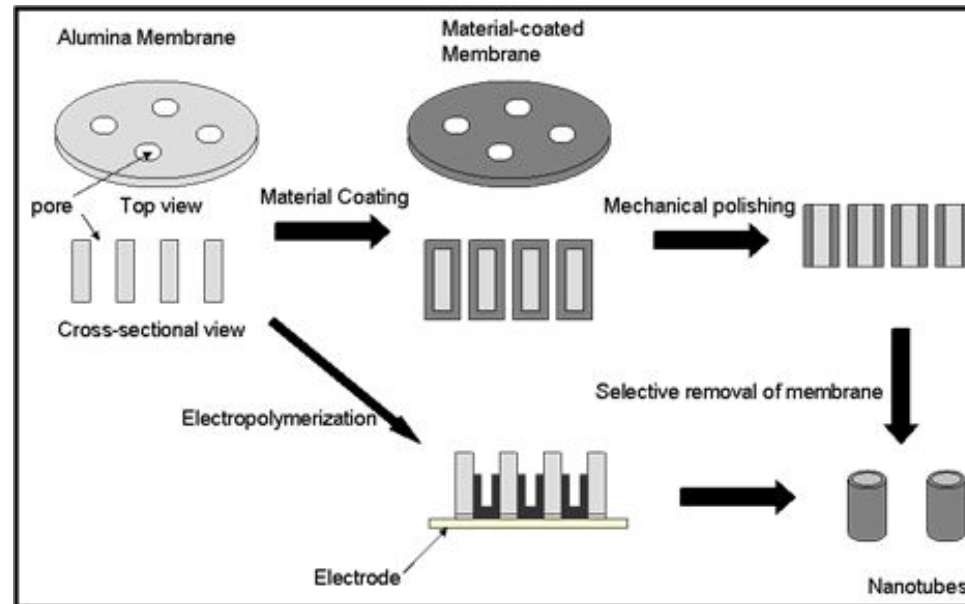


Figure 1. Schematic representation of the energy-level alignment in different core/shell systems realized with semiconductor NCs to date. The upper and lower edges of the rectangles correspond to the positions of the conduction- and valence-band edge of the core (center) and shell materials, respectively.

Template Synthesis



Porous Materials

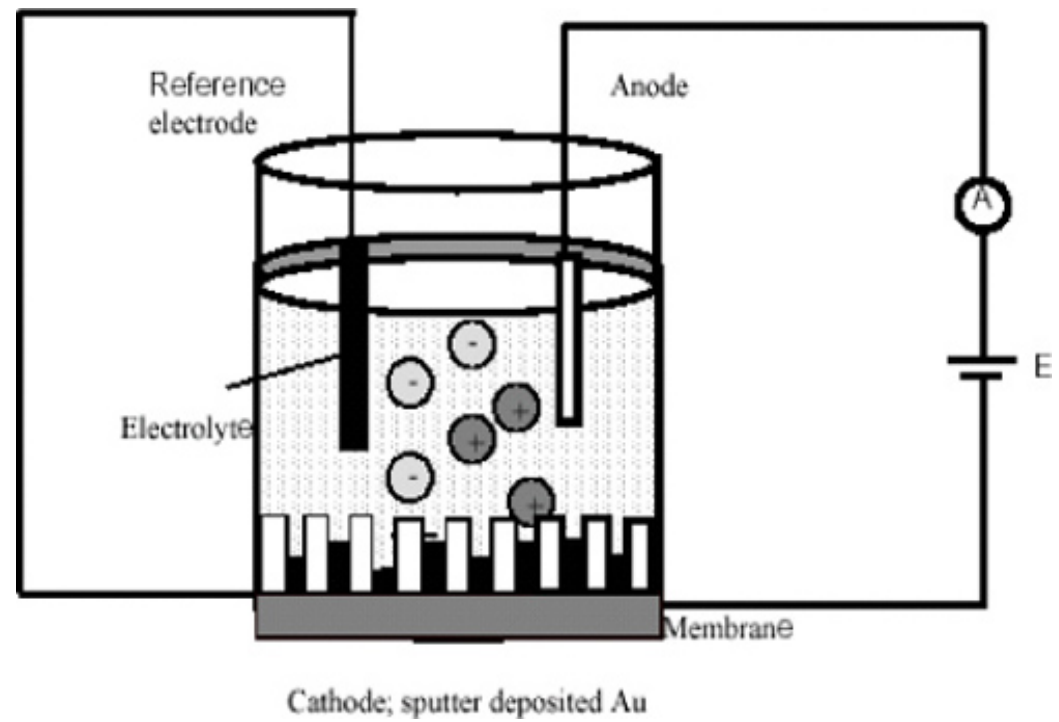
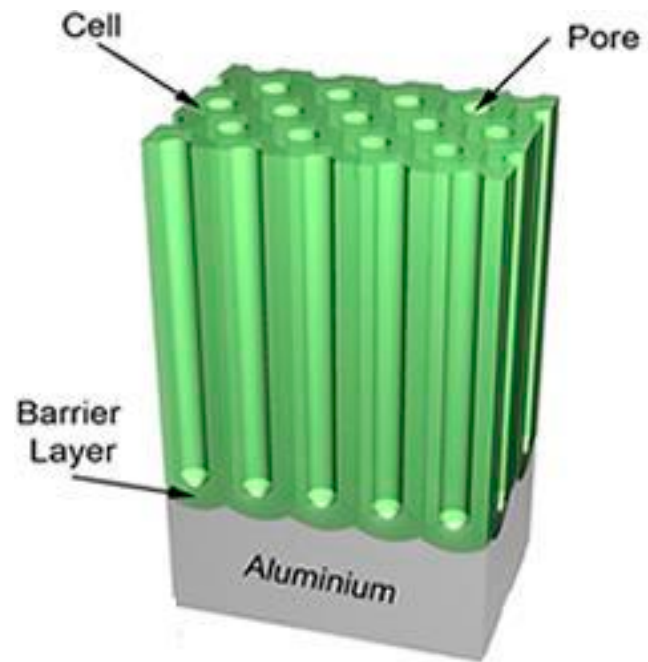
- AAO
- MCM-41

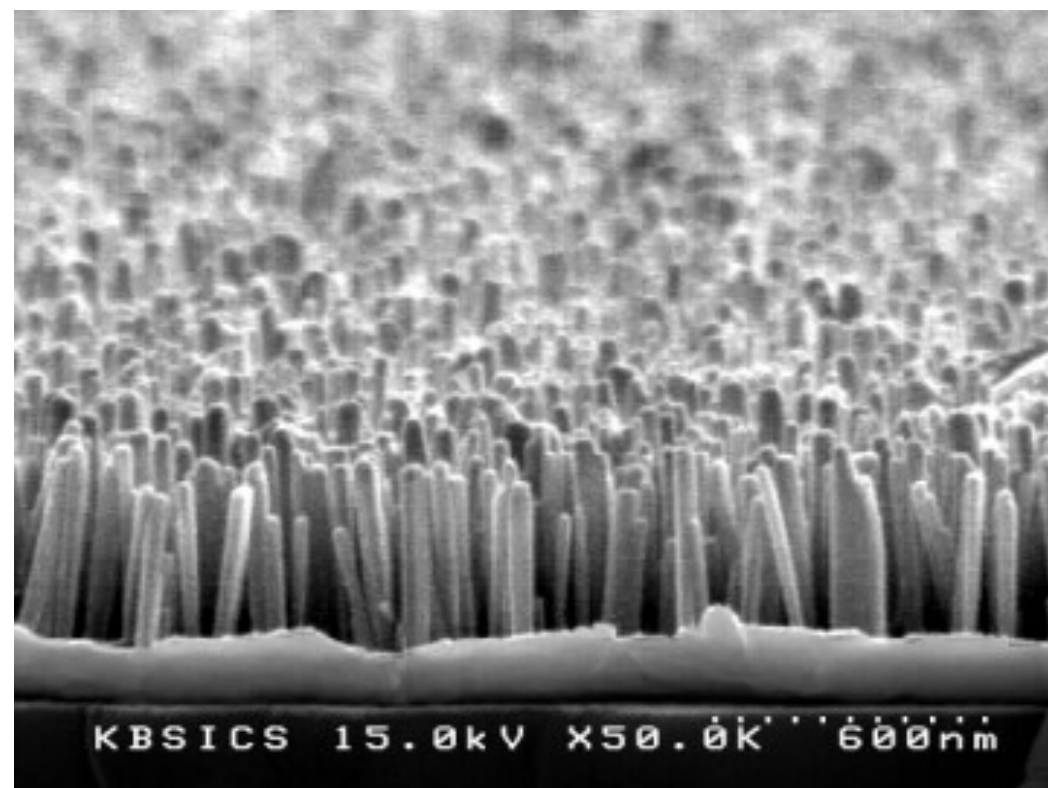
Mobil Crystalline Materials, or MCM-41

Santa Barbara Amorphous type material, or SBA-15

- Micro: $< 2\text{nm}$
- Meso:
- Macro: $> 50\text{nm}$

AAO





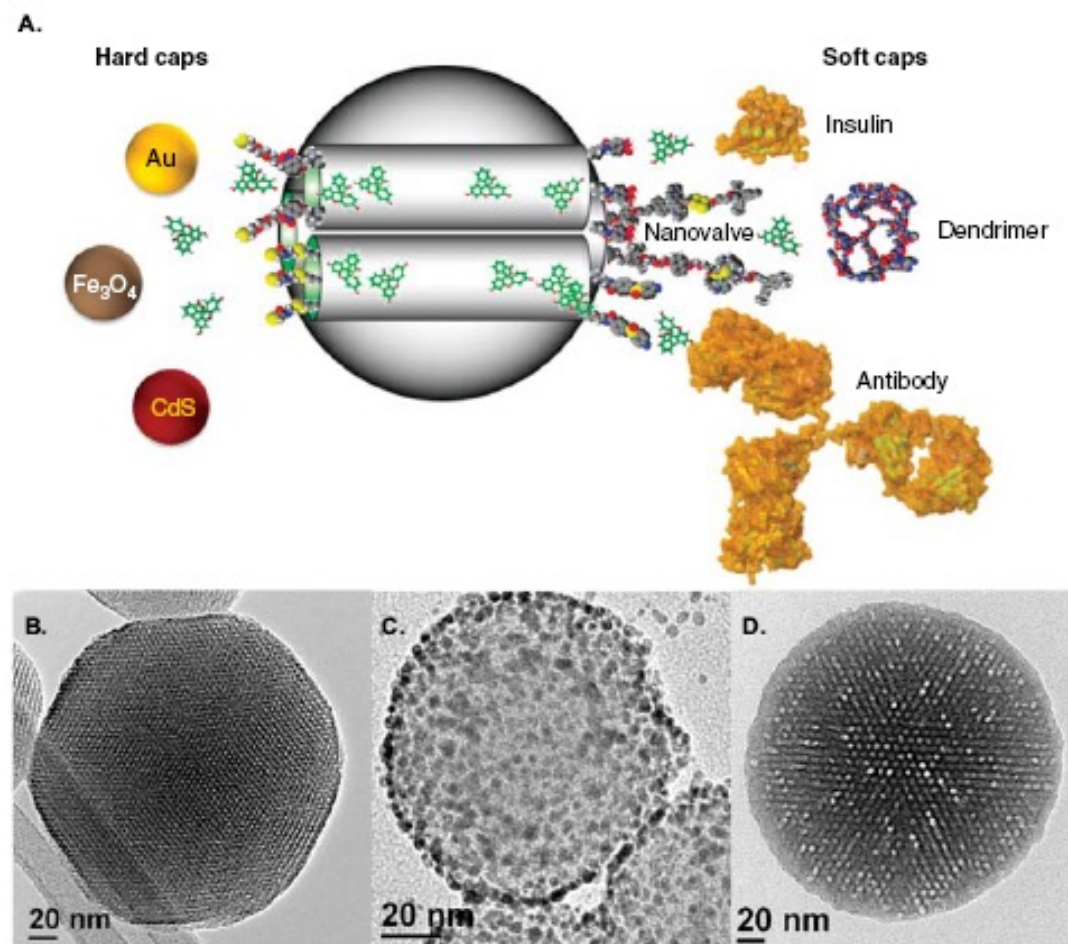
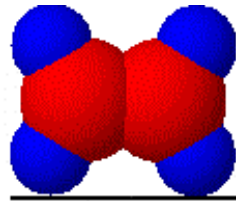


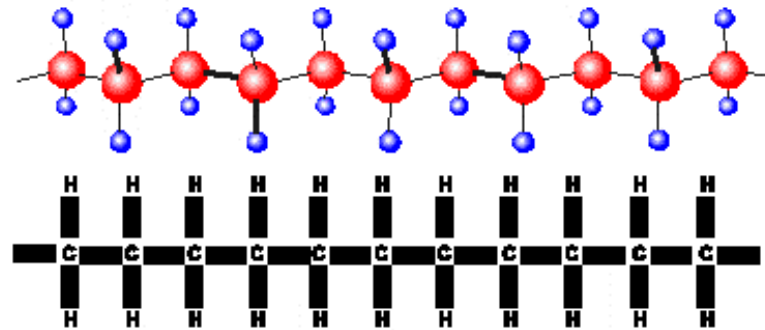
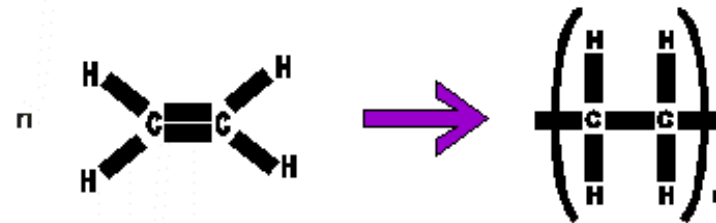
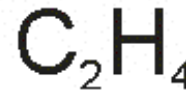
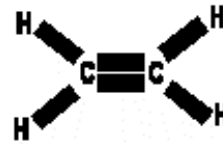
Figure 1. A. Schematic representation of a MSN loaded with drugs and capped with hard caps and soft caps highlighted in this review. Transmission electron microscopy images of (B) a MSN along the axis of the mesopores, (C) capped with hard (Au NP) and (D) with soft (polymer) caps.

MSN: Mesoporous silica nanoparticle.

Polymer



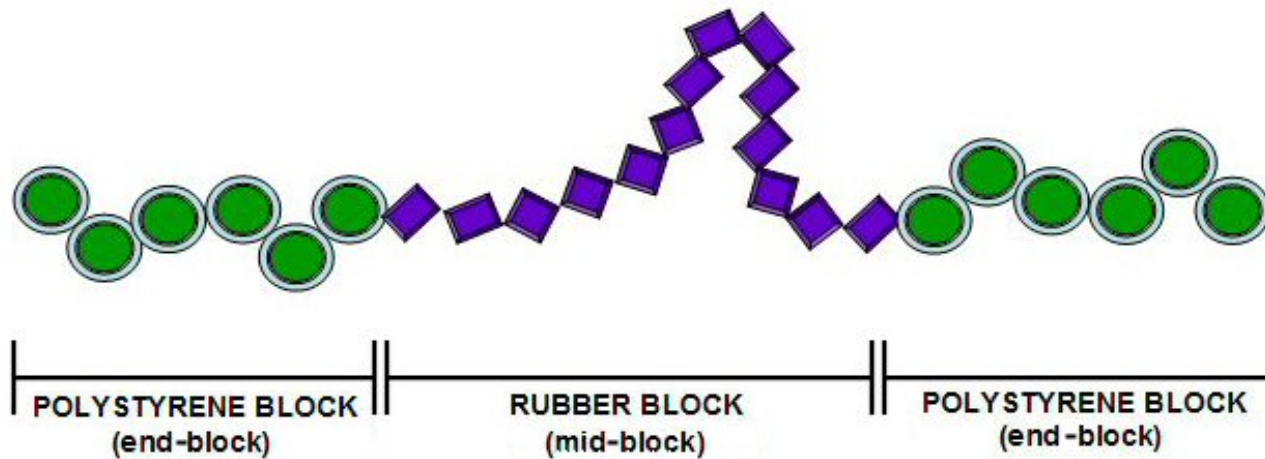
a monomer ethene



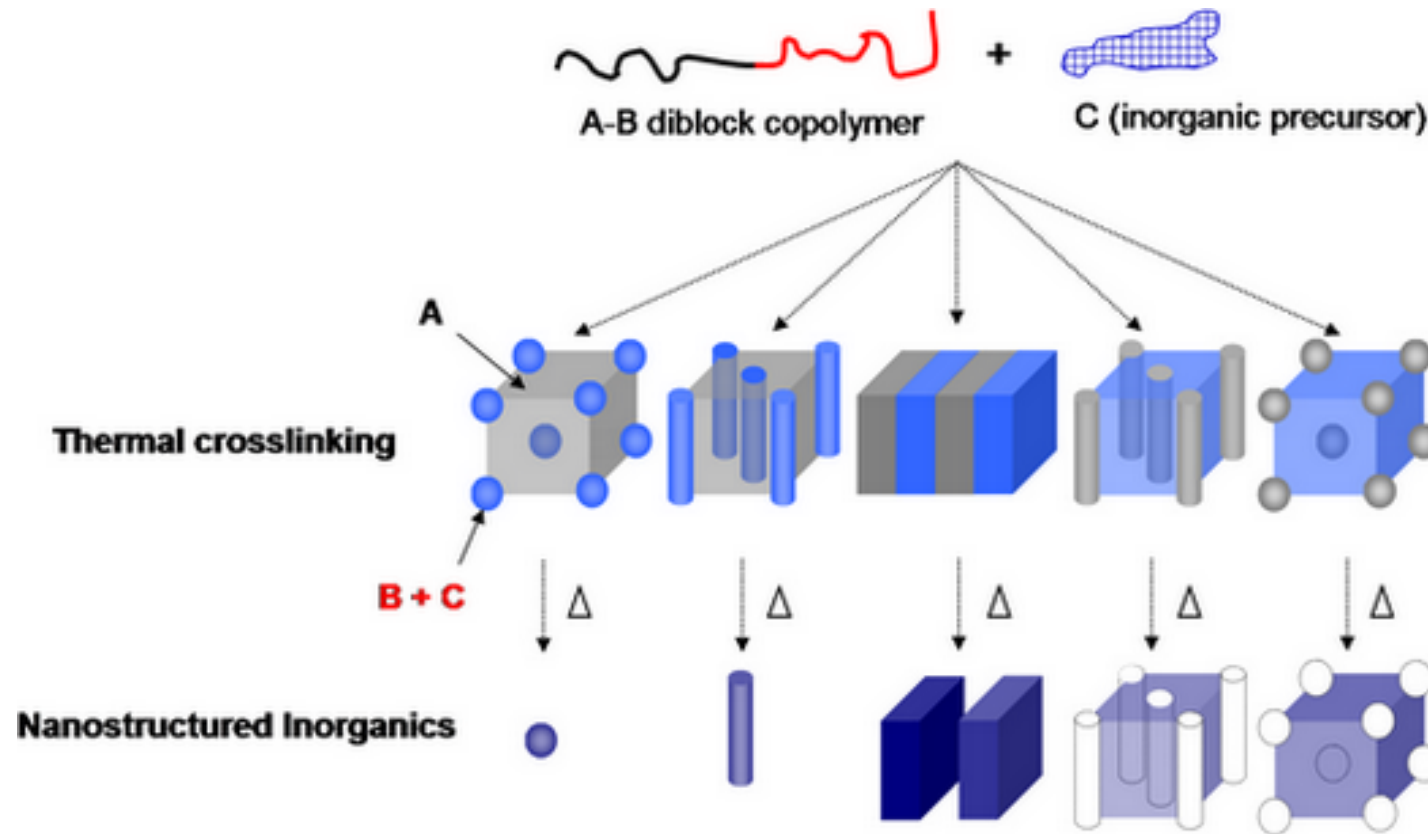
a polymer

poly(ethene)

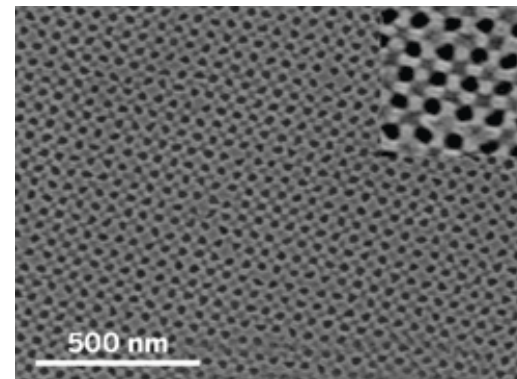
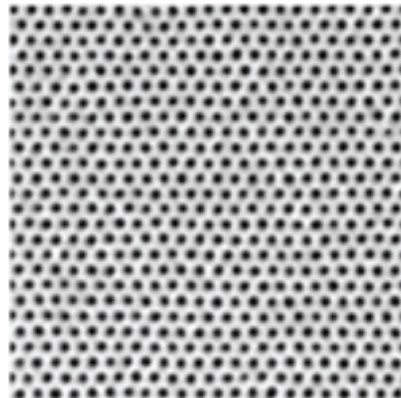
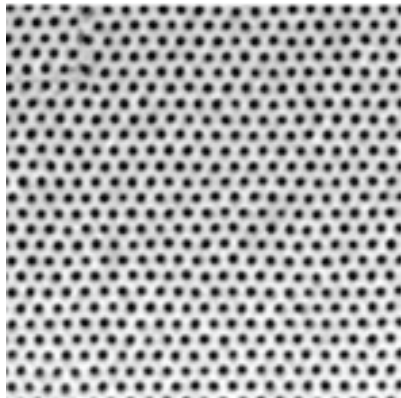
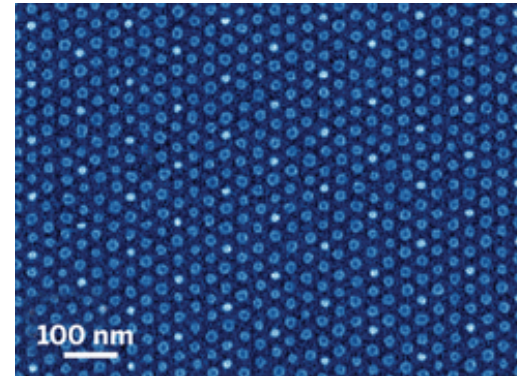
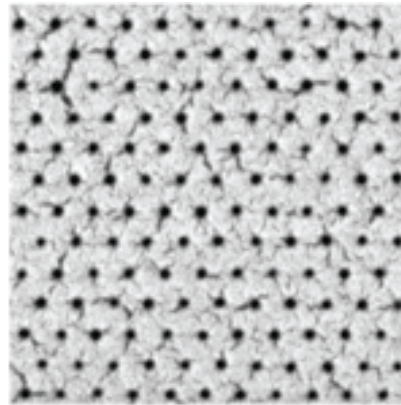
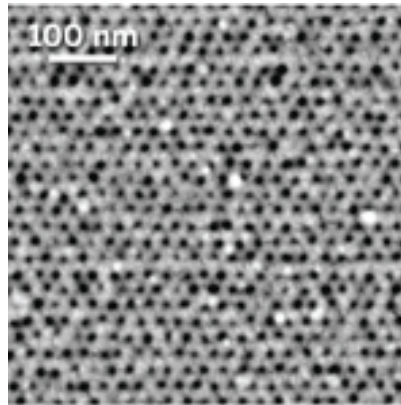
Block copolymer



Phase Segregation



Self-Assembled Block-copolymer



CNT

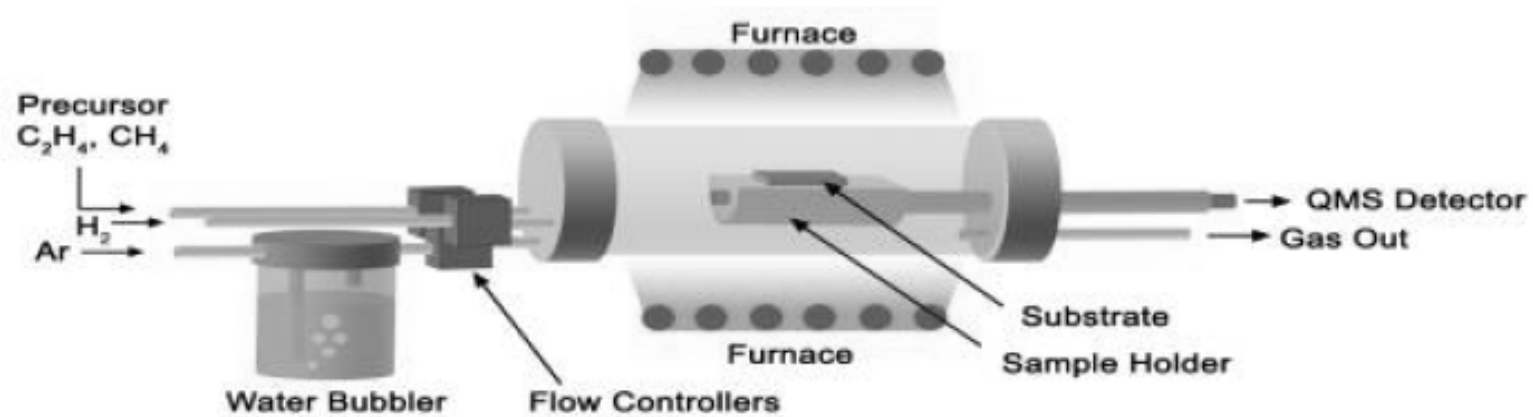
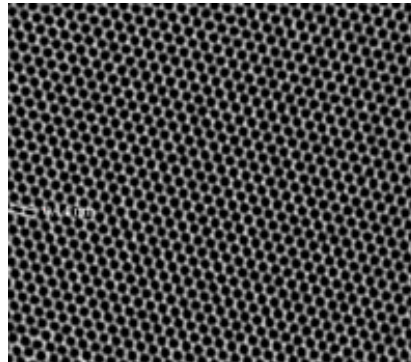
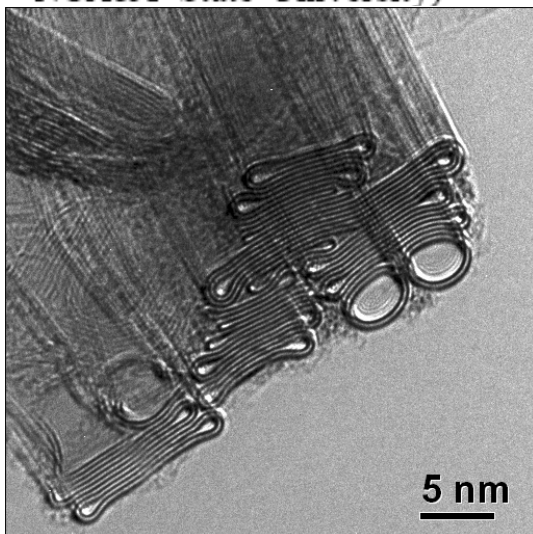


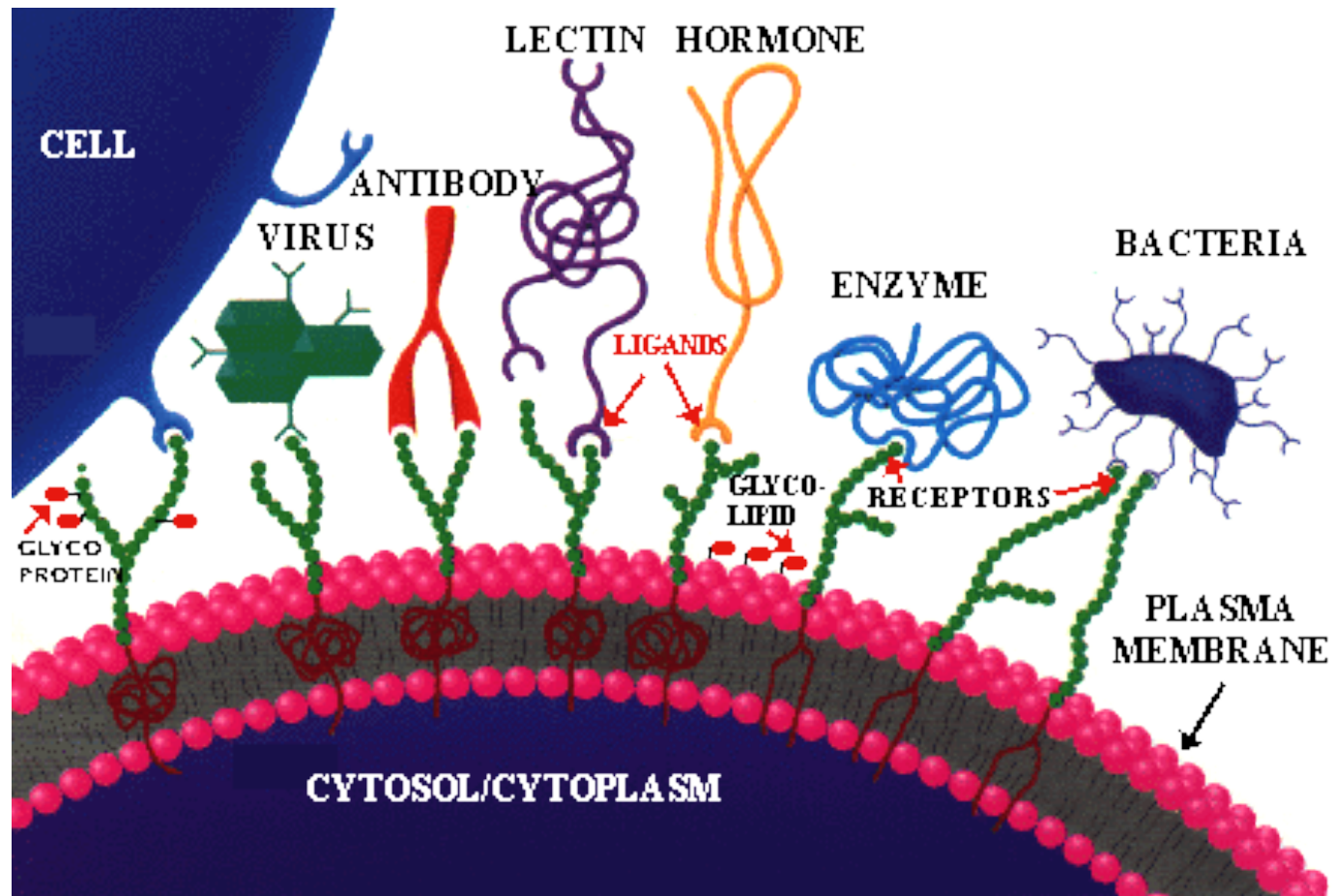
Fig. 1. Schematic of a CVD reactor for carbon nanotube growth. (Sketch by S. Yarmolenko from NCA&T State University)



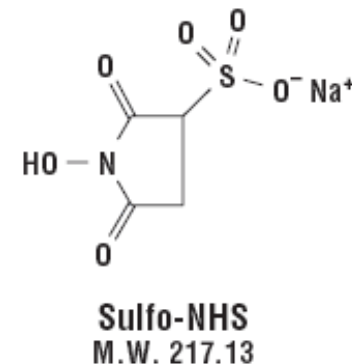
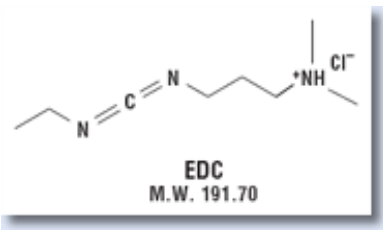
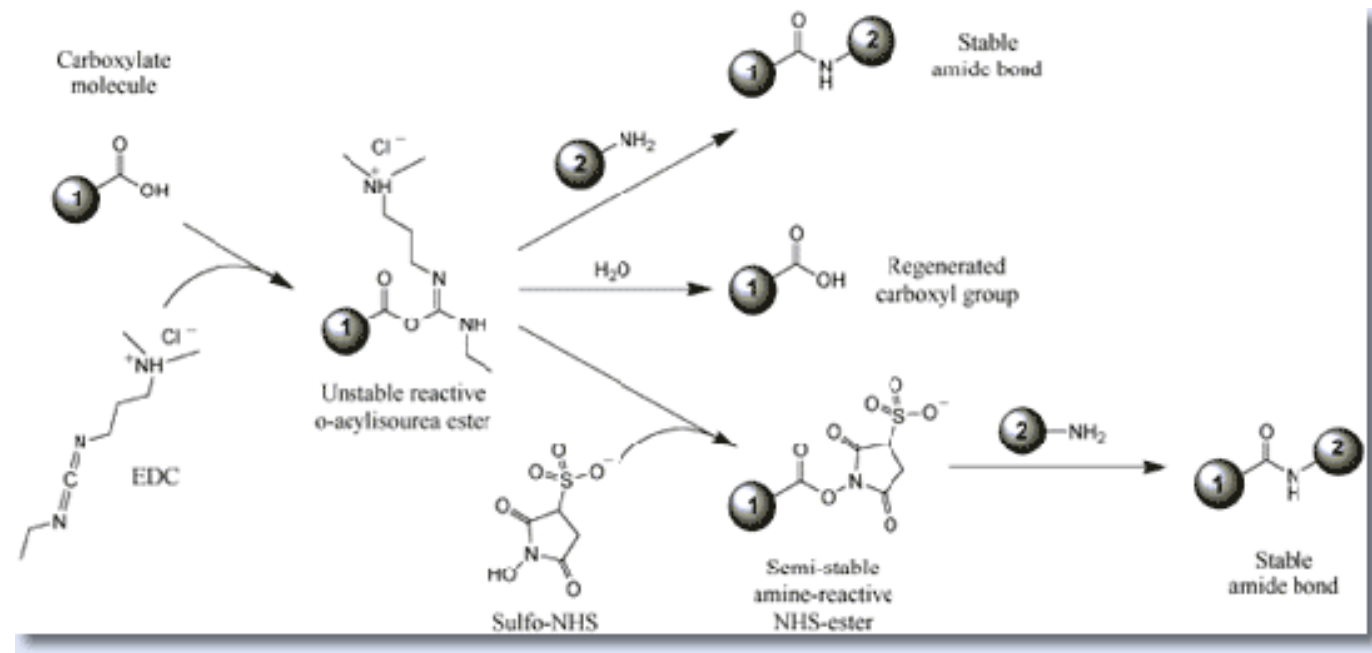
Surface Functionalization

- Recognition
 - Molecular Recognition
 - Protein
 - DNA
 - Saccharide
- Reporting/Detection
 - Dye
 - Quantum dots
 - SPR
 - SERS/LSPR
- Separation
 - Gel/Chromatography
 - Magnetic
- Surfaces
 - Gold and silver
 - Silicon oxide (glass)
 - Quantum dots
 - Polymer

Molecular Recognition

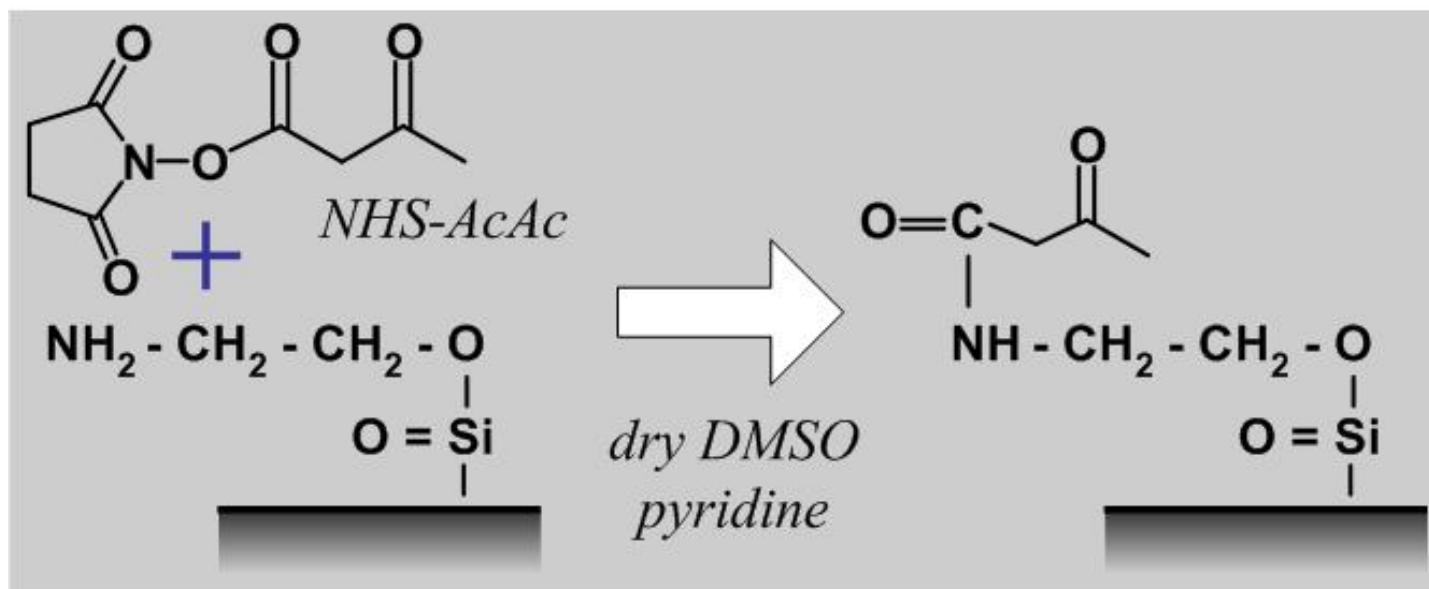


Carboxyl Presenting Surfaces

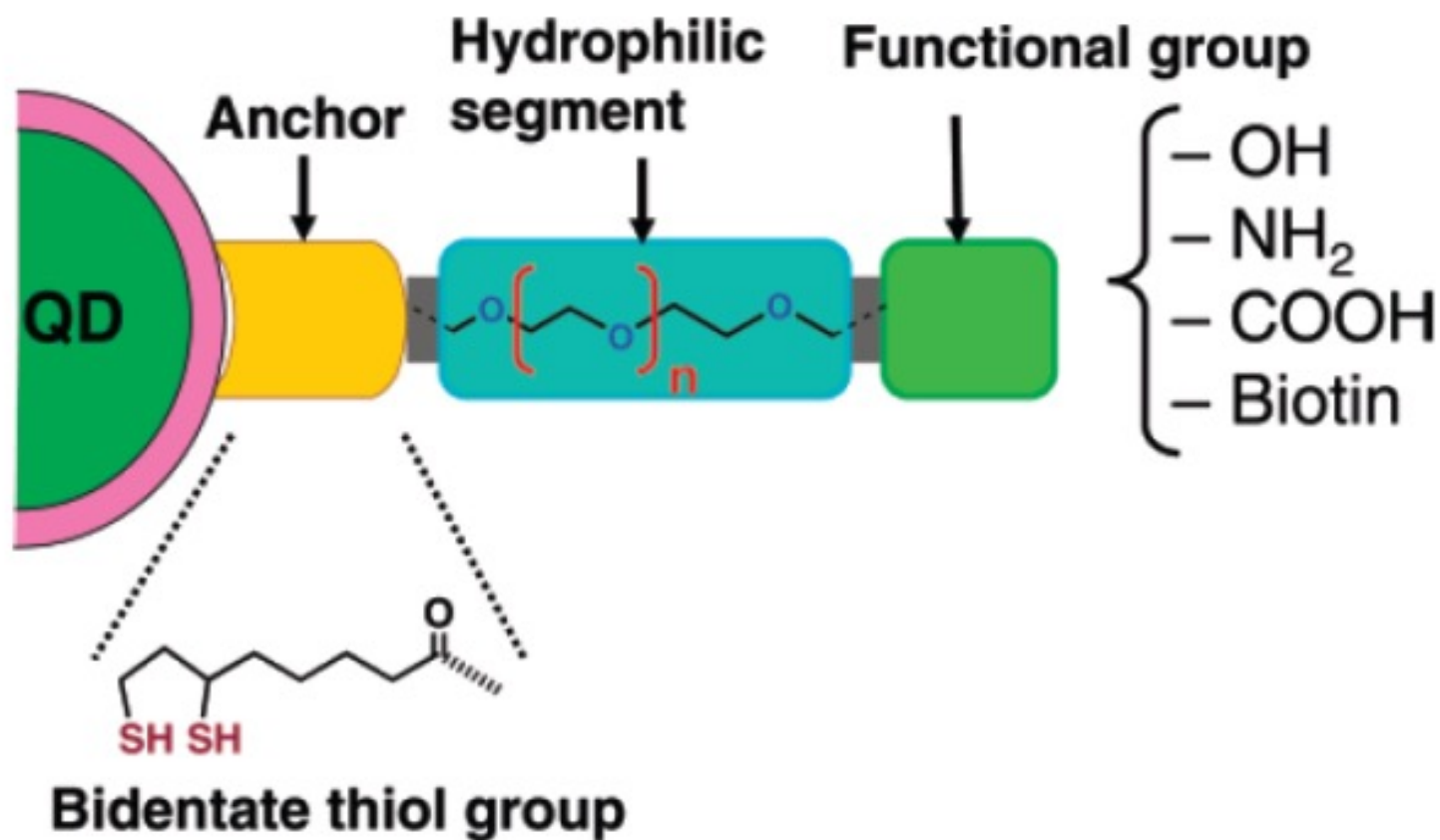


EDC (1-Ethyl-3-[3-dimethylaminopropyl]carbodiimide Hydrochloride)

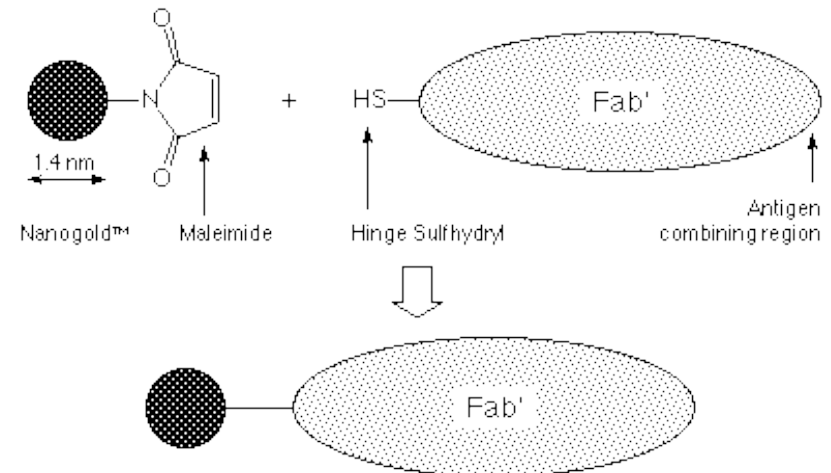
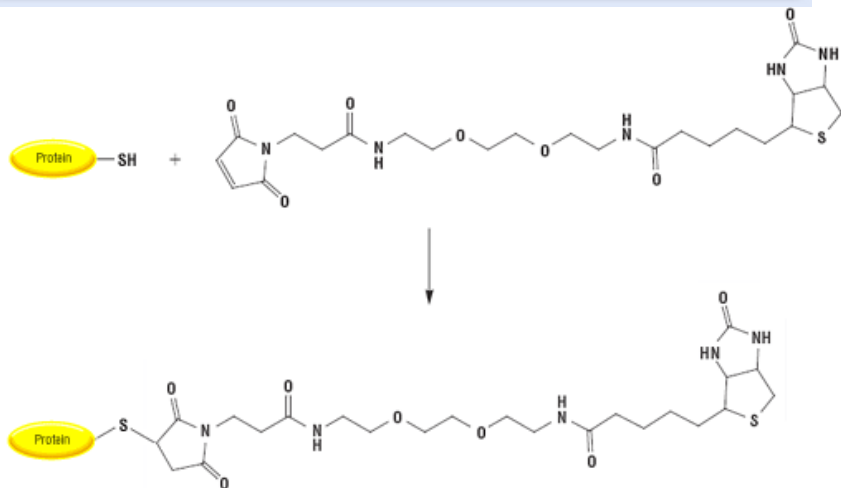
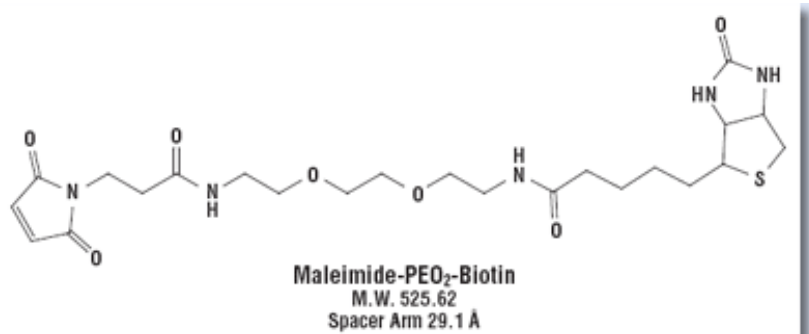
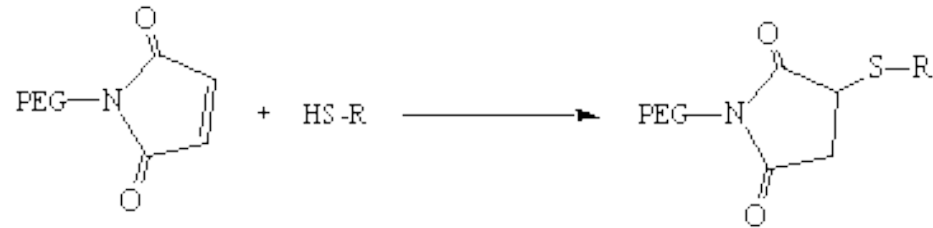
Amine Presenting Surface



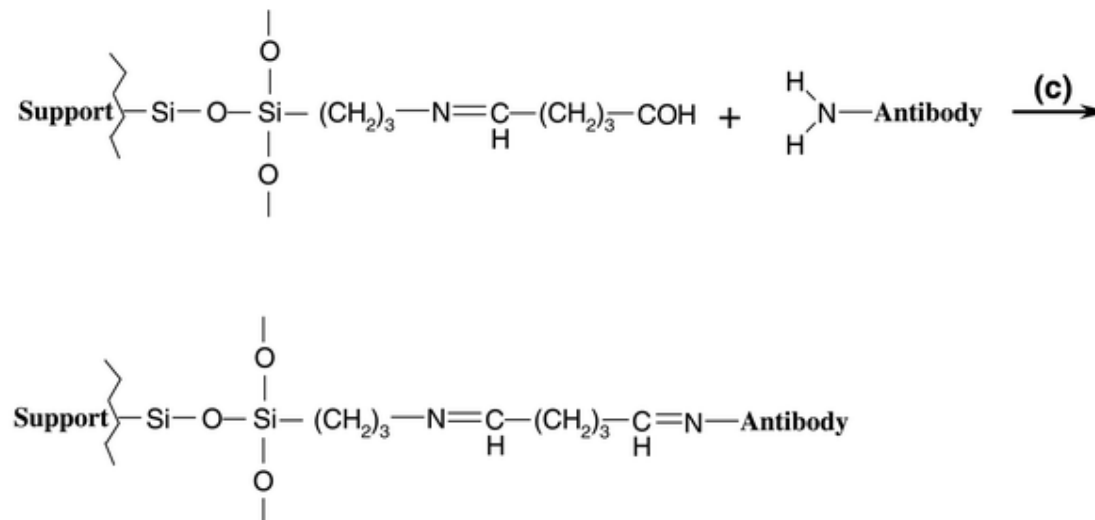
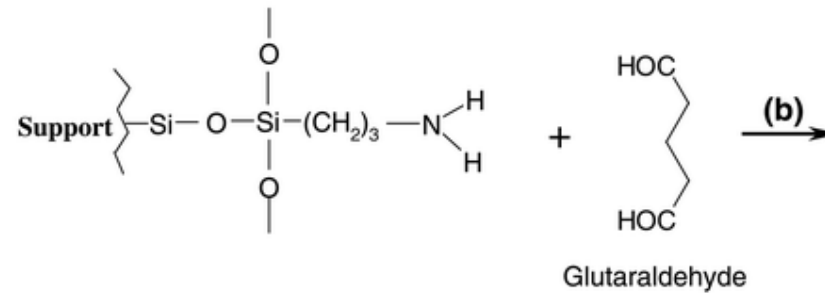
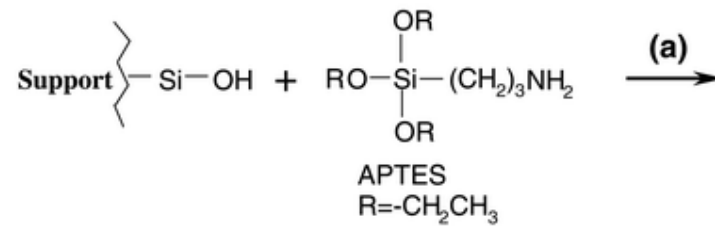
Scheme 1. Modular Design of Hydrophilic Ligands with Terminal Functional Groups Used in This Study



Sulfhydryl Labeling



Silica Modification



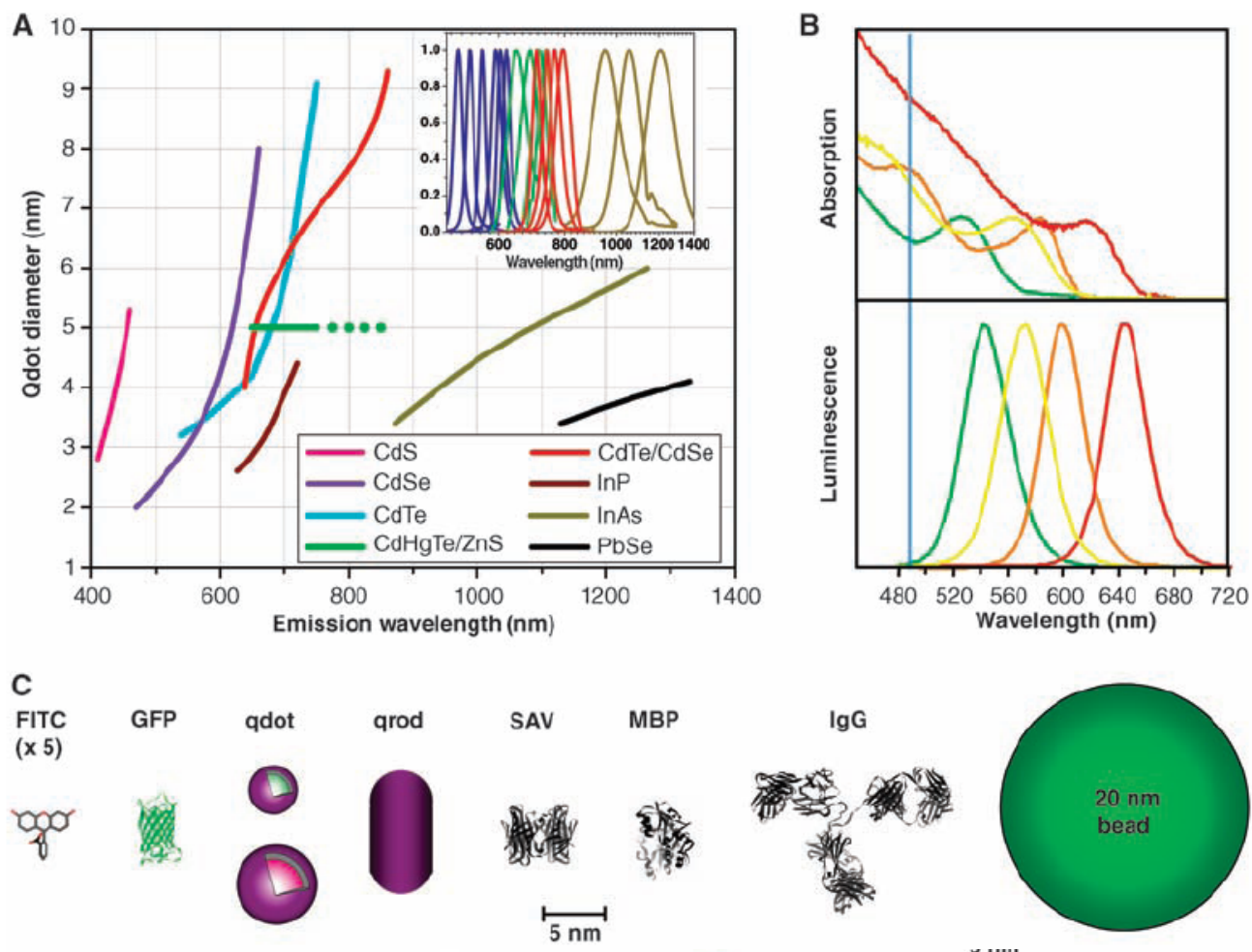
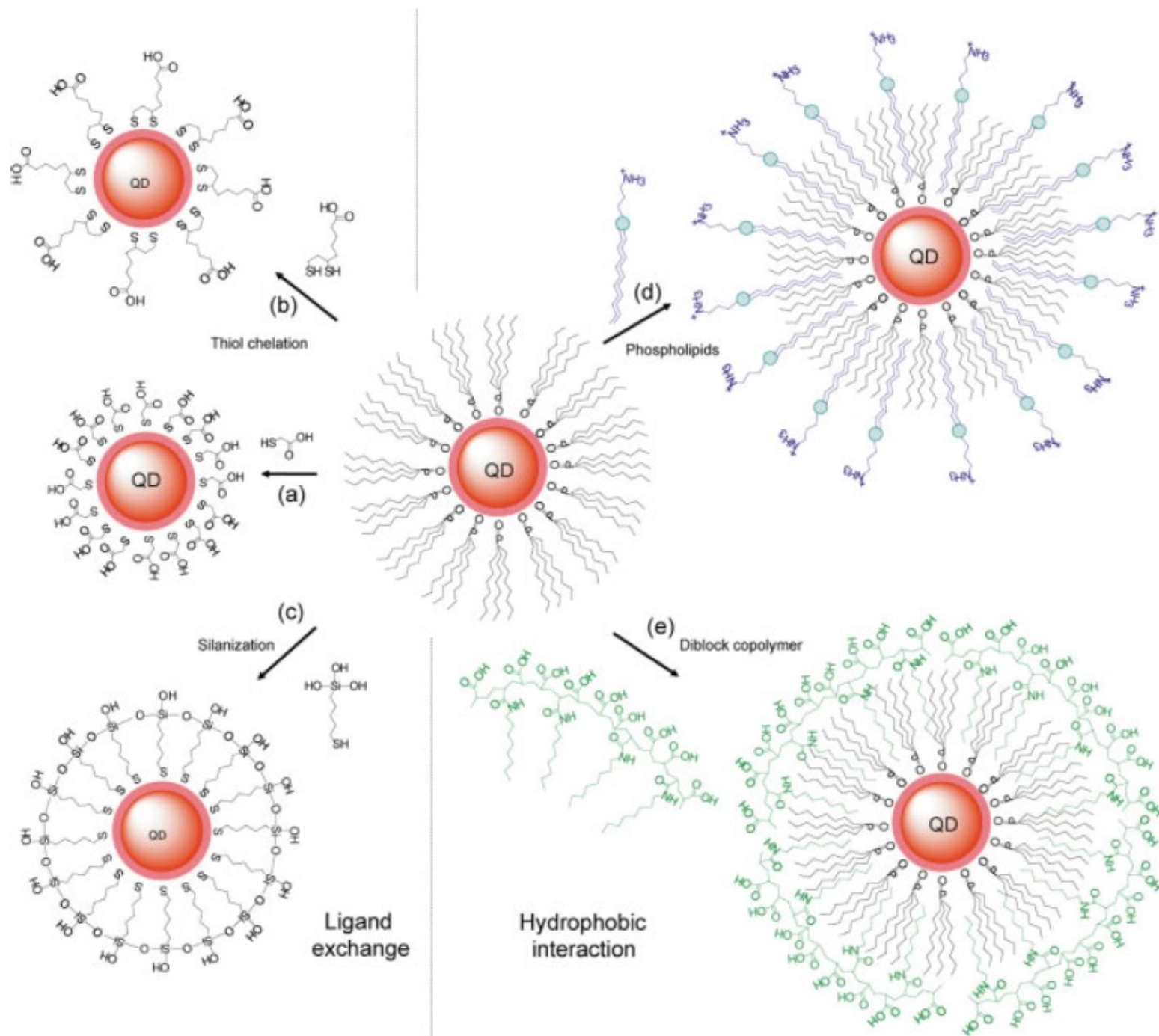


Fig. 1. (A) Emission maxima and sizes of quantum dots of different composition. Quantum dots can be synthesized from various types of semiconductor materials (II-VI: CdS, CdSe, CdTe...; III-V: InP, InAs...; IV-VI: PbSe...) characterized by different bulk band gap energies. The curves represent experimental data from the literature on the dependence of peak emission wavelength on qdot diameter. The range of emission wavelength is 400 to 1350 nm, with size varying from 2 to 9.5 nm (organic passivation/solubilization layer not included). All spectra are typically around 30 to 50 nm (full width at half maximum). Inset: Representative emission spectra for some materials. Data are from (12, 18, 27, 76–82). Data for CdHgTe/ZnS have been extrapolated to the maximum emission wavelength obtained in our group. (B) Absorption (upper curves) and emission (lower curves) spectra of four CdSe/ZnS qdot samples. The blue vertical line indicates the 488-nm line of an argon-ion laser, which can be used to efficiently excite all four types of qdots simultaneously. [Adapted from (28)] (C) Size comparison of qdots and comparable objects. FITC, fluorescein isothiocyanate; GFP, green fluorescent protein; qdot, green (4 nm, top) and red (6.5 nm, bottom) CdSe/ZnS qdot; qrod, rod-shaped qdot (size from Quantum Dot Corp.'s Web site). Three proteins—streptavidin (SAV), maltose binding protein (MBP), and immunoglobulin G (IgG)—have been used for further functionalization of qdots (see text) and add to the final size of the qdot, in conjunction with the solubilization chemistry (Fig. 2).



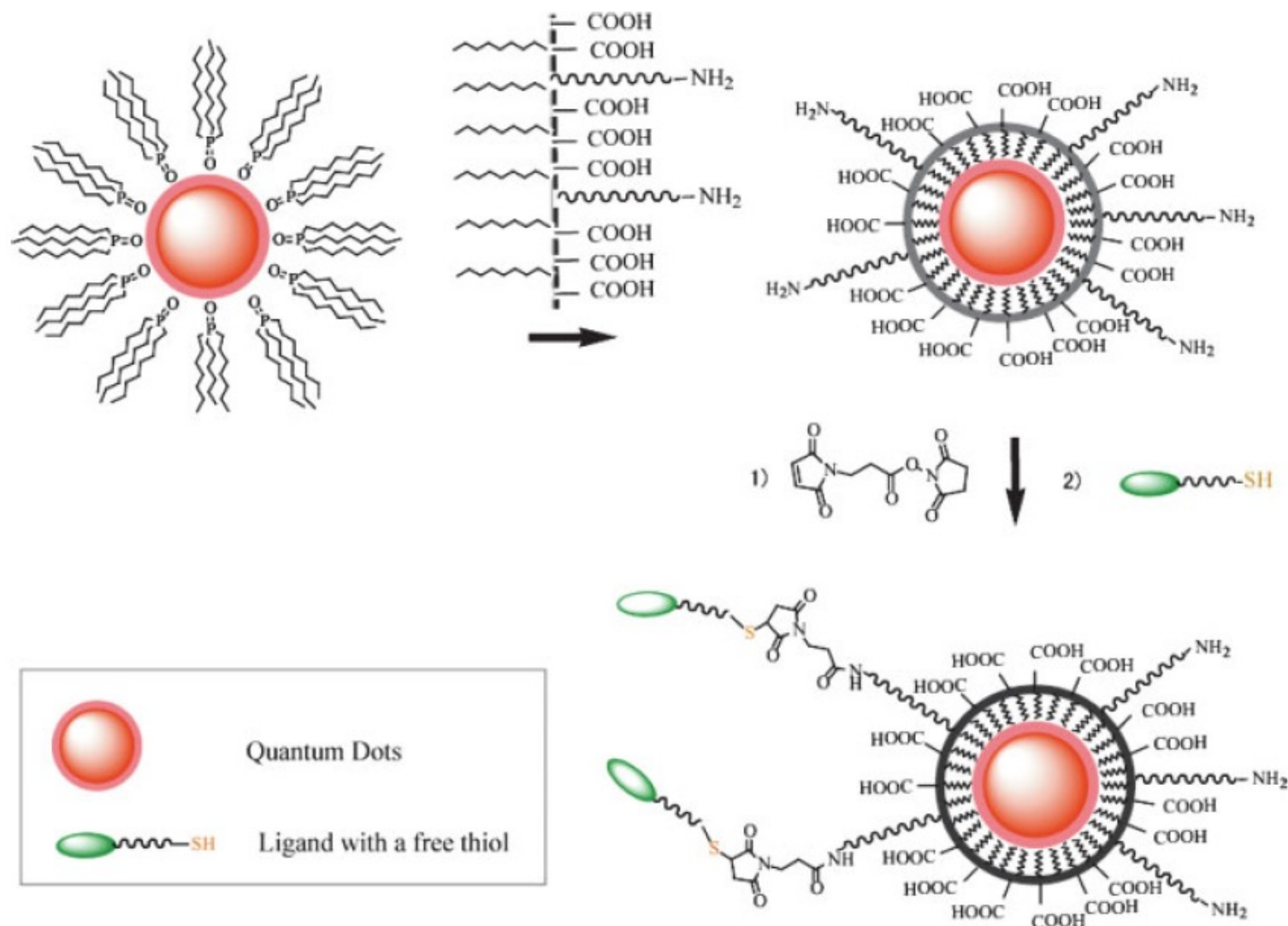
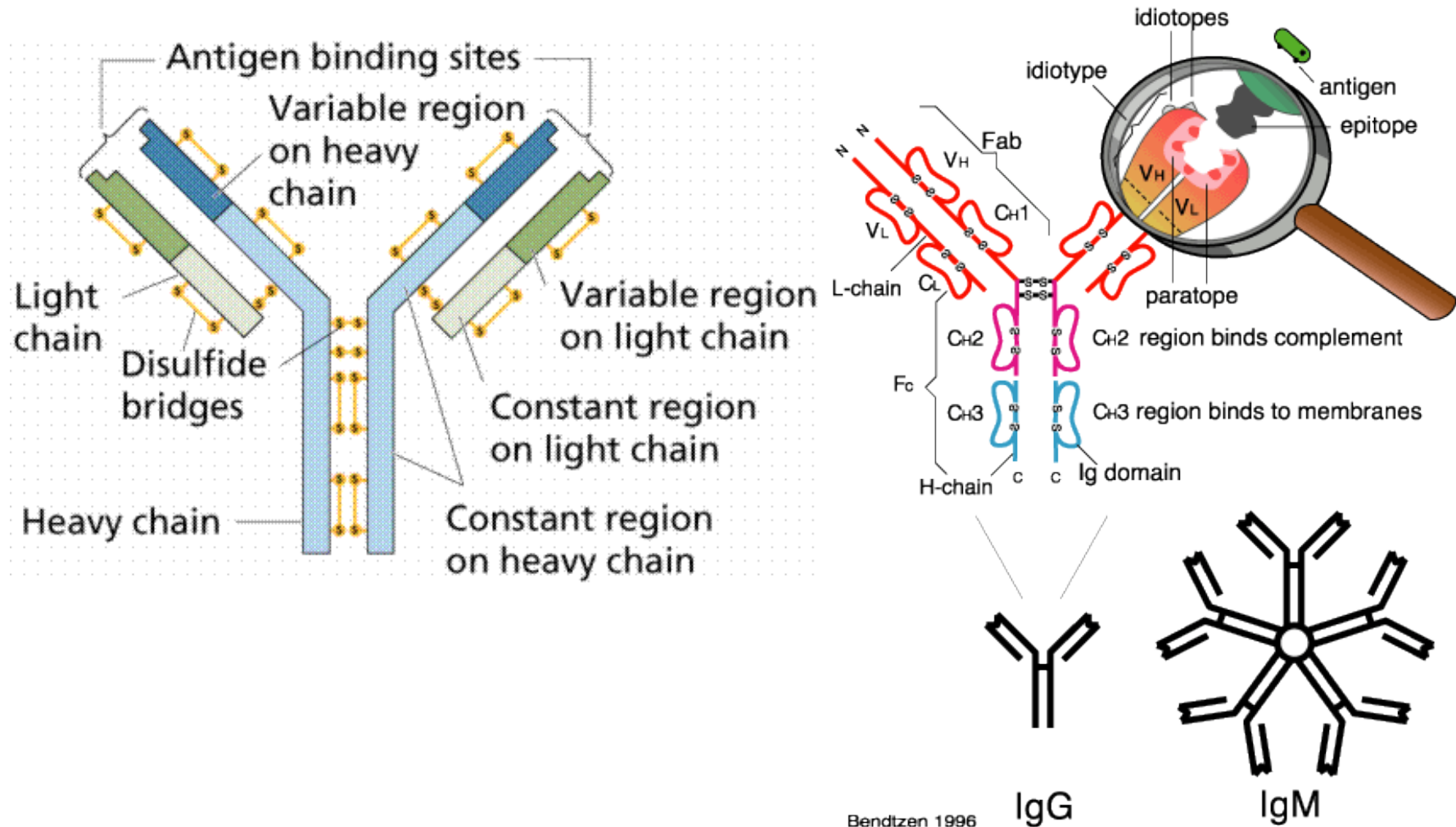
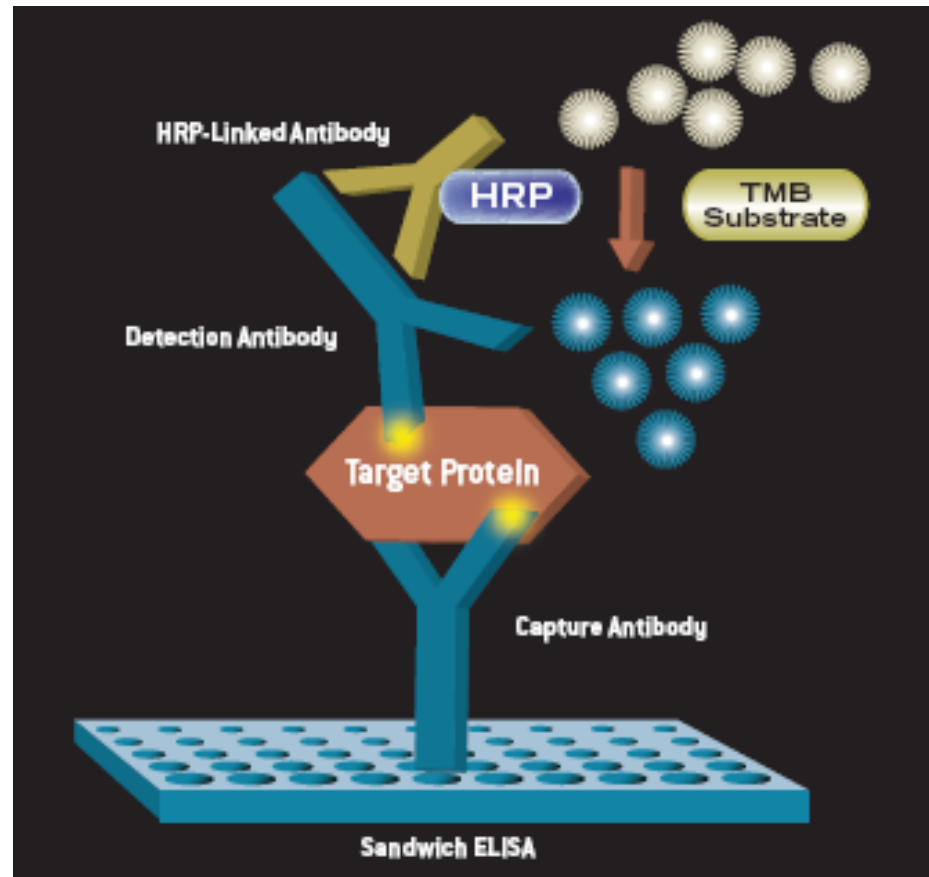


FIGURE 3 Maleimide functionalized QDs for conjugating thiol-containing ligands. TOPO stabilized QDs are coated with a primary amine functionalized tri-block amphiphilic copolymer for producing water-soluble QDs, which facilitate further conjugation to ligands with free thiols through bi-functional cross-linkers.

Antibody and Antigen



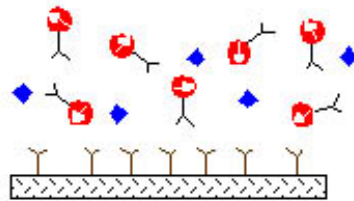
Enzyme-Linked ImmunoSorbent Assay (ELISA)



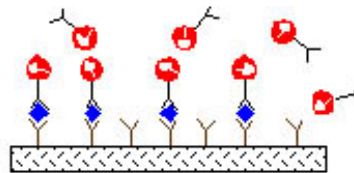
Labeling
BSA/PEG

Microarray

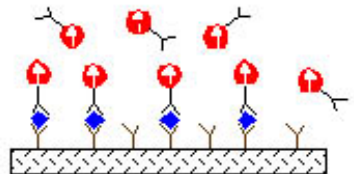
◆ Biomolecules of interest Y Capture antibody ▨ Solid support ● Magnetically labeled antibody



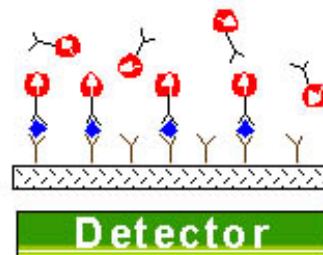
Add biomolecules of interest and magnetically labeled detect antibodies to well coated with capture antibody.



Immobilized immune complexes form on solid support.

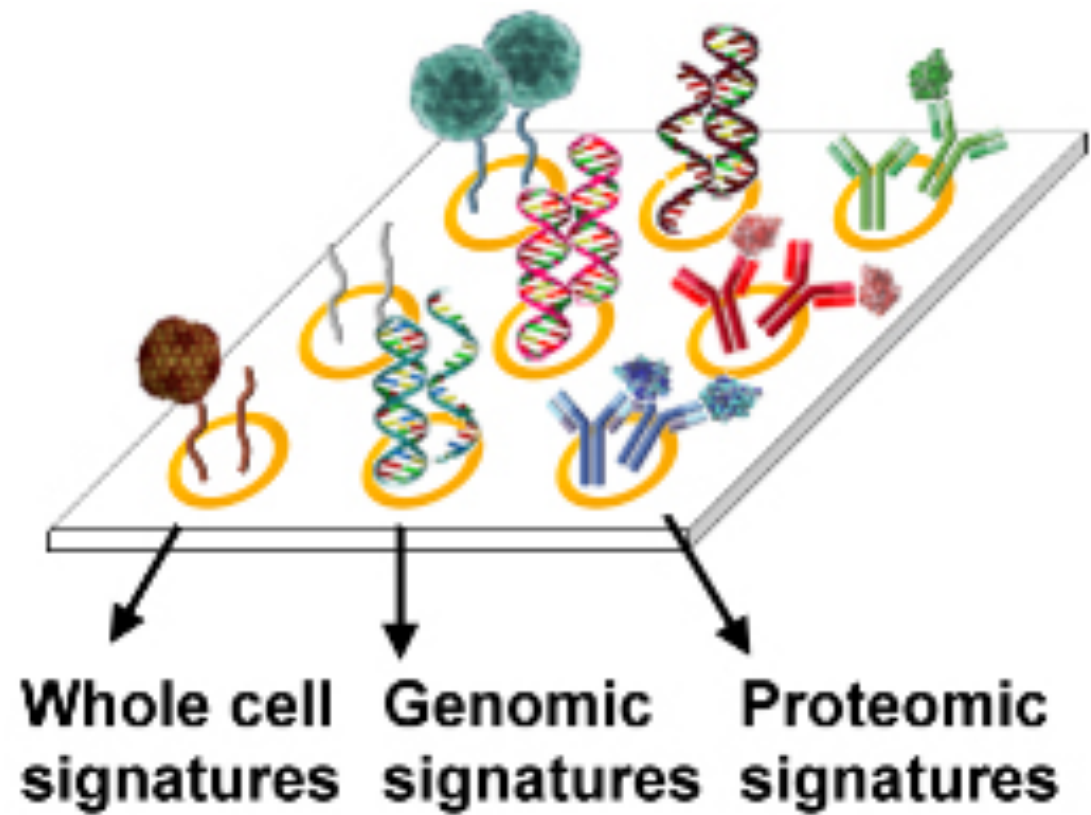


Apply external magnetic field, magnetic dipoles align.



Remove field, measure net magnetization due to bound antibody labels. Unbound labels randomize quickly and contribute no net signal.

Microarray



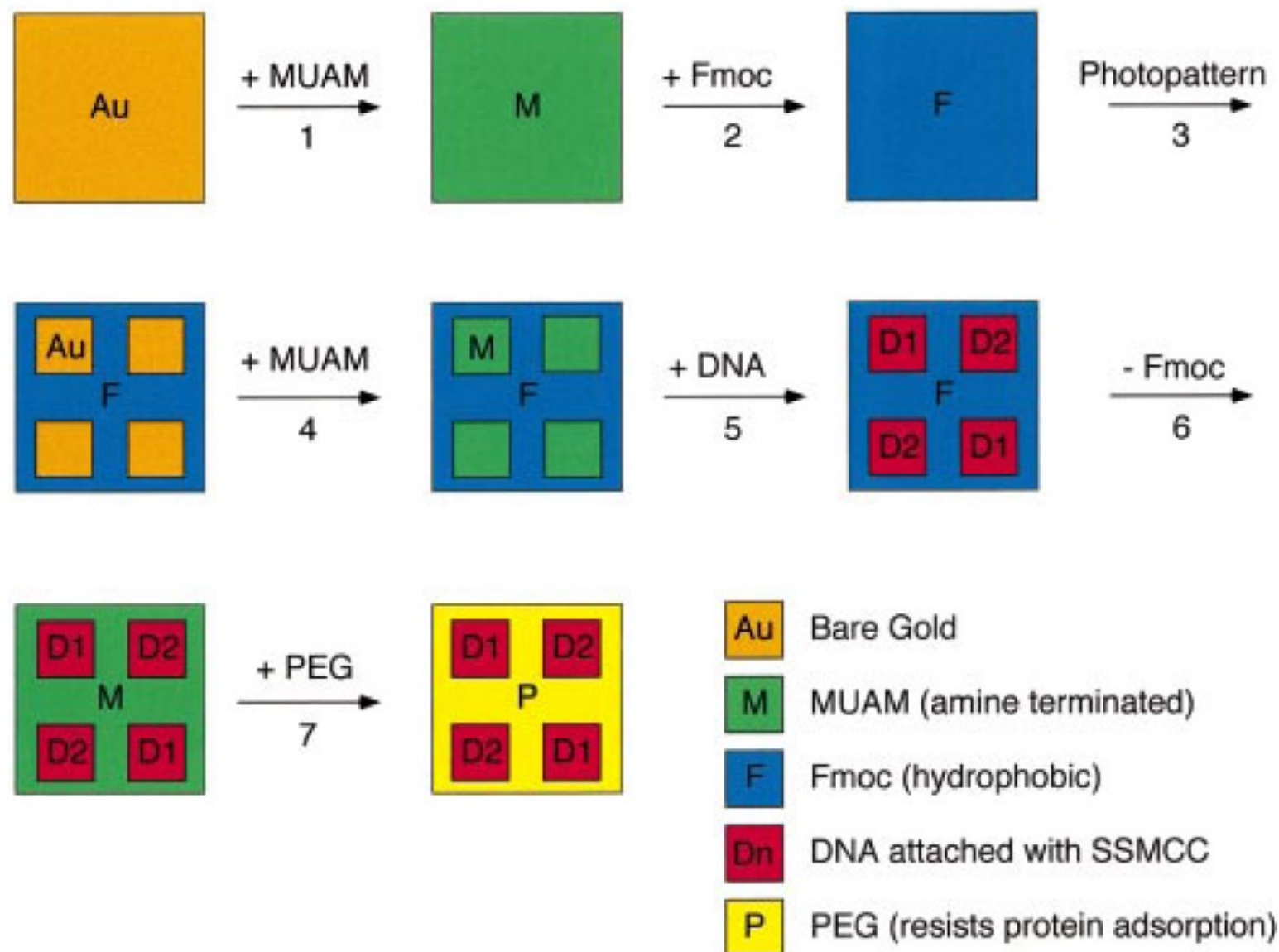


Figure 1. Fabrication scheme for the construction of multi-element DNA arrays. A clean gold surface is reacted with the amine-terminated alkanethiol MUAM, and subsequently reacted with Fmoc-NHS to create a hydrophobic surface. This surface is then exposed to UV radiation through a quartz mask and rinsed with solvent to remove the MUAM+Fmoc from specific areas of the surface, leaving bare gold pads. These bare gold areas on the sample surface are filled in with MUAM, resulting in an array of MUAM pads surrounded by a hydrophobic Fmoc background. Solutions of DNA are then delivered by pipet onto the specific array locations and are covalently bound to the surface via the bifunctional linker SSMCC. In the final two steps, the Fmoc-terminal groups on the array background are removed and replaced by PEG groups which prohibit the nonspecific binding of analyte proteins to the background.

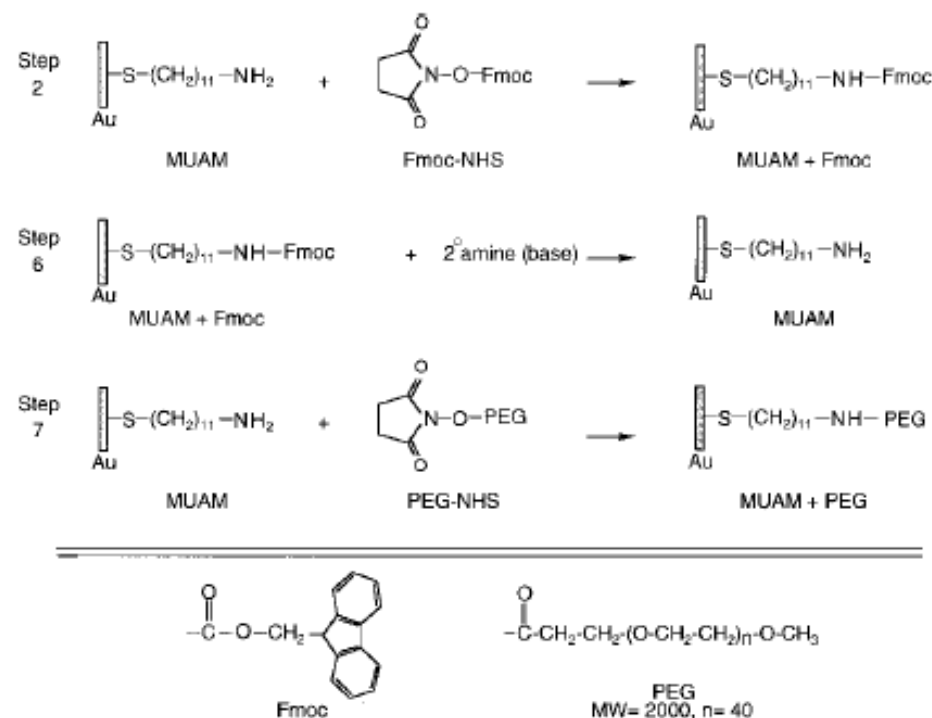


Figure 2. Surface reaction scheme showing the steps involved in the reversible modification of the array background. (Step 2) The starting amine-terminated alkanethiol surface (MUAM) is reacted with the Fmoc-NHS protecting group to form a carbamate linkage thus creating a hydrophobic Fmoc-terminated surface. (Step 6) After DNA immobilization (see Figure 3), the hydrophobic Fmoc group is removed from the surface with a basic secondary amine, resulting in the return of the original MUAM surface. (Step 7) In the final array fabrication step, the deprotected MUAM is reacted with PEG-NHS to form an amide bond that covalently attaches PEG to the array surface.

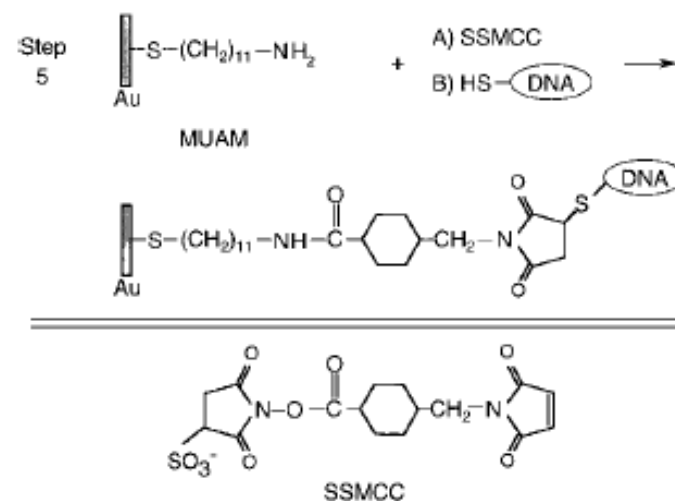
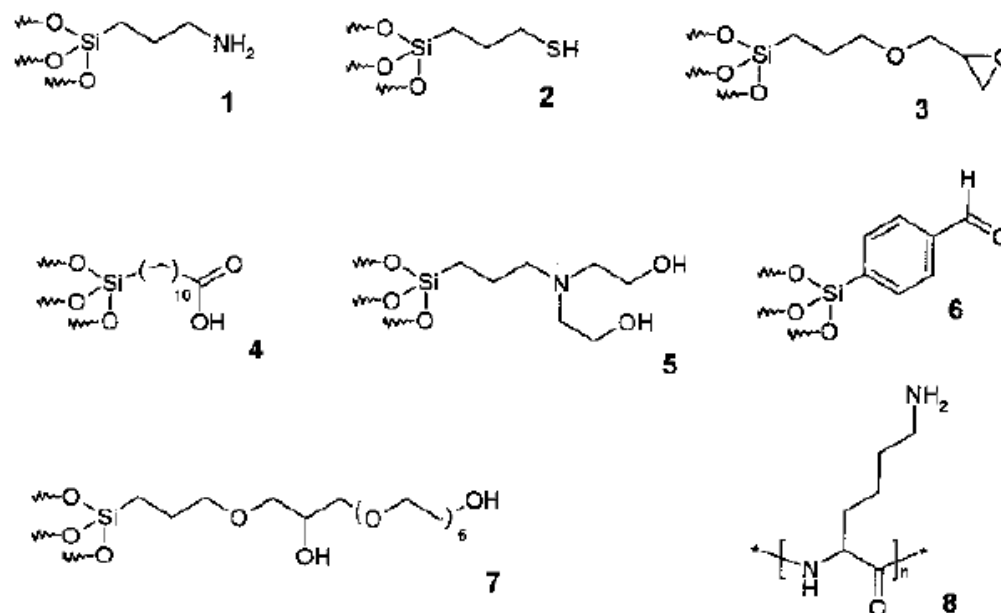
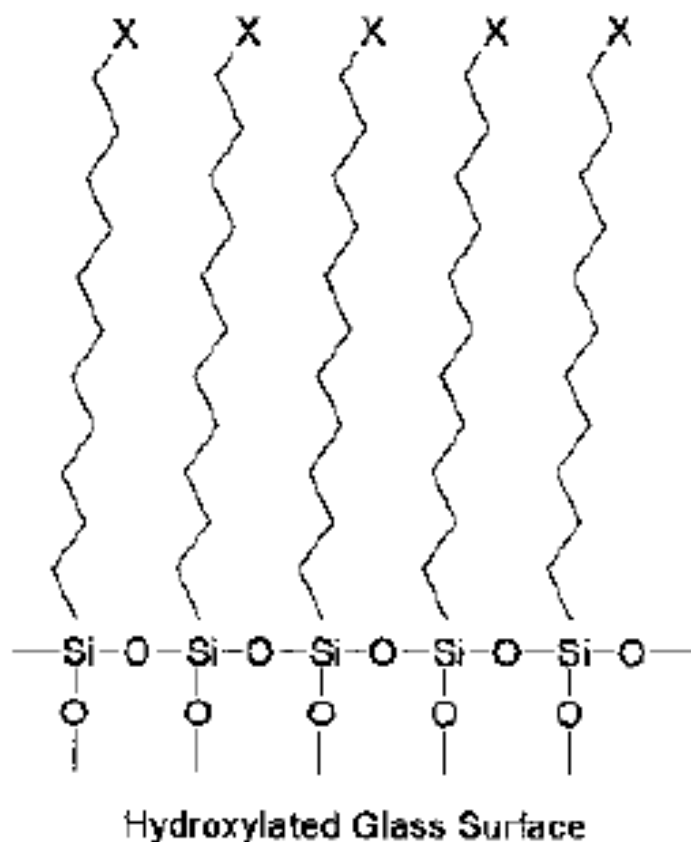


Figure 3. Surface reaction scheme showing the immobilization of thiol-terminated DNA to the array surface. In Step 5 of the DNA array fabrication, the heterobifunctional linker SSMCC is used to attach 5'-thiol modified oligonucleotide sequences to reactive pads of MUAM. This linker contains an NHSS ester functionality (reactive toward amines) and a maleimide functionality (reactive toward thiols). The surface is first exposed to a solution of the linker, whereby the NHSS ester end of the molecule reacts with the MUAM surface. Excess linker is rinsed away and the array surface is then spotted with 5'-thiol-modified DNA that reacts with the maleimide groups forming a covalent bond to the surface monolayer.

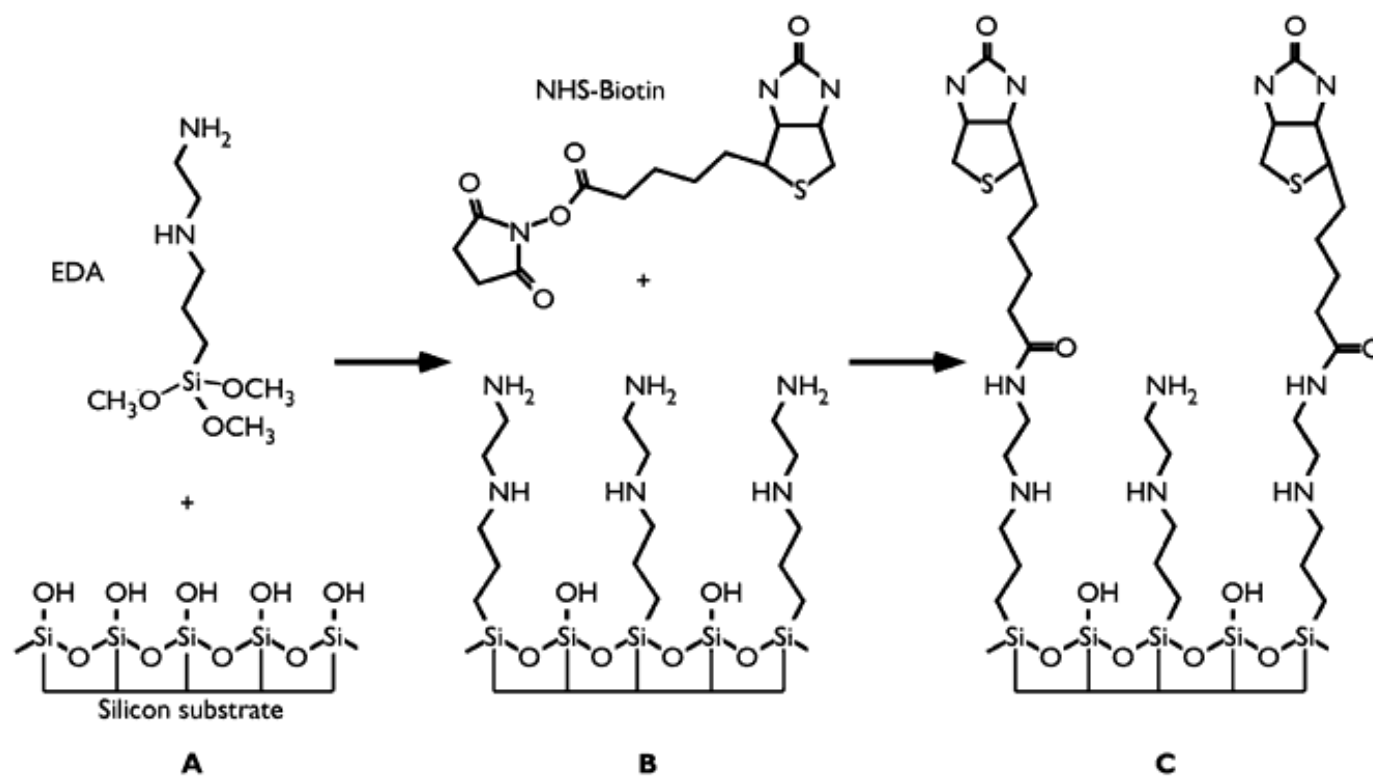
Glass Surface Modification



Scheme 2.2 Reagents for derivatization of glass surfaces. 1 APTES = aminopropyltriethoxysilane; 2 MPTS = 3-mercaptopropyltrimethoxysilane; 3 GPTS = glycidoxypropyltrimethoxysilane; 4 TETU = triethoxysilane undecanoic acid;

5 HE-APTS = bis(hydroxyethyl)aminopropyltriethoxysilane; 6 4-trimethoxysilylbenzaldehyde; 7 GPTS/HEG = glycidoxypropyltrimethoxysilane-hexaethylene glycol; 8 poly(lysine).

Scheme 2.1 2D schematic description of a polysiloxane monolayer on a glass surface (X = terminal functional)



Biotin-Streptavidin

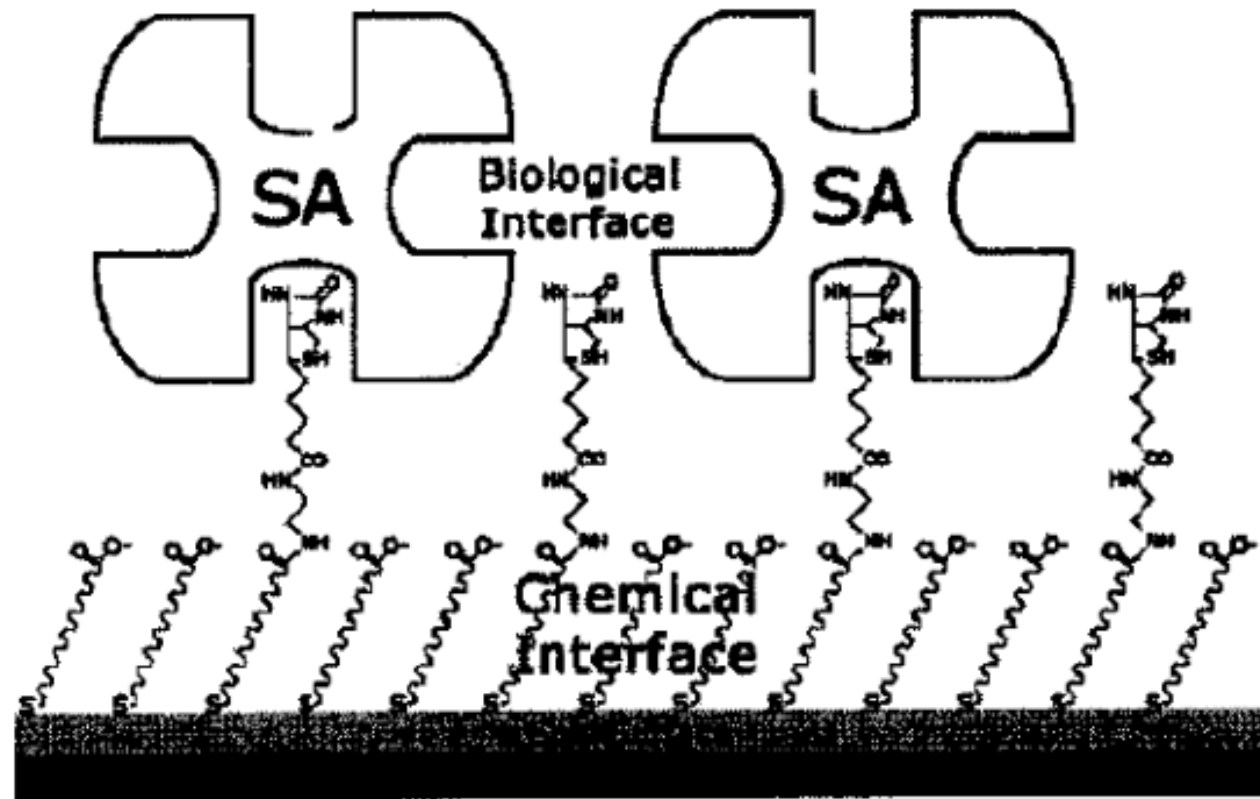
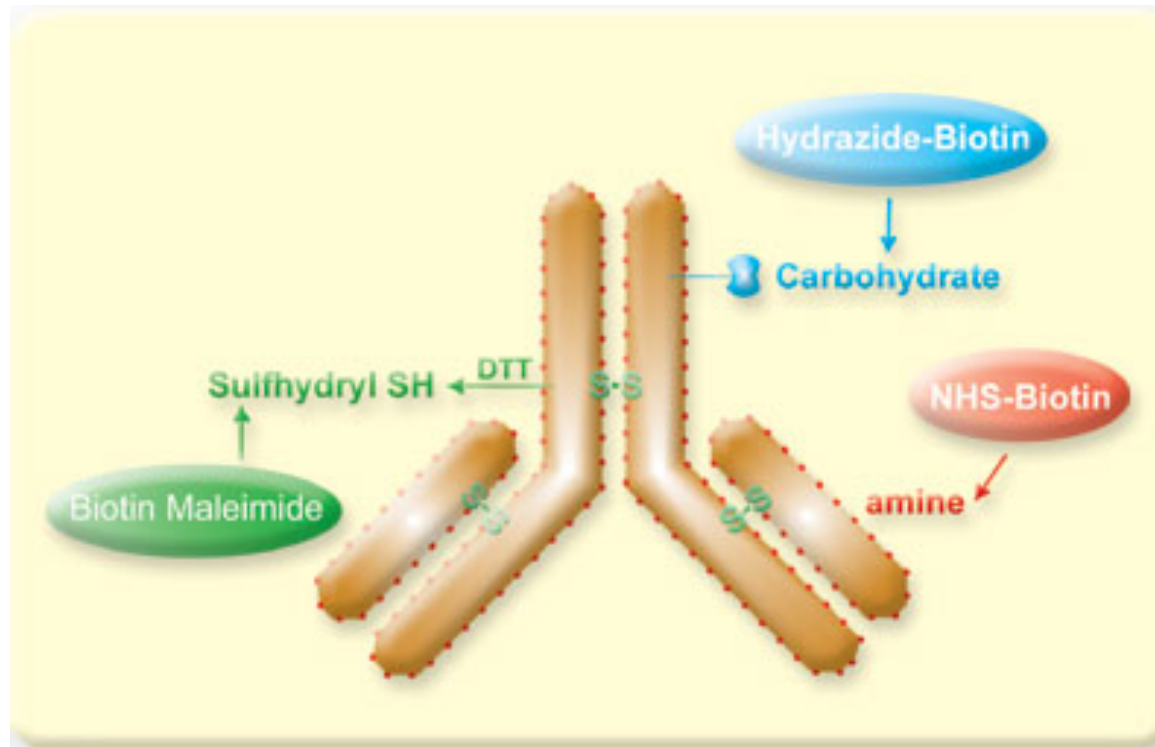
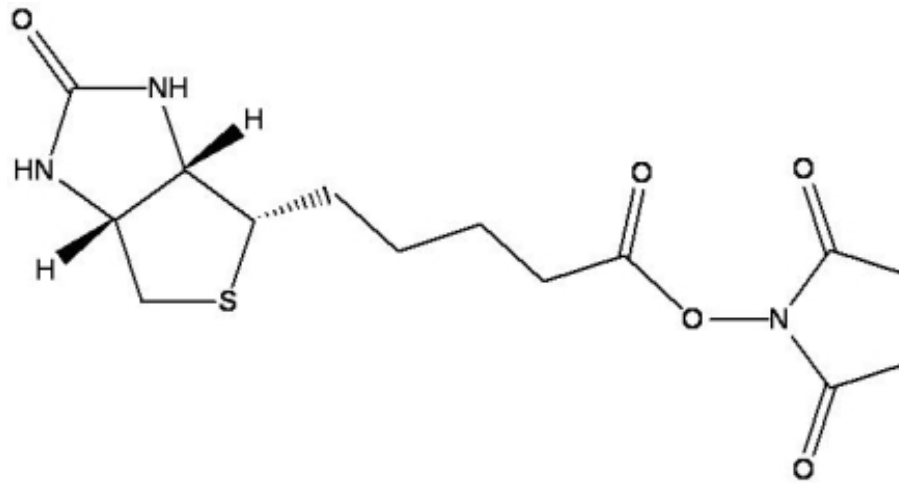


Figure 2.3 Schematic representation of a streptavidin sensor surface assembled on a reaction-controlled biotinylated SAM [28].

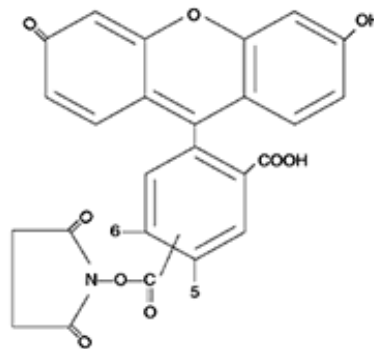
Protein Labeling



Amine Reactive Labeling

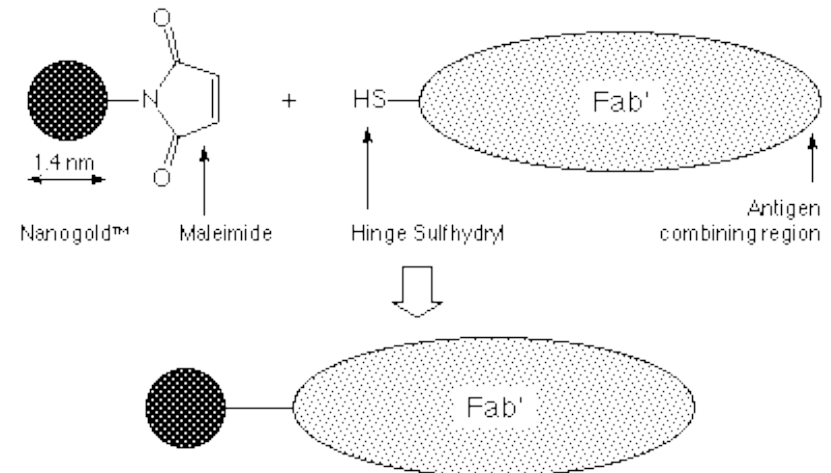
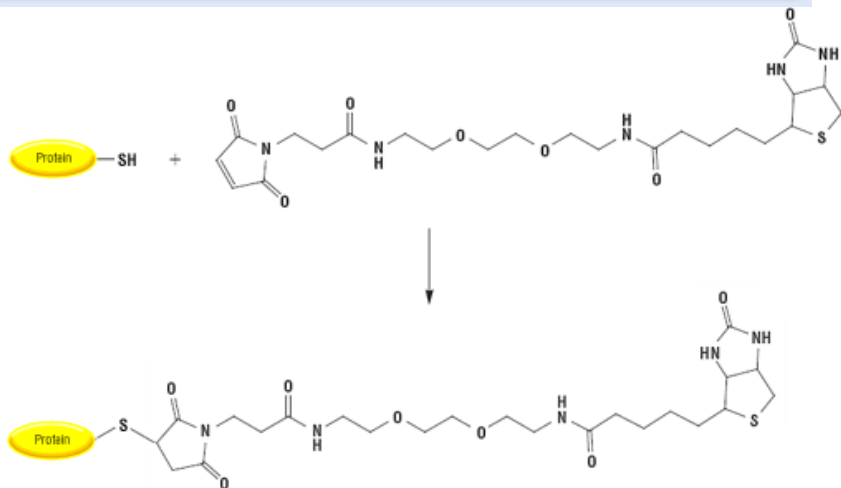
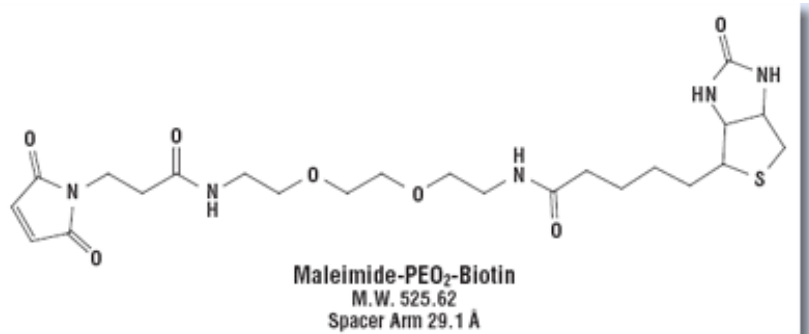
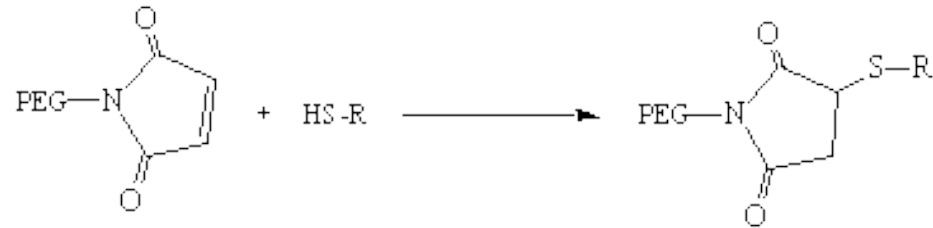


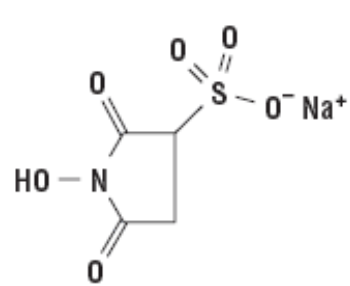
NHS ester



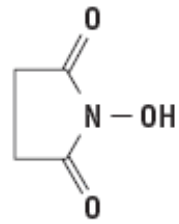
NHS-Fluorescein
MW 473.4

Sulfhydryl Labeling



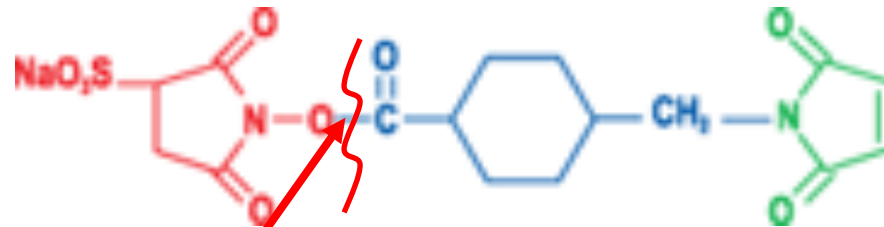


Sulfo-NHS
M.W. 217.13



NHS
M.W. 115.09

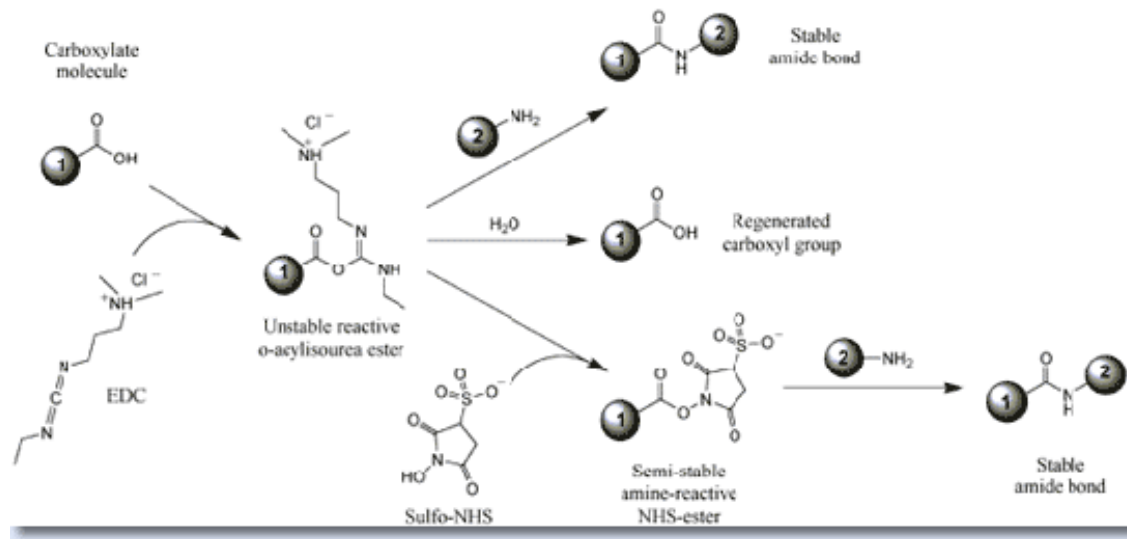
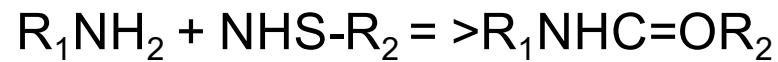
N-hydroxysuccinimide



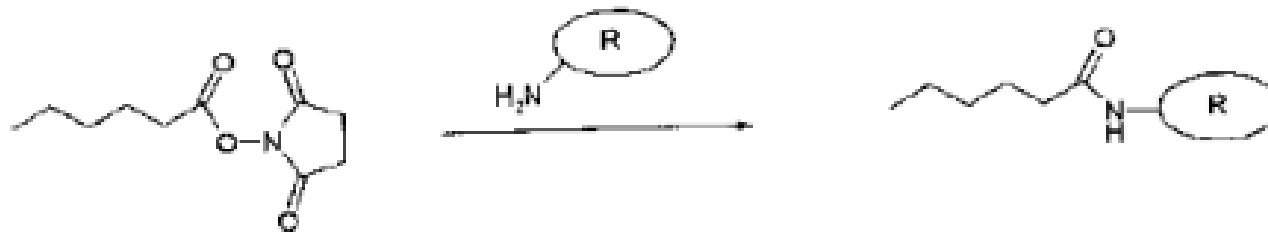
SulfoSuccinimidyl 4-(N-Maleimidomethyl)Cyclohexane-1-Carboxylate
SSMCC

The most popular NH_2 - and SH - crosslinker

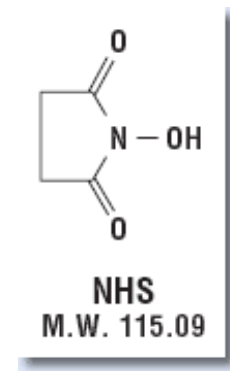
$\text{NH}_2 \Rightarrow$ amide



N-hydroxysuccinimide (NHS)

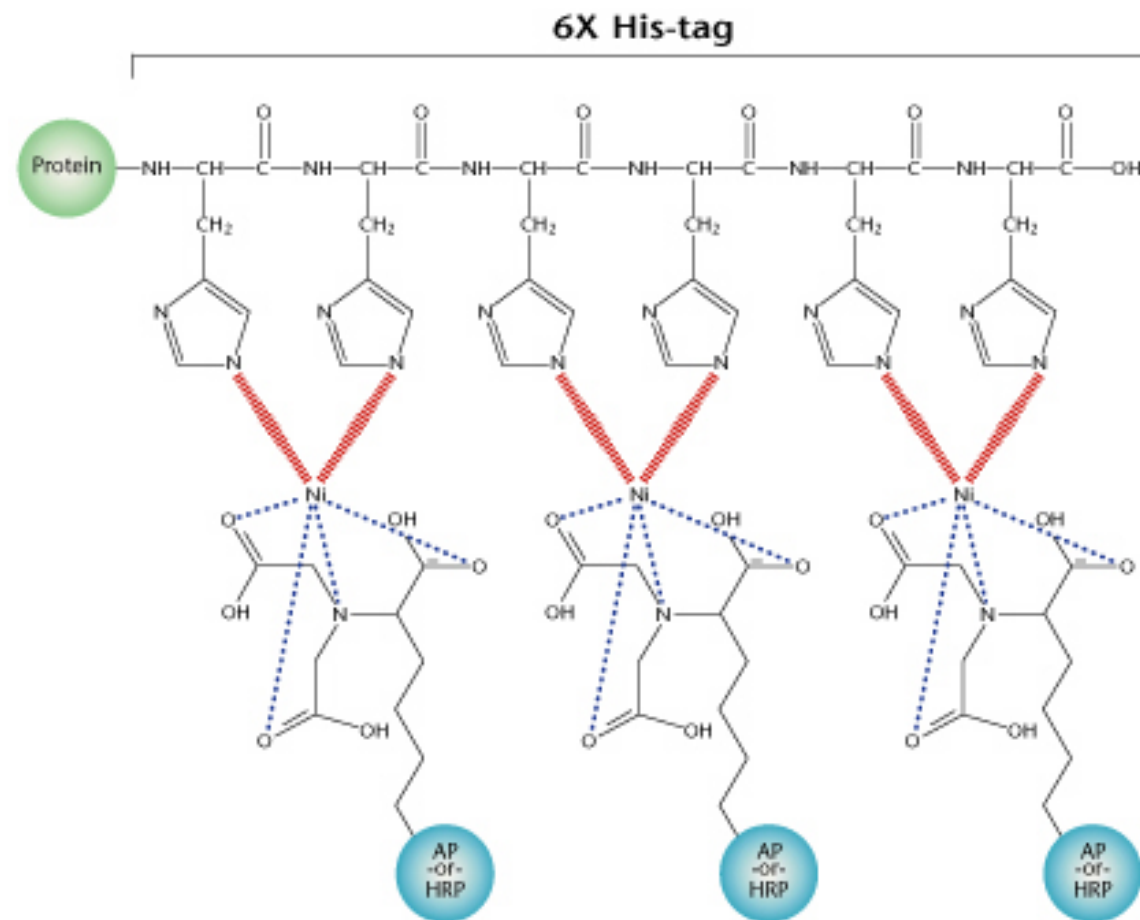


Scheme 2.6 Surface coupling reaction of NHS-esters with the amino residues of the side-chains of polypeptides (lysine units). R, protein.

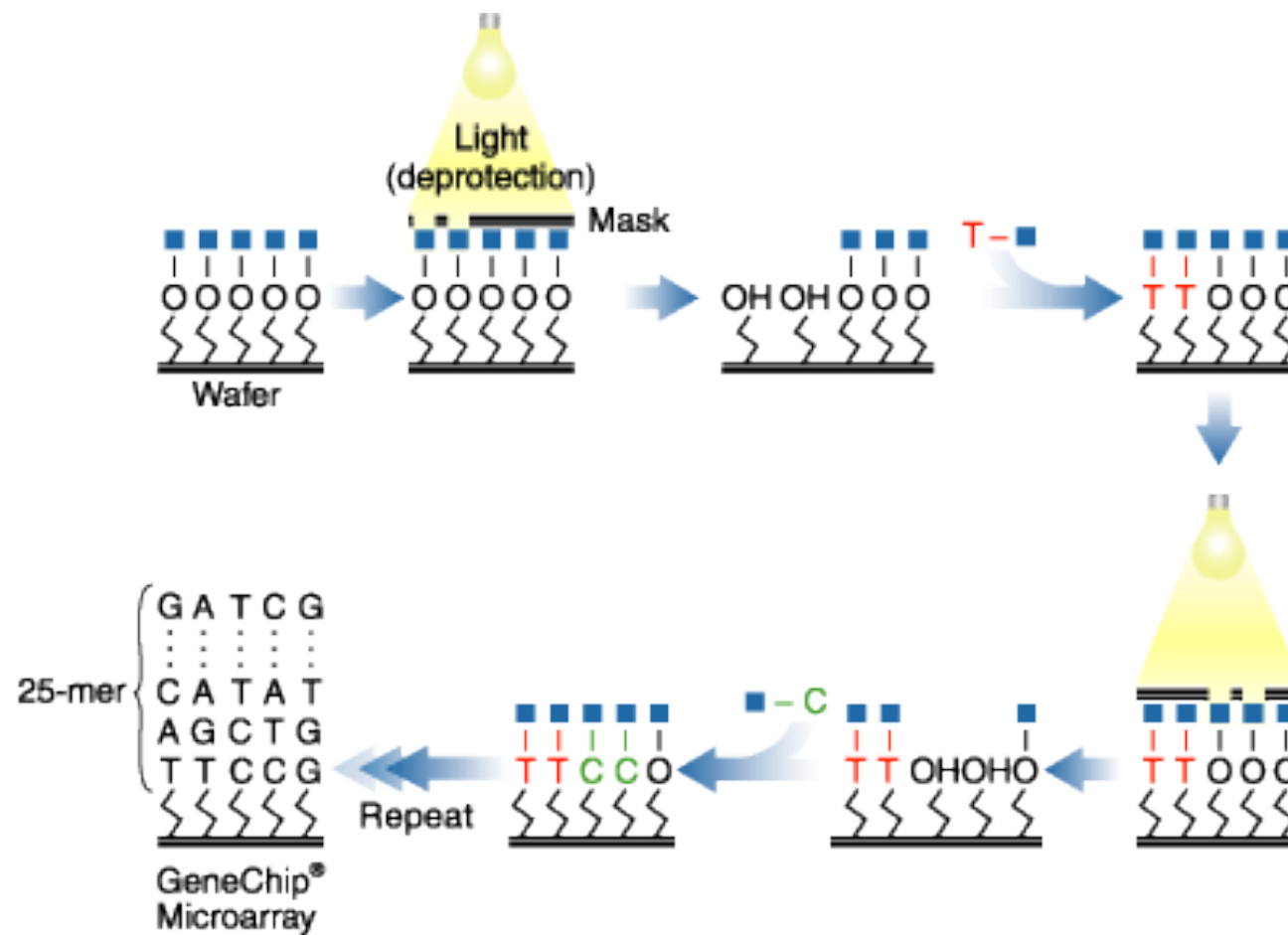


N-hydroxysuccinimide

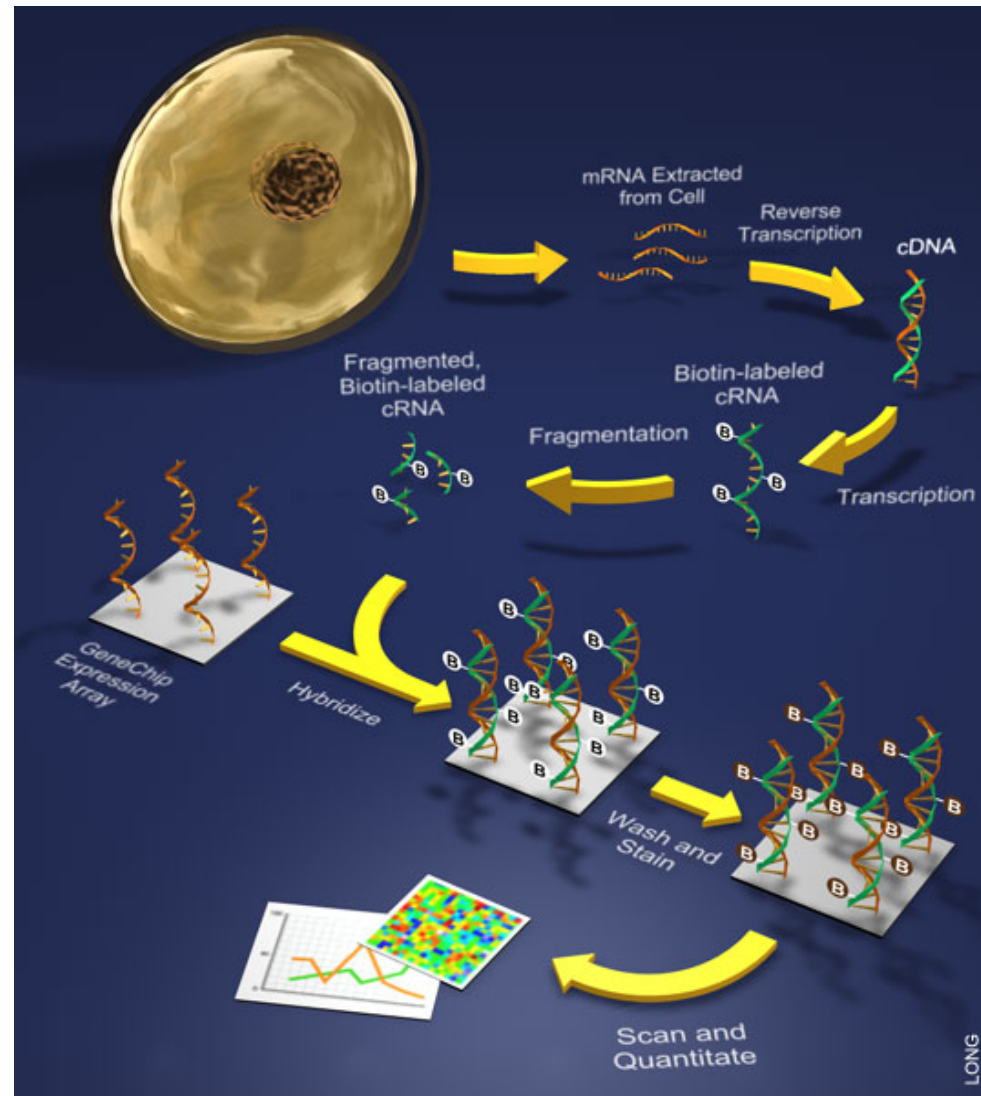
His Tag



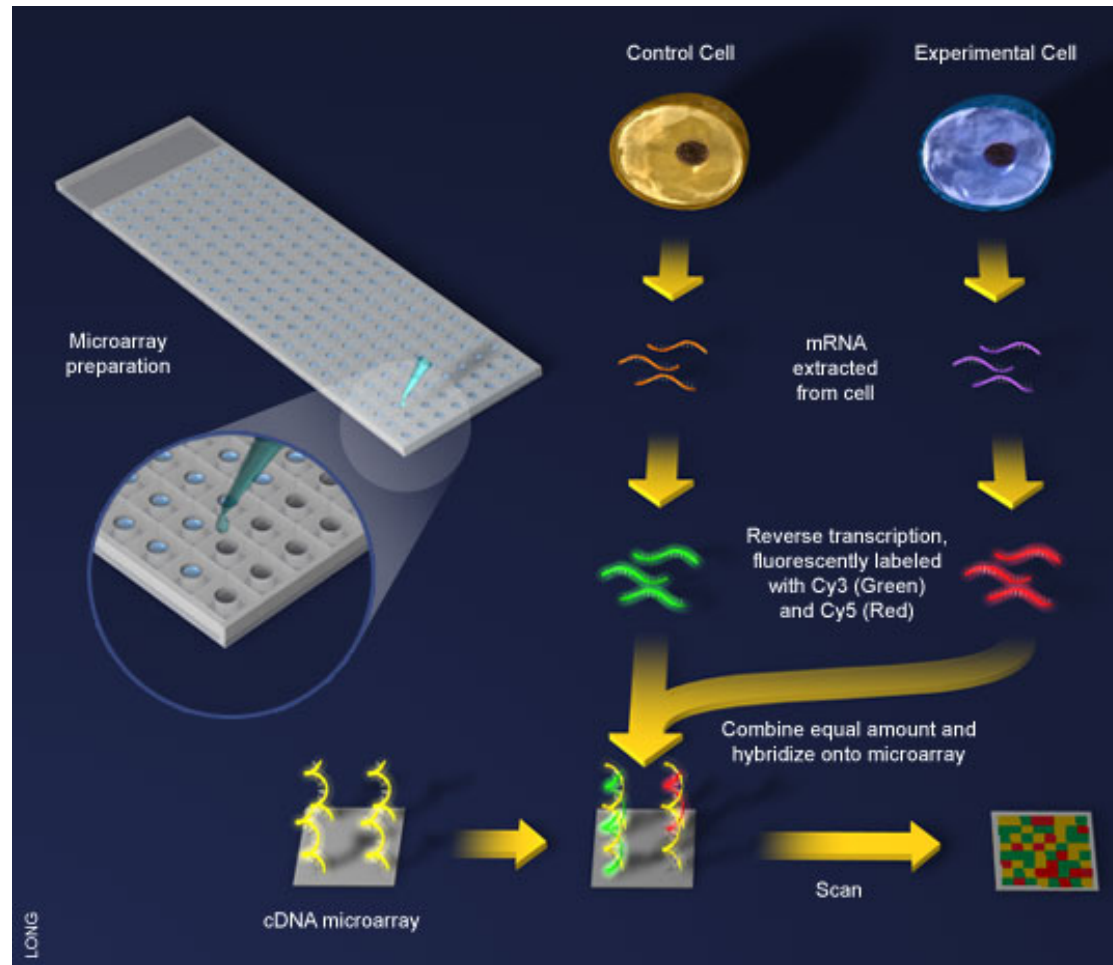
GeneChip



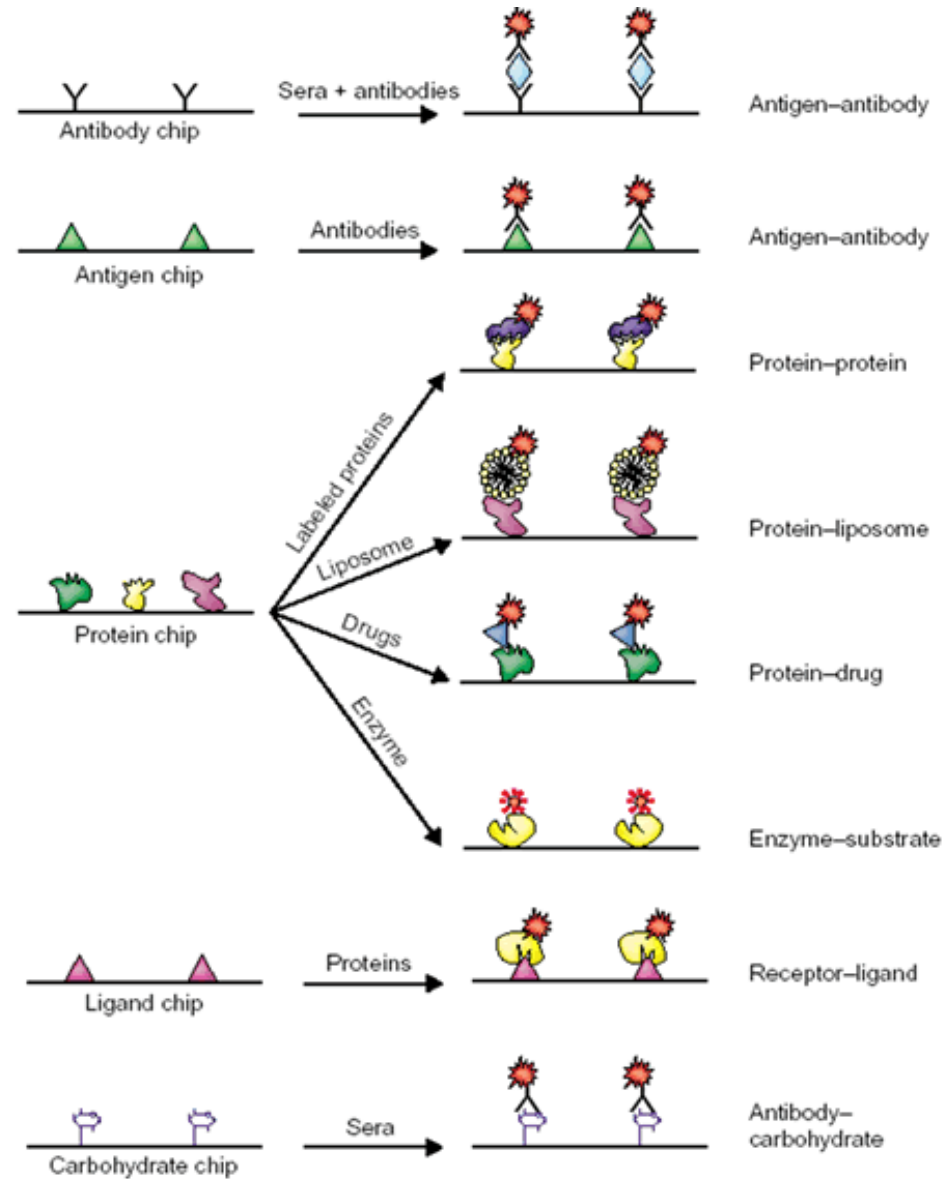
Scheme



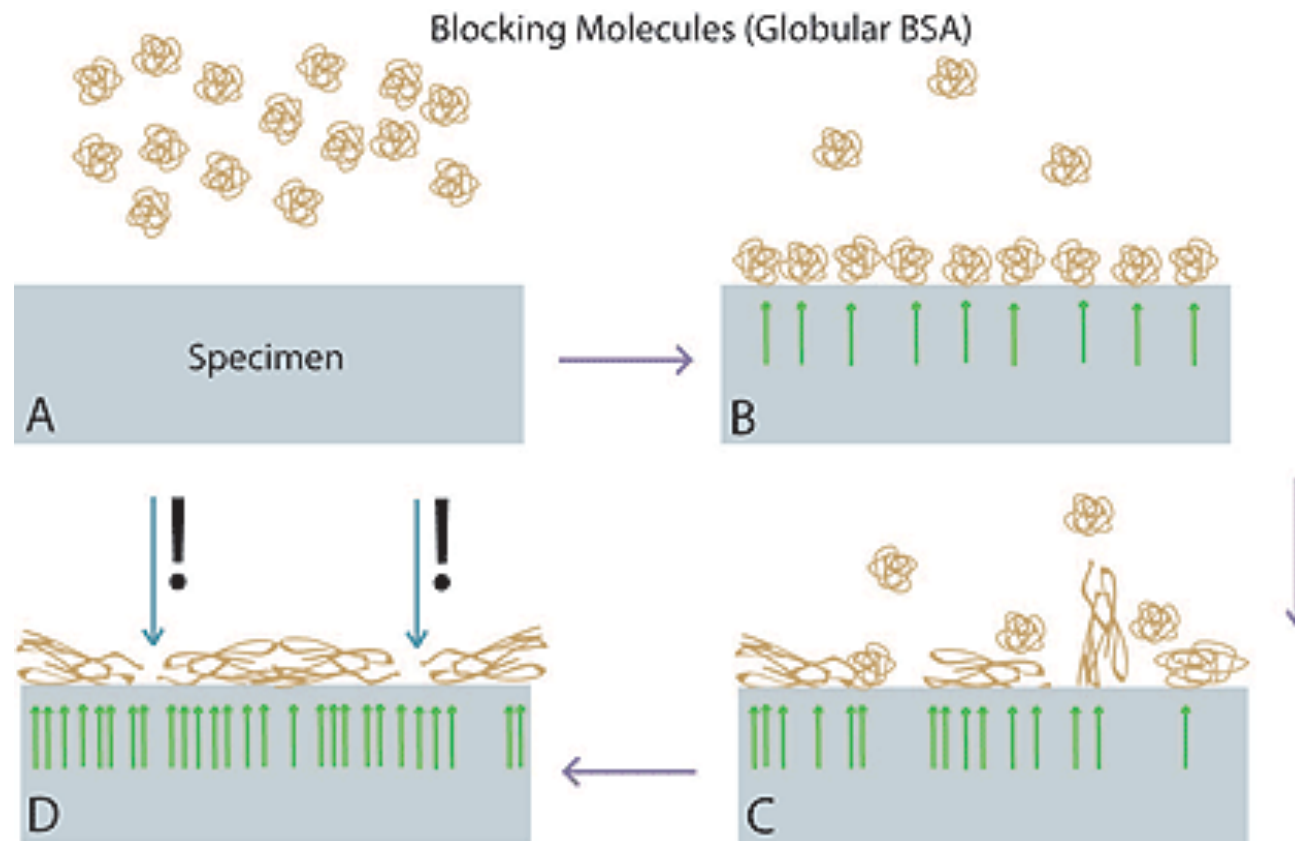
cDNA Microarray



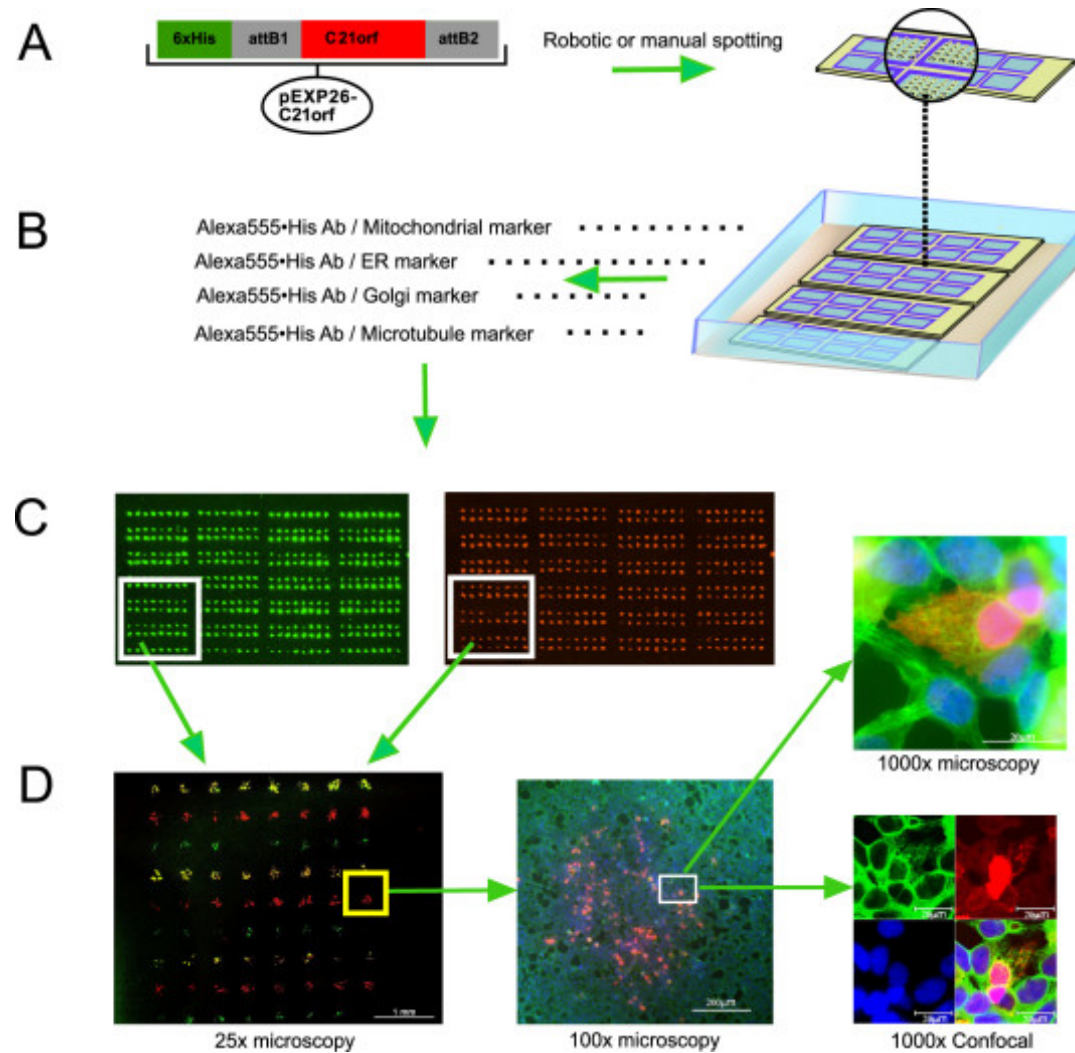
Protein Array



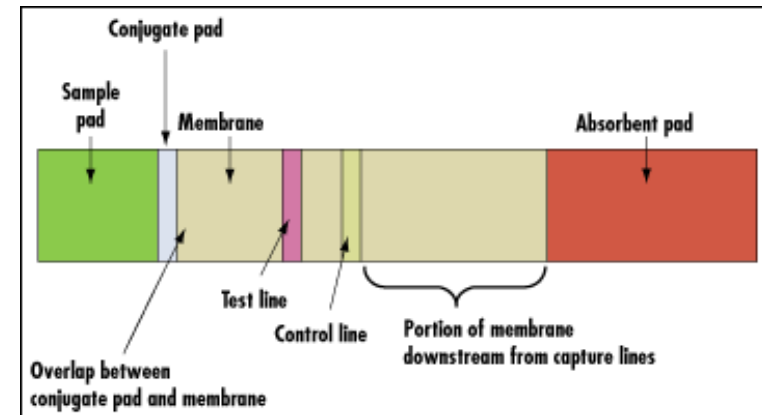
BSA Blocking



Cell Array



hCG immunoassay



human chorionic gonadotropin (hCG)

Nucleotide Sensor

